Title
Novel functions for autophagy during Ras transformation

Author
Lock, Rebecca

Publication Date
2012

Peer reviewed|Thesis/dissertation

Novel functions for autophagy during Ras transformation

by

Rebecca Lock

DISSERTATION

Submitted in partial satisfaction of the requirements for the degree of

DOCTOR OF PHILOSOPHY

in

Biomedical Sciences

in the

GRADUATE DIVISION

of the

UNIVERSITY OF CALIFORNIA, SAN FRANCISCO

[redacted]

Dedication

This work is dedicated to my brothers, Tim and Casey, and my parents, Mary Ann and Paul, for instilling creativity and encouraging my curiosity during my childhood in the woods of Maine.

Acknowledgements

First, I would like to thank Jayanta Debnath, my graduate advisor, for allowing me to perform my thesis research in his laboratory. When I started my thesis work in Jay's lab in 2006, the lab was less than a year old and I will forever be grateful for his confidence in me as a scientist, even as he was just beginning his lab, and for creating an atmosphere where I always felt comfortable in pursuing my own ideas.

Second, I would like to thank my thesis advisors Gerard Evan and William Weiss for their time, support, and their invaluable suggestions on how to improve my projects. I would also like to thank Diane Barber for her support and inspiration as a fellow woman scientist. I have the utmost respect for each of them for their enthusiasm and time they commit towards teaching and training young scientists.

Next, I would like to thank the members of the Debnath Laboratory. Thanks to the incredibly hard work of Chris Fung and Eduardo Salas the lab always ran smoothly making all of our work profoundly easier. A special thanks goes to Srirupa Roy and Candia Kenific who performed the metabolic flux and migration assays presented here. I would like to thank Lyndsay Murrow, my benchmate, for her time reading and editing my manuscripts and as my fellow foodie for introducing me to unbelievable new restaurants and delicious recipes. Lastly, I would like to thank Nan Chen. In lab Nan was always excited to discuss our current projects and even listen to my half-reasoned ideas. She always took

an honest, critical look at my research and the work I present here is much improved because of her thoughtful advice. Outside of lab she has become one of my best friends and I thank her for all of her support and always making me laugh with her fantastic, dry sense of humor.

Finally, I would like to thank Silas Laudon and my family. I would like to convey my deepest thanks to Silas for taking a huge chance and moving with me to San Francisco. Without his unconditional support, patience, and ability to always make me laugh this would have been a much more difficult pursuit. I would like to thank my brothers, Tim and Casey, for always inspiring me to be creative-I am a much better scientist for it. Lastly, thank you to my parents, Mary Ann and Paul for instilling in me a strong sense of commitment and hard work and always supporting and encouraging me in my pursuits.

Contributions to presented work

Statement from Dr. Jayanta Debnath:

"I directed and supervised the work in this dissertation. Rebecca Lock completed ninety five percent of the work included. This dissertation is an original contribution to scientific knowledge and meets the standard for a doctoral dissertation in the Biomedical Sciences Program at the University of California, San Francisco."

The contents of the Introduction are modified and reproduced from the following publications:

1. Lock, R., and J. Debnath. 2008. Extracellular matrix regulation of autophagy. *Curr Opin Cell Biol*. 20:583-8.

2. Lock, R., S. Roy, C.M. Kenific, J.S. Su, E. Salas, S.M. Ronen, and J. Debnath. 2011. Autophagy facilitates glycolysis during Ras-mediated oncogenic transformation. *Mol Biol Cell*. 22:165-78.

The contents of Chapter 1 are reproduced from the following publication:

1. Lock, R., S. Roy, C.M. Kenific, J.S. Su, E. Salas, S.M. Ronen, and J. Debnath. 2011. Autophagy facilitates glycolysis during Ras-mediated oncogenic transformation. *Mol Biol Cell*. 22:165-78.

The contents of the Discussion are modified and reproduced from the following publications:

1. Lock, R., S. Roy, C.M. Kenific, J.S. Su, E. Salas, S.M. Ronen, and J. Debnath. 2011. Autophagy facilitates glycolysis during Ras-mediated oncogenic transformation. *Mol Biol Cell*. 22:165-78.

2. Lock, R., and J. Debnath. 2011. Ras, autophagy and glycolysis. *Cell Cycle*. 10:1516-7.

Abstract

Novel functions for autophagy during Ras transformation

by

Rebecca Lock

Autophagy is a highly regulated catabolic process that degrades cytosolic organelles and macromolecules. Deregulation of the autophagic process has been linked to the development of several pathologies, including cancer, where it is associated with both pro- and anti-tumor functions. Although multiple studies have provided mechanistic insight into how autophagy suppresses tumorigenesis, the mechanisms explaining a pro-tumor role for autophagy have been limited to its capacity to promote tumor cell viability in response to stress. We hypothesized that autophagy contributes to additional cellular processes that support oncogenic transformation, and here we identify previously unrecognized pro-tumor functions for autophagy in the context of oncogenic Ras.

Using autophagy deficient cells, generated through genetic deletion or RNAi-mediated depletion of critical autophagy genes, we have identified a unique function for autophagy in supporting Ras-mediated anchorage-independent growth and proliferation. Furthermore, in the context of constitutively active Ras autophagy facilitates an enhanced rate of glycolysis, which supports robust anchorage-independent growth. Using a three-dimensional epithelial culture model, we demonstrate a requirement for autophagy in facilitating tumor cell

invasion and motility in Ras transformed cells. This reduction in invasive capacity correlates with a partial restoration in cell-cell junctional integrity and polarized secretion of basement membrane proteins. In addition, autophagy supports Ras-driven mesenchymal differentiation and the production of multiple secreted factors required for cell migration and invasion. Overall, these data reveal multiple tumor-promoting functions for autophagy during Ras transformation. Based on our findings we propose that in addition to its widely established function in promoting tumor cell survival, autophagy facilitates a larger repertoire of pro-tumor activities that support cancer progression and metastasis.

Table of Contents

List of Figures

Introduction

Macroautophagy (hereafter referred to as autophagy) is a tightly regulated catabolic process that degrades long-lived cytosolic proteins and organelles. The process is initiated by the formation of a double membrane structure termed a phagophore or isolation membrane. The isolation membrane then expands, engulfing cytosolic constituents and eventually fuses to form an intact double membrane vesicle called an autophagosome. The final step in the process is the delivery and fusion of the autophagosome with the lysomal compartment resulting in the degradation of the enclosed cargo as well as the inner autophagosomal membrane (Figure 1) (Levine and Klionsky, 2004; Mizushima, 2007; Ohsumi, 2001). The autophagic process is controlled by a large set of genes that are highly conserved from yeast to humans, termed autophagy genes (ATGs), and include genes that mediate two ubiquitin-like reactions that promote the expansion of the isolation membrane (Figure 1). The first reaction involves the conjugation of Atg12 to Atg5 and the second covalently links LC3 (the mammalian homologue of yeast Atg8) to a lipid, phosphatidylethanolamine (PE). Both reactions are catalyzed by the same E1 like enzyme, Atg7 (Ohsumi, 2001). Importantly, genetic deletion of *Atg5*, *Atg7*, *Atg3*, or *Atg12* (unpublished data) is sufficient to prevent conjugation of LC3 to PE and the formation of a mature autophagosome. Thus, targeting any of these genes individually by RNA interference or through genetic deletion is sufficient to inhibit the autophagic process.

Autophagy mediates cellular homeostasis and promotes survival in response to environmental stress

In nutrient replete conditions a baseline level of autophagy, or basal autophagy, provides a necessary housekeeping function by sequestering and degrading long-lived proteins and damage organelles (Baehrecke, 2005). This homeostatic role for autophagy is most prominently revealed in mice with tissue specific deletions of autophagy genes in the nervous system and liver. Mice deficient in either *Atg5* or *Atg7* in the central nervous system succumb to spontaneous neurodegeneration and genetic deletion of *Atg7* in hepatocytes results in cellular swelling and hepatomegaly. At the cellular level, autophagy deficient neurons and hepatocytes display an accumulation in ubiquitin-positive protein aggregates and deformed mitochondria, indicating basal autophagy is critical for the clearance of cytosolic proteins and in maintaining proper organelle turnover (Hara et al., 2006; Komatsu et al., 2006; Komatsu et al., 2005).

Exposure to a wide range of environmental stressors, such as, nutrient deprivation, growth factor withdrawal, ischemia, and extracellular matrix detachment, stimulates an increase in autophagy levels (Baehrecke, 2005; Levine and Klionsky, 2004). The increase in autophagy that occurs in response to environmental stress is regulated by signaling pathways that sense nutrient, growth factor, and energy levels and converge on the mTORC1 complex, the master regulator of cell growth. mTORC1 associates with and negatively regulates the activity of the ULK1-Atg13-FIP200 complex, which is involved in the earliest steps of autophagy induction (Jung et al., 2010). Thus, through

mTORC1 the major energy and growth sensing signaling pathways are linked to the regulation of autophagy, the major catabolic process within the cell.

Numerous studies have revealed that inhibition of autophagy in cells exposed to environmental stress results in reduced cell viability, highlighting its importance as a major stress response pathway (Degenhardt et al., 2006; Lum et al., 2005a; Onodera and Ohsumi, 2005). It is thought that the increase in autophagy that occurs in response to environmental stress promotes short-term cellular viability through the repurposing of autophagic degradation products into metabolic pathways in the cell. In fact, the decreased viability of autophagy deficient cells in response to stress can be partially rescued by the addition of exogenous metabolites, suggesting autophagy may in fact boost metabolic programs during times of stress (Lum et al., 2005a; Qu et al., 2007). Although these results suggest the by-products from autophagic degradation are important in supporting certain metabolic functions, there is no direct evidence this occurs or knowledge of the specific metabolic pathways that are affected by alterations in autophagy levels.

Role of autophagy during tumorigenesis

Autophagy and tumor suppression

Due to its critical role in maintaining cellular homeostasis and promoting viability in response to stress it is not surprising that alterations in autophagy have been associated with several human diseases, including cancer where it has both tumor suppressive and tumor promoting functions (Chen and Debnath,

2010). Autophagy was initially proposed to function as a tumor suppressor based on genetic studies of *BECN1*, the mammalian orthologue of yeast *ATG6*. *BECN1* is located in a tumor susceptibility locus that is monoallelically deleted in a high percentage of human epithelial cancers (Aita et al., 1999; Liang et al., 1999). Furthermore, mice lacking a single copy of *Becn1* (*Becn1+/-*) display increased rates of spontaneous tumor development (Aita et al., 1999; Liang et al., 1999; Qu et al., 2003; Yue et al., 2003). However, it was unclear from these initial studies whether the enhanced rate of spontaneous tumorigenesis in *Beclin+/-* mice was in fact the result of decreased autophagy as Beclin 1 also functions in a second protein complex involved in endocytosis (Itakura et al., 2008). More recent studies have confirmed a role for autophagy in tumor suppression through the finding that mice with systemic mosaic deletion of *Atg5* or hepatic-specific deletion of *Atg7* develop spontaneous liver tumors (Inami et al., 2011; Takamura et al., 2011).

In addition, based on the findings that several oncogenes and tumor suppressor genes have been shown to inhibit and activate autophagy, respectively, it has been speculated that autophagy levels might be reduced in tumor cells harboring these genetic lesions (Kondo et al., 2005). Specifically, components of the class I PI3K signaling pathway have been shown to inhibit autophagy and several tumor suppressors including PTEN, LKB1, and TSC1/2 have been shown to enhance autophagy (Arico et al., 2001; Kondo et al., 2005; Petiot et al., 2000). All the major regulators described above are thought either to restrict or enhance autophagy through their downstream effects on mTORC1

activity. Although these pathways have been shown to influence tumor growth and autophagy, there is no evidence that regulation of autophagy influences their oncogenic or tumor suppressive functions.

Multiple mechanisms have been uncovered that explain autophagy's function in tumor suppression. A large body of work from Eileen White and colleagues has indicated a role for autophagy in preventing genomic instability. *Beclin+/-* and *Atg5-/-* cells display increased levels of DNA damage and genomic instability following exposure to metabolic stress, and these cells display enhanced tumorigenicity in immunodeficient mice (Karantza-Wadsworth et al., 2007; Mathew et al., 2007). In support of a role for autophagy in maintaining genome integrity, hepatic adenomas that arise in *atg5* or *atg7* deficient tumors also stain positive for markers of genomic damage (Inami et al., 2011; Takamura et al., 2011). These studies raise the hypothesis that a decreased rate of autophagy could enhance DNA damage particularly in cells exposed to environmental stress resulting in an increased mutation rate. One potential mechanism contributing to the increase in DNA damage that occurs in autophagy deficient cells is the accumulation of p62/SQSTM1, an autophagy specific substrate. Overexpression of p62 in *Beclin+/-* or *Atg5* deficient cells increases the levels of reactive oxygen species, enhances genome damage, and results in enhanced xenograft tumor growth (Mathew et al., 2009). Furthermore, the genetic deletion of p62 in combination with *Atg7* deletion in the liver reduces the growth of liver adenomas (Takamura et al., 2011).

In addition to protecting cells against DNA damage, autophagy facilitates oncogene-induced senescence suggesting an alternative mechanism of autophagy-mediated tumor suppression. In response to oncogene-induced senescence the transcription of several autophagy genes is enhanced and this correlates with an increase in autophagy levels. Suppression of autophagy through the RNAi-mediated depletion of autophagy genes limits the induction of senescence in response to acute oncogenic Ras activation and suppresses the production of senescence-associated cytokines (Young et al., 2009).

Autophagy as a pro-tumorigenic factor

In contrast to the above described role for autophagy in tumor suppression, growing evidence indicates autophagy may promote tumorigenesis by supporting the viability of tumor cells that encounter environmental stress and in response to chemotherapeutic treatments (Hippert et al., 2006). As a tumor expands and outgrows its supporting vasculature, many cells within the tumor are deprived of nutrients and oxygen. Enhanced levels of autophagy have been observed in poorly vascularized tumor regions and loss of autophagy is associated with increased levels of necrosis when apoptosis is inhibited (Degenhardt et al., 2006). Furthermore, several studies indicate that autophagy is activated and promotes cell survival in both normal and cancer cells in response to glucose starvation and ischemia (Degenhardt et al., 2006; DiPaola et al., 2008; Lum et al., 2005b).

In addition, our previous studies indicate a pro-survival function for autophagy during extracellular matrix (ECM). We have shown that autophagy is increased in cells detached from extracellular matrix and in cells located in the luminal space of 3-dimensional acini, which lack contact with the basement membrane (Debnath et al., 2002; Fung et al., 2008). Inhibiting autophagy enhances apoptosis and increases the rate of luminal clearance indicating autophagy protects cells from detachment-induced cell death (anoikis) (Frisch and Francis, 1994; Fung *et al.*, 2008). Since the ability to overcome anoikis is viewed as a critical hurdle in tumor development, one can hypothesize that detachment-induced autophagy enables the viability and fitness of tumor cells deprived of contact with extracellular matrix.

Several chemotherapeutic agents have been shown to activate autophagy, including tamoxifen, γ-irradiation, and rapamycin and induction of autophagy in response to chemotherapeutic treatment likely serves as an adaptive response to aid tumor cell survival. Combined treatment of chemotherapeutics and autophagy inhibitors (typically through administration of chloroquine, a lysosomal inhibitor) has been tested in multiple tumor types and often results in enhanced tumor cell death (Chen and Debnath, 2010).

Using constitutive Ras activation as system to uncover novel functions for autophagy

The studies summarized above indicate tumor cells are able to enhance and utilize the autophagic process to respond to environmental stress and

chemotherapeutic agents. However, prior to the work presented here little was known about the mechanisms mediating autophagy's cell intrinsic pro-tumor functions beyond its role in promoting cell survival in response to stress. In particular it was unknown how autophagy, a critical homeostatic pathway proposed to sustain core metabolic functions, contributes to oncogenic transformation. We speculated that autophagy might have additional functions in the context of a strong oncogenic insult as these mutations impose additional cellular stress and coordinately alter diverse cellular programs that support transformation and decided to examine this hypothesis in the context of oncogenic Ras.

The Ras proteins are members of a family of small GTPases critical for mediating cellular responses following activation by upstream extracellular signals, such as growth factors. Oncogenic mutations in Ras, which result in constitutive activation and loss in sensitivity to upstream cues, are found in approximately 30% of human cancers and are highly prevalent in several carcinomas, including lung, pancreas, and colon (Schubbert et al., 2007). Notably, oncogenic Ras drives diverse cellular programs-proliferation, cell survival, migration, invasion and alterations in differentiation-that support tumor initiation as well as progression and metastasis.

Recent studies have begun to highlight the importance of the metabolic switch to aerobic glycolysis (termed the "Warburg effect") that takes place in cancer cells as a critical driver of tumorigenesis (Vander Heiden *et al.*, 2009). Oncogenic Ras has been found to promote glycolysis through transcriptional

alterations in multiple metabolic genes, and this switch to an enhanced glycolytic phenotype is critical for its capacity to support growth and proliferation during oncogenic transformation (Chiaradonna *et al.*, 2006). Two proteins that mitigate cell stress, Oct1 and Hsf1, have been demonstrated to facilitate tumorigenesis through the enhancement of glucose metabolism (Dai *et al.*, 2007; Shakya *et al.*, 2009). These studies broach important interconnections between stress pathways and cancer cell metabolism. Surprisingly, although autophagy is similarly viewed as a salvage mechanism that affords basic components to sustain core metabolic functions during starvation or stress, the relationship between autophagy and metabolism was previously unclear.

The studies described begin to address functions for autophagy during tumor initiation and primary tumor development. However, few studies have addressed a role for autophagy during tumor progression and mounting evidence suggests a minimal level of autophagy is essential for metastasis. Loss of the second allele of *Becn1* is not observed in mouse tumors, which strikingly resembles the haploinsufficiency found in human patients (Qu et al., 2003). In addition, although deletion of *Atg7* or *Atg5* in the liver results in spontaneous tumorigenesis, the hepatic adenomas that arise fail to exhibit any invasive behavior or distant metastasis (Inami et al., 2011; Takamura et al., 2011). Furthermore, deletion of *FIP200,* a gene involved in the initial steps of autophagosome induction, in a polyoma middle T (MMTV-PyMT) driven transgenic breast cancer model suppresses lung metastasis raising the intriguing possibility that autophagy impacts additional cell biological processes that

influence the later stages of tumor progression (Wei et al., 2011). In addition to supporting changes in metabolism, oncogenic Ras has been shown to drive cellular programs, including invasion, migration and mesenchymal differentiation that are associated with enhanced tumor progression and metastasis (Shin et al., 2010; Thiery, 2003).

Here, we delineate a requirement for autophagy in facilitating diverse pro-tumor functions downstream of oncogenic Ras. We find that in cells ectopically expressing oncogenic H-Ras as well as human cancer cell lines harboring endogenous K-Ras mutations, autophagy is induced following extracellular matrix detachment. Inhibiting autophagy due to the genetic deletion or RNAi-mediated depletion of multiple autophagy genes attenuates Ras-mediated adhesion-independent transformation and proliferation, and also reduces glycolytic capacity. Furthermore, in contrast to autophagy competent cells, both proliferation and transformation in autophagy deficient cells expressing oncogenic Ras are insensitive to reductions in glucose availability**.**

Using a three-dimensional culture system, we demonstrate that autophagy inhibition restricts Ras-driven cell invasion and restores several aspects of normal epithelial architecture, including the polarized deposition of basement membrane and cell-cell junctional integrity. Autophagy inhibition in oncogenic Ras expressing cells significantly diminishes *in vitro* cell motility and reverses certain aspects of Ras-driven mesenchymal differentiation. We find that autophagy facilitates the production of multiple secreted factors that promote cell migration and invasion during oncogenic Ras transformation, including

interleukin-6, matrix metalloproteinase 2 and Wnt5a. Overall, these results point to a broader role for autophagy in supporting Ras-driven anchorage-independent growth, glycolysis, and invasion suggesting unique mechanisms by which autophagy may promote Ras-driven tumorigenesis.

References

Aita, V.M., X.H. Liang, V.V. Murty, D.L. Pincus, W. Yu, E. Cayanis, S. Kalachikov, T.C. Gilliam, and B. Levine. 1999. Cloning and genomic organization of beclin 1, a candidate tumor suppressor gene on chromosome 17q21. *Genomics*. 59:59-65.

Arico, S., A. Petiot, C. Bauvy, P.F. Dubbelhuis, A.J. Meijer, P. Codogno, and E. Ogier-Denis. 2001. The tumor suppressor PTEN positively regulates macroautophagy by inhibiting the phosphatidylinositol 3-kinase/protein kinase B pathway. *J Biol Chem*. 276:35243-6.

Baehrecke, E.H. 2005. Autophagy: dual roles in life and death? *Nat Rev Mol Cell Biol*. 6:505-10.

Chen, N., and J. Debnath. 2010. Autophagy and tumorigenesis. *FEBS Lett*. 584:1427-35.

Chiaradonna, F., E. Sacco, R. Manzoni, M. Giorgio, M. Vanoni, and L. Alberghina. 2006. Ras-dependent carbon metabolism and transformation in mouse fibroblasts. *Oncogene*. 25:5391-404.

Dai, C., L. Whitesell, A.B. Rogers, and S. Lindquist. 2007. Heat shock factor 1 is a powerful multifaceted modifier of carcinogenesis. *Cell*. 130:1005-18.

Debnath, J., K.R. Mills, N.L. Collins, M.J. Reginato, S.K. Muthuswamy, and J.S. Brugge. 2002. The role of apoptosis in creating and maintaining luminal space within normal and oncogene-expressing mammary acini. *Cell*. 111:29-40.

Degenhardt, K., R. Mathew, B. Beaudoin, K. Bray, D. Anderson, G. Chen, C. Mukherjee, Y. Shi, C. Gelinas, Y. Fan, D.A. Nelson, S. Jin, and E. White. 2006. Autophagy promotes tumor cell survival and restricts necrosis, inflammation, and tumorigenesis. *Cancer Cell*. 10:51-64.

DiPaola, R.S., D. Dvorzhinski, A. Thalasila, V. Garikapaty, D. Doram, M. May, K. Bray, R. Mathew, B. Beaudoin, C. Karp, M. Stein, D.J. Foran, and E. White. 2008. Therapeutic starvation and autophagy in prostate cancer: a new paradigm for targeting metabolism in cancer therapy. *Prostate*. 68:1743-52.

Frisch, S.M., and H. Francis. 1994. Disruption of epithelial cell-matrix interactions induces apoptosis. *J Cell Biol*. 124:619-26.

Fung, C., R. Lock, S. Gao, E. Salas, and J. Debnath. 2008. Induction of Autophagy during Extracellular Matrix Detachment Promotes Cell Survival. *Mol Biol Cell*. 19:797-806.

Hara, T., K. Nakamura, M. Matsui, A. Yamamoto, Y. Nakahara, R. Suzuki-Migishima, M. Yokoyama, K. Mishima, I. Saito, H. Okano, and N. Mizushima. 2006. Suppression of basal autophagy in neural cells causes neurodegenerative disease in mice. *Nature*. 441:885-9.

Hippert, M.M., S. O'Toole P, and A. Thorburn. 2006. Autophagy in cancer: good, bad, or both? *Cancer Res*. 66:9349-51.

Inami, Y., S. Waguri, A. Sakamoto, T. Kouno, K. Nakada, O. Hino, S. Watanabe, J. Ando, M. Iwadate, M. Yamamoto, M.S. Lee, K. Tanaka, and M. Komatsu. 2011. Persistent activation of Nrf2 through p62 in hepatocellular carcinoma cells. *J Cell Biol*. 193:275-84.

Itakura, E., C. Kishi, K. Inoue, and N. Mizushima. 2008. Beclin 1 forms two distinct phosphatidylinositol 3-kinase complexes with mammalian Atg14 and UVRAG. *Mol Biol Cell*. 19:5360-72.

Jung, C.H., S.H. Ro, J. Cao, N.M. Otto, and D.H. Kim. 2010. mTOR regulation of autophagy. *FEBS Lett*. 584:1287-95.

Karantza-Wadsworth, V., S. Patel, O. Kravchuk, G. Chen, R. Mathew, S. Jin, and E. White. 2007. Autophagy mitigates metabolic stress and genome damage in mammary tumorigenesis. *Genes Dev*. 21:1621-35.

Komatsu, M., S. Waguri, T. Chiba, S. Murata, J. Iwata, I. Tanida, T. Ueno, M. Koike, Y. Uchiyama, E. Kominami, and K. Tanaka. 2006. Loss of autophagy in the central nervous system causes neurodegeneration in mice. *Nature*. 441:880-4.

Komatsu, M., S. Waguri, T. Ueno, J. Iwata, S. Murata, I. Tanida, J. Ezaki, N. Mizushima, Y. Ohsumi, Y. Uchiyama, E. Kominami, K. Tanaka, and T. Chiba. 2005. Impairment of starvation-induced and constitutive autophagy in Atg7-deficient mice. *J Cell Biol*. 169:425-34.

Kondo, Y., T. Kanzawa, R. Sawaya, and S. Kondo. 2005. The role of autophagy in cancer development and response to therapy. *Nat Rev Cancer*. 5:726-34.

Levine, B., and D.J. Klionsky. 2004. Development by self-digestion: molecular mechanisms and biological functions of autophagy. *Dev Cell*. 6:463-77.

Liang, X.H., S. Jackson, M. Seaman, K. Brown, B. Kempkes, H. Hibshoosh, and B. Levine. 1999. Induction of autophagy and inhibition of tumorigenesis by beclin 1. *Nature*. 402:672-6.

Lum, J.J., D.E. Bauer, M. Kong, M.H. Harris, C. Li, T. Lindsten, and C.B. Thompson. 2005a. Growth factor regulation of autophagy and cell survival in the absence of apoptosis. *Cell*. 120:237-48.

Lum, J.J., R.J. DeBerardinis, and C.B. Thompson. 2005b. Autophagy in metazoans: cell survival in the land of plenty. *Nat Rev Mol Cell Biol*. 6:439-48.

Mathew, R., C.M. Karp, B. Beaudoin, N. Vuong, G. Chen, H.Y. Chen, K. Bray, A. Reddy, G. Bhanot, C. Gelinas, R.S. Dipaola, V. Karantza-Wadsworth, and E. White. 2009. Autophagy suppresses tumorigenesis through elimination of p62. *Cell*. 137:1062-75.

Mathew, R., S. Kongara, B. Beaudoin, C.M. Karp, K. Bray, K. Degenhardt, G. Chen, S. Jin, and E. White. 2007. Autophagy suppresses tumor progression by limiting chromosomal instability. *Genes Dev*. 21:1367-81.

Mizushima, N. 2007. Autophagy: process and function. *Genes Dev*. 21:2861-73.

Ohsumi, Y. 2001. Molecular dissection of autophagy: two ubiquitin-like systems. *Nat Rev Mol Cell Biol*. 2:211-6.

Onodera, J., and Y. Ohsumi. 2005. Autophagy is required for maintenance of amino acid levels and protein synthesis under nitrogen starvation. *J Biol Chem*. 280:31582-6.

Petiot, A., E. Ogier-Denis, E.F. Blommaart, A.J. Meijer, and P. Codogno. 2000. Distinct classes of phosphatidylinositol 3'-kinases are involved in signaling pathways that control macroautophagy in HT-29 cells. *J Biol Chem*. 275:992-8.

Qu, X., J. Yu, G. Bhagat, N. Furuya, H. Hibshoosh, A. Troxel, J. Rosen, E.L. Eskelinen, N. Mizushima, Y. Ohsumi, G. Cattoretti, and B. Levine. 2003. Promotion of tumorigenesis by heterozygous disruption of the beclin 1 autophagy gene. *J Clin Invest*. 112:1809-20.

Qu, X., Z. Zou, Q. Sun, K. Luby-Phelps, P. Cheng, R.N. Hogan, C. Gilpin, and B. Levine. 2007. Autophagy gene-dependent clearance of apoptotic cells during embryonic development. *Cell*. 128:931-46.

Schubbert, S., K. Shannon, and G. Bollag. 2007. Hyperactive Ras in developmental disorders and cancer. *Nat Rev Cancer*. 7:295-308.

Shakya, A., R. Cooksey, J.E. Cox, V. Wang, D.A. McClain, and D. Tantin. 2009. Oct1 loss of function induces a coordinate metabolic shift that opposes tumorigenicity. *Nat Cell Biol*. 11:320-7.

Shin, S., C.A. Dimitri, S.O. Yoon, W. Dowdle, and J. Blenis. 2010. ERK2 but not ERK1 induces epithelial-to-mesenchymal transformation via DEF motif-dependent signaling events. *Mol Cell*. 38:114-27.

Takamura, A., M. Komatsu, T. Hara, A. Sakamoto, C. Kishi, S. Waguri, Y. Eishi, O. Hino, K. Tanaka, and N. Mizushima. 2011. Autophagy-deficient mice develop multiple liver tumors. *Genes Dev*. 25:795-800.

Thiery, J.P. 2003. Epithelial-mesenchymal transitions in development and pathologies. *Curr Opin Cell Biol*. 15:740-6.

Vander Heiden, M.G., L.C. Cantley, and C.B. Thompson. 2009. Understanding the Warburg effect: the metabolic requirements of cell proliferation. *Science*. 324:1029-33.

Wei, H., S. Wei, B. Gan, X. Peng, W. Zou, and J.L. Guan. 2011. Suppression of autophagy by FIP200 deletion inhibits mammary tumorigenesis. *Genes Dev*. 25:1510-27.

Young, A.R., M. Narita, M. Ferreira, K. Kirschner, M. Sadaie, J.F. Darot, S. Tavare, S. Arakawa, S. Shimizu, F.M. Watt, and M. Narita. 2009. Autophagy mediates the mitotic senescence transition. *Genes Dev*. 23:798-803.

Yue, Z., S. Jin, C. Yang, A.J. Levine, and N. Heintz. 2003. Beclin 1, an autophagy gene essential for early embryonic development, is a haploinsufficient tumor suppressor. *Proc Natl Acad Sci U S A*. 100:15077-82.

FIGURE LEGEND

Figure 1. Overview of the autophagic process.

The autophagic process begins with the formation of a double membrane structure termed the “isolation membrane”. The autophagic membrane then expands and eventually fuses resulting in the engulfment of cytosolic proteins and organells. Autophagic vesicles then fuse with the lysosome where the contents of the autophagosome and the inner membrane are degraded. The expansion of the isolation membrane requires two ubiquitin-like conjugation systems, which are highly conserved from yeast to humans.

Figure 1

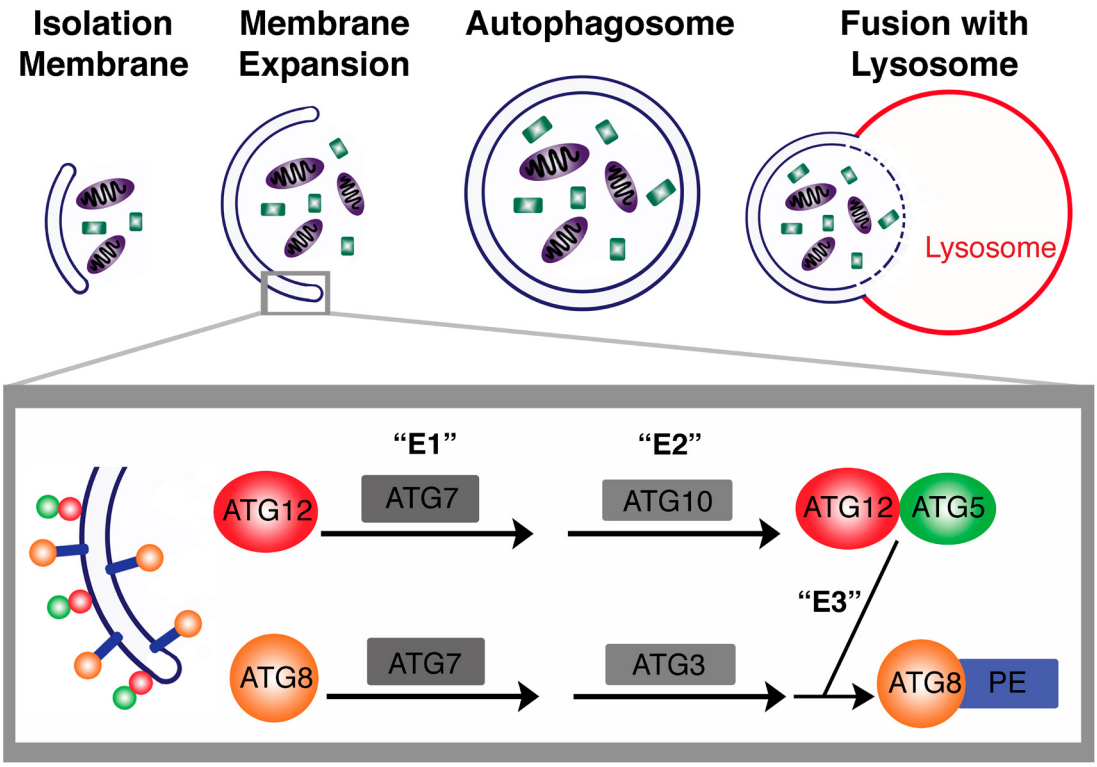
Isolation Membrane
Membrane Expansion
Autophagosome
Fusion with Lysosome
Lysosome
"E1"
"E2"
ATG12
ATG7
ATG10
ATG12
ATG5
"E3"
ATG8
ATG7
ATG3
ATG8
PE

Chapter 1

Autophagy facilitates glycolysis during Ras-mediated oncogenic transformation

Oncogenic Ras does not suppress ECM detachment-induced autophagy.

Several studies demonstrate that constitutive activation of Ras suppresses autophagy induction while others indicate that Ras/MAPK pathway activation can enhance autophagy during nutrient starvation (Berry and Baehrecke, 2007; Furuta et al., 2004; Pattingre et al., 2003). Given these paradoxical results, we first sought to clarify how oncogenic Ras modulates autophagy upon loss of cell-matrix contact, a cardinal stress during adhesion-independent transformation. We generated stable pools of MCF10A human mammary epithelial cells expressing oncogenic H-Ras (H-Ras^{V12}) as well as control cells expressing an empty vector (BABE) (Figure 2-1A, left). We then tested autophagy levels following substratum detachment by plating cells on poly-HEMA coated plates to prevent cell-matrix adhesion. As previously reported, in BABE control cells, we observed an increase in the lysosomal turnover of phosphotidylethanolamine (PE) lipidated LC3/ATG8 (LC3-II), commonly termed autophagic flux, following matrix detachment. (Figure 1A, right). (Fung *et al.*, 2008). Furthermore, MCF10A cells expressing H-Ras^{V12} displayed an increase in LC3-II induction and lysosomal turnover following matrix detachment. (Figure 2-1A, right). To further verify autophagosome induction in H-Ras^{V12} transformed MCF10A cells, we stably expressed GFP-LC3 in H-Ras^{V12} and vector control cells, and assessed autophagosome formation (punctate GFP-LC3) using fluorescence microscopy. Following detachment, we observed robust induction of GFP-LC3 puncta in both empty vector and RasV12 expressing MCF10A cells in comparison to attached controls (Figure 2-1B). Because detached epithelial cells exhibit extensive

clustering, we were unable to precisely enumerate puncta per cell; nonetheless, we consistently observed similar levels of punctate GFP-LC3 in H-Ras^{V12} transformed MCF10A compared to BABE controls.

We next evaluated the effects of H-Ras^{V12} on detachment-induced autophagy in immortalized mouse embryonic fibroblasts (MEFs) (Figure 2-1C). Remarkably, both H-Ras^{V12} and control fibroblasts exhibited a high baseline level of LC3-II when grown in attached conditions; upon suspension, LC3-II levels decreased dramatically in the H-Ras^{V12} expressing MEFs and to a lesser extent, in vector controls during suspension. Upon addition of E/P, LC3-II levels increased following detachment in both cell types, indicating that both control and RasV12 fibroblasts exhibit LC3-II turnover during matrix detachment (Figure 2-1C, center). To more conclusively validate these results, we assessed the degradation of p62 (SQSTM), a scaffold protein specifically degraded by autophagy, following detachment (Figure 2-1C, right). In both vector control and H-Ras^{V12} transformed MEFs, we observed significantly reduced p62 levels following 24h of suspension. In contrast, p62 levels remained elevated in both control and H-Ras^{V12} transformed *atg5-/-* MEFs, supporting that the degradation of p62 during substratum detachment requires an intact autophagy pathway.

To extend these results, we evaluated detachment-induced autophagy in epithelial cancer cell lines that naturally harbor oncogenic Ras mutations. In three different carcinoma lines that possess activating KRas mutations, MDA-MB-231 breast carcinoma cells, HCT116 colon carcinoma cells, and PANC-1 pancreatic carcinoma cells, both LC3-II induction and turnover increased upon

substratum detachment (Figure 2-1D). In parallel, we examined autophagosome formation (GFP-LC3 puncta) following suspension. Similar to MCF 10A cells, all three carcinoma cell lines displayed an increase in GFP-LC3 puncta following 24 h matrix detachment (Figure 2-1E). Altogether, our results support the robust induction of autophagy in both epithelial and fibroblast cells expressing H-Ras^{V12} as well as in cancer cell lines harboring activating KRas mutations following matrix detachment; hence, Ras activation does not suppress autophagy during ECM detachment.

We next assessed whether constitutive Ras activation was sufficient to maintain activation of downstream signaling pathways following ECM detachment. We first tested if oncogenic activation of Ras sustained activation of the MAPK pathway by examining levels of phosphorylated ERK. Both MCF10A cells and mouse fibroblasts (expressing empty vector) displayed a reduction in phosphorylated ERK1/2 levels following 24h ECM detachment. In contrast, the phosphorylation of ERK1/2 remained elevated in both H-Ras^{V12} transformed MCF10As and MEFs during ECM detachment (Figure 2-2A-B). ERK1/2 phosphorylation was similarly maintained in MDA-MB-231 cells and HCT 116; remarkably, in PANC-1 cells ERK1/2 phosphorylation was increased in matrix-detached cells when compared to attached controls. (Figure 2-2C).

Sustained activation of mTORC1, the archetypal negative regulator of autophagy, has been proposed to mediate autophagy inhibition downstream of oncogenic Ras (Furuta *et al.*, 2004; Maiuri *et al.*, 2009). Thus, we measured mTORC1 activation in H-Ras^{V12} transformed cells following ECM detachment by

assessing the phosphorylation status of ribosomal protein S6, a downstream mTOR target. Upon detachment, S6 phosphorylation decreased sharply in control MCF10A cells, supporting reduced activation of the mTORC1 pathway. Notably, S6 phosphorylation was partially decreased in H-Ras^{V12}-transformed cells following 24h suspension (Figure 2-2D). In fibroblasts, both control and H-Ras^{V12}-transformed MCF10A cells demonstrated decreased levels of phosphorylated S6 during suspension (Figure 2-2E). Similarly, in KRas mutant cancer cells, S6 phosphorylation was reduced following ECM detachment (Figure 2-2F). Because we observed a partial decrease in S6 phosphorylation during ECM detachment, particularly in H-Ras^{V12} MCF10A cells, we treated suspended cells with rapamycin to assess whether robust inhibition of mTORC1 was able to further enhance detachment-induced autophagy. Upon rapamycin treatment, we were unable to detect S6 phosphorylation in H-Ras^{V12} MCF10A cells following 24h suspension; however, we did not observe any further increase in LC3-II induction or turnover upon rapamycin treatment (Figure 2-2G). This result supports that autophagy can be potently induced in H-Ras^{V12} MCF10A cells following extracellular matrix detachment without complete suppression of mTORC1 activity.

Reduced H-Ras^{V12} driven soft agar transformation in autophagy deficient MEFs.

Because autophagy was robustly induced in Ras-transformed cells upon loss of cell-matrix contact, we next interrogated the functional contribution of

autophagy to H-Ras^{V12} driven anchorage-independent growth. For these experiments, we initially tested how the genetic deletion of three critical autophagy regulators, *atg5, atg7,* and *atg3,* individually influence anchorage-independent transformation by oncogenic Ras. All three proteins are essential components of the ubiquitin-like conjugation pathways that control the early step of autophagosome formation; thus, the genetic deletion of any of these ATGs is sufficient to completely inhibit autophagy (Komatsu et al., 2005; Kuma et al., 2004; Ohsumi, 2001; Sou et al., 2008). We first compared the ability of *atg5+/+* and *atg5-/-* MEFs transformed with H-Ras^{V12} to form colonies in soft agar. H-Ras^{V12} transformed *atg5-/-* MEFs displayed an approximate 4-fold decrease in colony formation compared to wild-type autophagy-competent controls (Figure 2-3A); importantly, both *atg5+/+* and *atg5-/-* cells expressed equivalent levels of H-Ras^{V12} (Figure 2-1C, left).

To verify that these differences directly resulted from autophagy inhibition upon ATG5 deletion, we constituted *atg5-/-* cells with either wild-type mouse ATG5 or ATG5 K130R, a lysine mutant unable to conjugate to ATG12 and therefore unable to induce autophagy. Rescue of H-Ras^{V12} *atg5-/-* MEFs with wild-type ATG5 restored ATG5-ATG12 complex levels whereas expression of ATG5 K130R did not (Figure 2-3B). This rescue of H-Ras^{V12} *atg5-/-* MEFs with wild-type ATG5 restored autophagy induction, indicated by the production of LC3-II in attached conditions and following suspension. In contrast, both H-Ras^{V12} *atg5-/-* MEFs, as well as those expressing ATG5 K130R, were unable to induce autophagy during suspension (Figure 2-3B). Furthermore, the rescue of

H-Ras^{V12} transformed *atg5-/-* MEFs with wild-type ATG5, but not ATG5 K130R, was able to restore soft agar colony formation (Figure 2-3C), further supporting that autophagy competence functionally contributes to Ras-driven transformation. Similarly, soft agar transformation mediated by H-Ras^{V12} was also abrogated in *atg7-/-* and *atg3-/-* cells. Colony formation was reduced almost four-fold in H-Ras^{V12} *atg7-/-* MEFs compared to wild-type controls (Figure 2-3D), and H-Ras^{V12} *atg3-/-* MEFs displayed the most profound defect in soft agar colony formation, almost 8 fold, compared to wild-type controls (Figure 2-3E). These results support that the elimination of autophagy in mouse fibroblasts, achieved via the genetic deletion of multiple ATGs, potently inhibits the transformation potential of H-Ras^{V12}.

Reduced soft agar transformation upon ATG knockdown in Ras-transformed epithelial cells.

We next determined if the acute reduction of autophagy in the context of preexisting oncogenic Ras activation was similarly able to inhibit adhesion-independent transformation. First, we stably expressed two independent shRNAs against ATG7 (shATG7-1 and shATG7-2) as well as a hairpin directed against ATG12 (shATG12-1) in MDA-MB-231 cells. Analysis of target protein levels by western blot revealed high level knockdown of ATG7 with both shATG7-1 and 2 and reduction of the ATG5-ATG12 complex in shATG12-1 expressing MDA-MB-231 cells (Figure 2-4A). Of these three hairpins, shATG7-2 gave the most robust reduction in autophagy; based on immunoblotting for LC3-II (data not shown).

MDA-MB-231 cells expressing this shRNA exhibited an approximately 50% decrease in both basal and detachment-induced autophagy (Figure 2-4B). Furthermore, the expression of all three of these shATGs in MDA-MB-231 cells resulted in a significant decrease in soft agar colony formation, ranging from approximately 50%-90% depending on the shRNA used (Figure 2-4C).

In parallel, we generated stable pools of H-Ras^{V12} MCF10A cells expressing shRNA against ATG7 (shATG7-2). These cells demonstrated potent ATG7 knockdown and decreased LC3-II in both attached and detached conditions (Figure 2-4D). Colony formation in H-Ras^{V12} MCF10A cultures expressing shATG7-2 was reduced by approximately 50% when compared to shCNT expressing cells (Figure 2-4E); suggesting ATG7 knockdown was sufficient to partially suppress H-Ras^{V12} induced soft agar growth in MCF10A cells. Hence, consistent with our data in ATG-deficient fibroblasts, epithelial cells with oncogenic Ras displayed a reduction in soft agar colony formation following RNAi-mediated knockdown of ATGs. Furthermore, it is important to note that although we were able to achieve high levels of ATG knockdown, such perturbations produced partial reductions in autophagic capacity, up to 50% of control. Nonetheless, such levels of autophagy reduction resulted in robust decreases in soft agar colony formation, pointing to a critical role for autophagy in Ras-mediated anchorage-independent transformation.

Effects of autophagy inhibition on detachment-induced apoptosis (anoikis) in Ras-transformed cells.

Because our previous work indicates that detachment-induced autophagy protects nontransformed MCF10A cells from anoikis, we hypothesized that autophagy may similarly promote the survival of Ras-transformed cells deprived of cell-matrix contact (Fung *et al.*, 2008). To test this prediction, H-Ras^{V12} *atg5+/+* and *atg5-/-* MEFs were either grown attached or suspended for 24-48h and protein lysates were immunoblotted for cleaved caspase-3. Although previous work indicates that fibroblasts do not undergo anoikis, we found that cleaved caspase-3 did indeed increase in H-Ras^{V12} autophagy-competent fibroblasts upon ECM detachment. Furthermore, compared to wild type controls, the levels of cleaved caspase-3 in H-Ras^{V12} *atg5-/-* MEFs following suspension were higher. This corroborates that autophagy deficiency leads to increased detachment-induced apoptosis in H-Ras^{V12}-transformed cells (Figure 2-5A).

Based on these results, we interrogated if the ectopic expression of the anti-apoptotic molecule Bcl-2 was sufficient to promote adhesion independent growth and survival in H-Ras^{V12} *atg5-/-* MEFs. To test this hypothesis, we generated H-Ras^{V12} *atg5+/+* and *atg5-/-* MEFs stably expressing Bcl-2 (Figure 2-5B). As Bcl-2 has previously been shown to suppress autophagy in certain cell types via its interaction with Beclin 1, we determined the effects of Bcl-2 expression on detachment-induced autophagy in H-Ras^{V12} MEFs, but did not identify any significant effects on LC3-II induction or turnover, or on p62 degradation during ECM detachment (Figure 2-5C) (Pattingre *et al.*, 2005). In

contrast, Bcl-2 potently reduced apoptosis in H-Ras^{V12}-transformed *atg5+/+* and *atg5-/-* cells following matrix detachment, as indicated by immunoblotting for cleaved caspase-3, (Figure 2-5D).

We next evaluated if Bcl-2 expression was sufficient to restore adhesion-independent transformation in H-Ras^{V12} *atg5-/-* MEFs. However, we continued to detect reduced levels of H-Ras^{V12} driven soft agar growth in Bcl-2-expressing autophagy-deficient cells when compared to wild-type counterparts (Figure 2-5E). These results indicate that autophagy inhibition in H-Ras^{V12} transformed cells can promote anoikis; however, protecting autophagy-deficient cells from apoptosis is not sufficient to restore adhesion-independent transformation, raising the possibility that autophagy facilitates Ras transformation via other mechanisms.

Autophagy inhibition results in decreased proliferation of Ras-transformed cells.

The aforementioned results motivated us to test the functional contributions of autophagy to the proliferation of H-Ras^{V12} transformed cells. First, we tested the effects of ECM detachment on the proliferation capacity of autophagy competent and deficient MEFs expressing either vector control (BABE) or H-Ras^{V12}. Cells grown attached or in suspension for 48h were subject to flow cytometric analysis for DNA content corresponding to the S+G2/M phases of the cell cycle (Figure 2-6A). In vector control (BABE) wild-type MEFs, we observed a decrease in the percentage of cycling cells (S+G2/M), from 67.3% +/-

1.3% in attached conditions to 40.7% +/-3.5% after 48h of suspension (Figure 2-6A, black bars). In contrast, 57.9% +/-1.5% of H-Ras^{V12} transformed wild-type (*atg5+/+)* cells remained in S+G2/M following 48h of suspension (Figure 2-6A, white bars). Thus, H-Ras^{V12} transformed cells continue to proliferate upon loss of cell-matrix contact. However, in H-Ras^{V12} *atg5-/-* MEFs, incapable of autophagy, the ability of H-Ras^{V12} to promote proliferation in the absence of cell-matrix contact was attenuated, with only 47.3% +/-2.1% of cells remaining in cycle following 48h of suspension (Figure 2-6A, light grey bars). Interestingly, we noted that control (BABE) *atg5-/-* MEFs (dark grey bars) proliferated slightly better than *atg5+/+* cells during detachment; such results are consistent with previous studies demonstrating that reduced autophagy due to Beclin/ATG6 haploinsufficiency or genetic deletion of Ambra1 can promote cell proliferation (Fimia et al., 2007; Qu et al., 2003). Nevertheless, in the context of H-Ras^{V12} expression, autophagy inhibition curtailed rather than enhanced proliferation during ECM detachment.

To extend these results, we then measured if H-Ras^{V12} transformed *atg5-/-* cells displayed similar defects in proliferation in the absence of the stresses imposed by substratum detachment. Thus, we grew the various cell types in nutrient replete, attached conditions in which only basal levels of autophagy were present. Upon enumerating cell numbers from cultures, we found that nontransformed wild type and *atg5-/-* MEFs exhibited minimal differences in proliferation (Figure 2-6B). In contrast, upon transformation with H-Ras^{V12}, autophagy-deficient cells failed to proliferate as well as controls (Figure 2-6C).

Similarly, acute ATG7 knockdown in MDA-MB-231 cells led to a profound decrease in proliferation compared to controls (Figure 2-6D). Overall, these results indicate that autophagy induction is necessary for optimal cell proliferation in H-Ras^{V12} expressing cells following ECM detachment, and that oncogenic Ras activation engenders an increased reliance on basal autophagy for cell expansion in attached conditions.

Increased glucose metabolism in autophagy competent cells.

Due to the decreased proliferation observed in Ras-transformed cells upon autophagy inhibition, we hypothesized that the difference in adhesion-independent transformation we observed between Ras-transformed autophagy competent and deficient cells may arise from changes in protein synthesis or in cellular metabolism, two processes that directly impact the capacity for cell growth and proliferation. Both nitrogen-starved, autophagy deficient yeast and early ATG5 deficient embryos display a decrease in *de novo* protein translation compared to wild-type controls (Onodera and Ohsumi, 2005; Tsukamoto *et al.*, 2008). Therefore, we speculated that H-Ras^{V12} *atg5-/-* MEFs would exhibit diminished rates of protein synthesis compared to H-Ras^{V12} wild-type MEFs in the absence of ECM contact. Although we observed decreased *de novo* protein synthesis in empty vector (BABE) expressing *atg5-/-* MEFs compared to wild-type following 24h detachment, only minor differences were present when we compared H-Ras^{V12} expressing wild-type and *atg5-/-* MEFs (Figure 2-7A and B).

Like many oncogenes, H-Ras^{V12} enhances glycolysis, which is associated with increased glucose uptake and lactate production; importantly, increased aerobic glycolysis is required for Ras driven tumors to maintain energy production and enhance biosynthetic pathways. Remarkably, we found that glucose uptake, determined by uptake of 2-[N-(7-nitrobenz-2-oxa-1,3-diazol-4-yl) amino]-2-deoxy-D-glucose (2-NBDG), was significantly reduced in empty vector *atg5-/-* MEFs compared to atg5+/+ controls (Figure 2-8A). As expected, H-Ras^{V12} expression resulted in increased glucose uptake (Figure 2-9A). When we compared glucose uptake between H-Ras^{V12} *atg5+/+* and H-Ras^{V12} *atg5-/-* MEFs over an 8h timecourse, we found reduced glucose uptake in H-Ras^{V12} *atg5-/-* MEFs compared to H-Ras^{V12} *atg5+/+* cells at all timepoints examined (Figure 2-8B). We also observed a decreased level of glucose uptake in H-Ras^{V12} *atg5-/-* MEFs following extracellular matrix detachment (Figure 2-9B). Enhanced glucose uptake is often associated with an increase in glycolytic flux, resulting in the enhanced production of lactate. Thus, to determine the glycolytic status of autophagy-proficient and deficient cells, we used ^{13}C-NMR spectroscopy to assess metabolic fluxes. Cells were labeled with [1-^{13}C]-glucose and *de novo* lactate production was monitored. Despite reduced glucose uptake in *atg5-/-* MEFs compared to *atg5+/+* controls, there was no concomitant decrease in lactate production in *atg5-/-* MEFs (Figure 2-8C). In fact, we observed equivalent levels of both intracellular and extracellular lactate production by wild type and *atg5-/-* MEFs. However, upon H-Ras^{V12} transformation, both intracellular and extracellular [3-^{13}C]-lactate production was decreased in H-Ras^{V12} transformed

atg5-/- cells in comparison to *atg5*+/+ controls (Figure 2-8C). Furthermore, compared to *atg5*+/+ controls, H-Ras^{V12} *atg5-/-* MEFs exhibited decreased levels of [3-^{13}C]-alanine, which is produced via the transamination of the glycolytic end product pyruvate (Figure 2-9C).

Next, we evaluated if defects in glucose metabolism were present in MDA-MB-231 cells upon ATG7 knockdown. Although glucose uptake was not significantly reduced in ATG7 depleted cells (data not shown), they did exhibit a significant decrease in the enzymatic activity of lactate dehydrogenase (LDH), which is required for the conversion of pyruvate to lactate. Furthermore, LDH-A protein levels were also decreased in ATG7 depleted MDA-MB-231 cells (Figure 2-9D). LDH-A levels were not altered in empty vector *atg5-/-* or H-Ras^{V12} *atg5-/-* MEFs compared to wild-type controls (Figure 2-9E). Altogether, these results implicate that reduced autophagy results in a concomitant decrease in glycolytic capacity.

Autophagy competent cells exhibit increased sensitivity to diminished glucose availability.

Because glycolysis was decreased in Ras-transformed, autophagy deficient cells, we next sought to determine the effects of varying glucose concentrations on autophagy competent versus deficient cells. We first assessed if autophagy is stimulated in response to decreasing media glucose concentrations, since previous studies support that autophagy is induced upon glucose starvation or treatment with 2-deoxy-glucose (Aki *et al.*, 2003; DiPaola *et*

al., 2008). Although we observed a robust induction of autophagy following 9h of complete glucose withdrawal, a similar increase in autophagy was not detected in H-Ras^{V12} expressing MEFs upon lowering glucose concentrations from the standard 25mM to 5.5mM for up to 48h (Figure 2-10A).

Glycolytic cells typically display exquisite sensitivity to diminishing concentrations of glucose; accordingly, we assessed how autophagy competence versus deficiency impacted glucose consumption and proliferation in H-Ras^{V12} expressing cells. First, we measured the consumption of glucose in H-Ras^{V12} *atg5+/+* and *atg5-/-* cells grown over 2d in 5.5mM glucose; in accordance with the results above, media glucose concentrations declined more precipitously in H-Ras^{V12} wild-type MEF cultures compared to H-Ras^{V12} *atg5-/-* cells (Figure 2-10B). Furthermore, following 4d of culture in 5.5mM glucose, cell numbers in H-Ras^{V12} wild-type cultures were reduced by 62.5% in comparison to those grown in 25mM. In contrast, the expansion of H-Ras^{V12} *atg5-/-* cells was not as profoundly attenuated by similar reductions in glucose concentration; these cells only exhibited a 40.4% reduction in cell number when cultured in 5.5mM glucose compared to 25mM glucose. This increased sensitivity of H-Ras^{V12} *atg5+/+* MEFs to lower media glucose levels is in accordance with the increases in glycolytic capacity and glucose uptake we observed in H-Ras^{V12} *atg5+/+* MEFs (Figure 2-10B). To corroborate these results, we performed parallel experiments in MDA-MB-231 cells following acute ATG7 depletion. When grown in 2.8mM glucose, cells expressing shATG7-2 consumed glucose at a lower rate than cells expressing control shRNA (shCNT) (Figure 2-10C). In addition, the expansion of

shATG7-2 cells was not as sensitive to lower glucose concentrations as shCNT cells (Figure 2-10C).

Based on these results, we hypothesized that declining glucose concentrations would attenuate the rate of adhesion-independent transformation of H-Ras^{V12}-transformed autophagy competent cells, but have little effect on autophagy-deficient counterparts. Accordingly, we observed a significant reduction in soft agar colony formation in H-Ras^{V12} *atg5+/+* MEFs grown in 5.5mM glucose compared to those grown in 25mM glucose. In contrast, adhesion-independent transformation in H-Ras^{V12} *atg5-/-* MEFs was not affected by declining glucose concentrations. Remarkably, at the lower glucose concentration (5.5mM), we observed comparable levels of soft agar colony formation between H-Ras^{V12} transformed autophagy-competent and deficient cells (Figure 2-10D). These results support that the ability of autophagy to promote adhesion independent transformation is highly dependent on glucose levels, and point to a previously unrecognized role for autophagy competence in facilitating glycolysis and proliferation during oncogenic Ras-mediated transformation.

References

Aki, T., K. Yamaguchi, T. Fujimiya, and Y. Mizukami. 2003. Phosphoinositide 3-kinase accelerates autophagic cell death during glucose deprivation in the rat cardiomyocyte-derived cell line H9c2. *Oncogene*. 22:8529-35.

Berry, D.L., and E.H. Baehrecke. 2007. Growth arrest and autophagy are required for salivary gland cell degradation in Drosophila. *Cell*. 131:1137-48.

DiPaola, R.S., D. Dvorzhinski, A. Thalasila, V. Garikapaty, D. Doram, M. May, K. Bray, R. Mathew, B. Beaudoin, C. Karp, M. Stein, D.J. Foran, and E. White. 2008. Therapeutic starvation and autophagy in prostate cancer: a new paradigm for targeting metabolism in cancer therapy. *Prostate*. 68:1743-52.

Fimia, G.M., A. Stoykova, A. Romagnoli, L. Giunta, S. Di Bartolomeo, R. Nardacci, M. Corazzari, C. Fuoco, A. Ucar, P. Schwartz, P. Gruss, M. Piacentini, K. Chowdhury, and F. Cecconi. 2007. Ambra1 regulates autophagy and development of the nervous system. *Nature*. 447:1121-5.

Fung, C., R. Lock, S. Gao, E. Salas, and J. Debnath. 2008. Induction of Autophagy during Extracellular Matrix Detachment Promotes Cell Survival. *Mol Biol Cell*. 19:797-806.

Furuta, S., E. Hidaka, A. Ogata, S. Yokota, and T. Kamata. 2004. Ras is involved in the negative control of autophagy through the class I PI3-kinase. *Oncogene*. 23:3898-904.

Komatsu, M., S. Waguri, T. Ueno, J. Iwata, S. Murata, I. Tanida, J. Ezaki, N. Mizushima, Y. Ohsumi, Y. Uchiyama, E. Kominami, K. Tanaka, and T. Chiba. 2005. Impairment of starvation-induced and constitutive autophagy in Atg7-deficient mice. *J Cell Biol*. 169:425-34.

Kuma, A., M. Hatano, M. Matsui, A. Yamamoto, H. Nakaya, T. Yoshimori, Y. Ohsumi, T. Tokuhisa, and N. Mizushima. 2004. The role of autophagy during the early neonatal starvation period. *Nature*. 432:1032-6.

Maiuri, M.C., E. Tasdemir, A. Criollo, E. Morselli, J.M. Vicencio, R. Carnuccio, and G. Kroemer. 2009. Control of autophagy by oncogenes and tumor suppressor genes. *Cell Death Differ*. 16:87-93.

Ohsumi, Y. 2001. Molecular dissection of autophagy: two ubiquitin-like systems. *Nat Rev Mol Cell Biol*. 2:211-6.

Onodera, J., and Y. Ohsumi. 2005. Autophagy is required for maintenance of amino acid levels and protein synthesis under nitrogen starvation. *J Biol Chem*. 280:31582-6.

Pattingre, S., C. Bauvy, and P. Codogno. 2003. Amino acids interfere with the ERK1/2-dependent control of macroautophagy by controlling the activation of Raf-1 in human colon cancer HT-29 cells. *J Biol Chem*. 278:16667-74.

Pattingre, S., A. Tassa, X. Qu, R. Garuti, X.H. Liang, N. Mizushima, M. Packer, M.D. Schneider, and B. Levine. 2005. Bcl-2 antiapoptotic proteins inhibit Beclin 1-dependent autophagy. *Cell*. 122:927-39.

Qu, X., J. Yu, G. Bhagat, N. Furuya, H. Hibshoosh, A. Troxel, J. Rosen, E.L. Eskelinen, N. Mizushima, Y. Ohsumi, G. Cattoretti, and B. Levine. 2003. Promotion of tumorigenesis by heterozygous disruption of the beclin 1 autophagy gene. *J Clin Invest*. 112:1809-20.

Sou, Y.S., S. Waguri, J. Iwata, T. Ueno, T. Fujimura, T. Hara, N. Sawada, A. Yamada, N. Mizushima, Y. Uchiyama, E. Kominami, K. Tanaka, and M. Komatsu. 2008. The Atg8 conjugation system is indispensable for proper development of autophagic isolation membranes in mice. *Mol Biol Cell*. 19:4762-75.

Tsukamoto, S., A. Kuma, M. Murakami, C. Kishi, A. Yamamoto, and N. Mizushima. 2008. Autophagy is essential for preimplantation development of mouse embryos. *Science*. 321:117-20.

FIGURE LEGENDS

Figure 2-1. Oncogenic Ras does not suppress ECM detachment-induced autophagy.

(A) Left: Ras expression in MCF10A cells expressing empty vector (BABE) or H-Ras^{V12}. Right: BABE and H-Ras^{V12} MCF10A cells were grown attached (A) or suspended (susp) for the indicated times in the presence or absence of E64d and pepstatin A (E/P), lysed, and subject to immunoblotting with antibodies against LC3 and tubulin.

(B) GFP-LC3 puncta in MCF10A cells expressing empty vector (BABE) or H-Ras^{V12}grown attached or suspended for 24h.

(C) Left: Ras expression in *atg5+/+* (WT) and *atg5-/-* MEFs expressing empty vector or H-Ras^{V12}. Center: *atg5+/+* (WT) MEFs expressing empty vector (BABE) and H-Ras^{V12} were growth attached (A) or suspended (susp) for 24h in the presence or absence of E64d and pepstatin A (E/P), lysed, and subject to immunoblotting with antibodies against LC3 and tubulin. Right: *atg5+/+* (WT) and *atg5-/-* MEFs expressing H-Ras^{V12} or empty vector (BABE) were grown attached (A) or suspended (susp) for 24h, lysed, and subject to immunobloting with antibodies against p62 and tubulin.

(D) MDA-MB-231, HCT 116 and PANC-1 cells were grown attached (A) or suspended (susp) for 24h in the presence or absence of E64d and pepstatin A (E/P) and subject to immunoblotting with antibodies against LC3 and tubulin. (E)

GFP-LC3 puncta in MDA-MB-231, HCT 116 and PANC-1 cells that were grown attached or detached for 24h. Bar, 25 mm.

Figure 2-2. Effects of ECM detachment on MAPK and mTORC1 signaling in Ras transformed cells.

(A-C) Empty vector (BABE) and H-Ras^{V12} expressing MCF10A cells (A), *atg5*+/+ (WT) and *atg5*-/- MEFs (B), and K-Ras mutant carcinoma cell lines (C) were grown attached (A) or suspended (susp) for the indicated times, and subject to immunoblotting with antibodies against phosphorylated-ERK1+2 and total ERK1+2 protein.

(D-F) Empty vector (BABE) and H-Ras^{V12} expressing MCF10A cells (D), *atg5*+/+ (WT) and *atg5*-/- MEFs (E), and K-Ras mutant carcinoma cell lines (F) were grown attached (A) or suspended (susp) for the indicated times, and subject to immunoblotting with antibodies against phosphorylated-S6 and total ribosomal S6 protein.

(G) H-Ras^{V12} MCF10A cells were grown attached (A) or suspended (susp) for 24h in the presence or absence of E64d and pepstatin A (E/P) and subject to immunoblotting with antibodies against phosphorylated-S6, S6, LC3, and tubulin. When indicated, cells were treated with 25nM rapamycin for 5h prior to harvest.

Figure 2-3. Decreased anchorage-independent growth in autophagy deficient MEFs expressing H-Ras^{V12}.

(A) Soft agar colony formation in H-Ras^{V12} expressing *atg5+/+* (WT) and *atg5-/-* MEFs.

(B) *atg5-/-* MEFs reconstituted with wild-type murine ATG5 or ATG5 K130R were subject to immunoblotting with antibodies against ATG12 (to detect the ATG12-ATG5 complex) and tubulin. As indicated, cells were grown attached (A) or suspended for 24h (susp) in the presence or absence of E64d and pepstatin A (E/P) and subject to immunoblotting with antibodies against LC3 and tubulin as a loading control.

(C) Soft agar colony formation in H-Ras^{V12} expressing *atg5-/-* MEFs expressing ATG5 or ATG5K130R.

(D-E) Soft agar colony formation in H-Ras^{V12} expressing wild type (WT), *atg7-/-*, and *atg3-/-* MEFs. Above results represent the mean+/-SEM from 3 or more independent experiments. P-value was calculated using Student's t-test.

Figure 2-4. Effects of ATG knockdown on adhesion independent transformation in MDA-MB-231 cells and H-Ras^{V12} MCF10A cells.

(A) MDA-MB-231 cells transduced with lentiviral vectors encoding shRNAs against the indicated ATGs (shATGs) were subject to immunoblotting with antibodies against ATG7, ATG5 (to detect ATG12-ATG5 complex), and tubulin.

(B) MDA-MB-231 cells expressing shATG7-2 or shCNT were grown attached (A) or suspended (susp) for the indicated times in the presence or absence of E64d

and pepstatin A (E/P) and subject to immunoblotting with antibodies against LC3 and tubulin.

(C) Representative images and quantification of soft agar colony formation in MDA-MB-231 cells expressing the indicated shATGs.

(D) H-Ras^{V12} MCF10A cells expressing shCNT or shATG7-2 were grown attached (A) or suspended (susp) for the indicated times in the presence or absence of E64d and pepstatin A (E/P) and subject to immunoblotting with antibodies against ATG7, LC3, and tubulin.

(E) Representative images and quantification of soft agar colony formation in H-Ras^{V12} MCF10A cells expressing shCNT or shATG7-2. Above results represent the mean+/-SEM from 3 or more independent experiments. P-value was calculated using Student's t-test.

Figure 2-5. Bcl-2 inhibition of apoptosis is not sufficient to restore anchorage-independent growth in autophagy deficient cells.

(A) H-Ras^{V12} expressing *atg5+/+* (WT) and *atg5-/-* MEFs were grown attached (A) or suspended (susp) for the indicated times and subject to immunoblotting with antibodies against cleaved capase-3 and tubulin.

(B) Bcl-2 expression levels in H-Ras^{V12} *atg5+/+* (WT) and *atg5-/-* MEFs in the presence or absence of stable ectopic expression of Bcl-2.

(C) The indicated cell types were grown attached (A) or suspended (susp) for 24h with or without E64d and pepstatin A (E/P) and subject to immunoblotting with antibodies against LC3, p62 and tubulin.

(D) The indicated cell types were grown attached (A) or suspended (susp) for 24h and subject to immunoblotting with antibodies against cleaved caspase-3, and tubulin.

(E) Soft agar colony formation of H-Ras^{V12} *atg5*+/+ (WT) and *atg5-/-* MEFs stably expressing BCL-2. Results represent the mean+/-SEM from 3 independent experiments. P-value was calculated using Student's t-test.

Figure 2-6. Reduced proliferation upon autophagy inhibition in H-Ras^{V12} expressing MEFs and MDA-MB-231 cells.

(A) The indicated cell types were grown attached or subject to ECM detachment for 48h and analyzed by flow cytometry to quantify the percent of cells with DNA content corresponding to the S and G2/M (S+G2/M) phases of the cell cycle. Results are the mean+/-SEM from 3 or more independent experiments. Statistical significance was calculated using ANOVA.

(B) Proliferation curves of empty vector (BABE) *atg5*+/+ (WT) and *atg5-/-* MEFs cultured in attached, nutrient-rich conditions.

(C) Proliferation curves of H-Ras^{V12} expressing *atg5*+/+ (WT) and *atg5-/-* MEFs in attached, nutrient-rich conditions.

(D) Proliferation curves of MDA-MB-231 cells expressing shCNT or shATG7-2 in attached, nutrient-rich conditions. For (B-D), P-value was calculated at each timepoint using Student's t-test, with statistical significance indicated as follows: * $p<0.05$; ** $p<0.01$.

Figure 2-7. *De novo* protein synthesis following ECM detachment.

(A) Left: Empty vector (BABE) and H-Ras^{V12} expressing wild type and *atg5-/-* MEFs were grown attached (A) or suspended (susp) for 24h and labeled using TAMRA Click-iT Protein Analysis Detection Kit to detect newly translated proteins. Right: Total protein levels from the same SDS-PAGE gel.

(B) Quantification of translated protein levels normalized to total protein (middle column) and quantification of the decrease in protein synthesis following suspension expressed as percent of translated protein relative to the attached condition (right column). Results are representative of three independent experiments.

Figure 2-8. Reduced glucose metabolism in autophagy deficient MEFs.

(A) Levels of glucose uptake (2-NBDG uptake, mean fluorescence intensity) in empty vector (BABE) *atg5+/+* (WT) and *atg5-/-* MEFs following 2.5h incubation. Statistical significance was calculated using Student's t-test.

(B) 2-NBDG uptake (mean fluorescence intensity) after 1h (left histogram) and over an 8h timecourse (right graph) in H-Ras^{V12} expressing *atg5+/+* (WT) and *atg5-/-* MEFs. P-value was calculated at each timepoint using Student's t-test, with statistical significance indicated as follows: * $p<0.05$; ** $p<0.01$; ***$p<0.001$.

(C) Levels of ^{13}C labeled intracellular lactate and extracellular lactate detected by NMR following 24h of labeling with 1-^{13}C-glucose. Results represent the mean+/- SEM from 3 independent experiments. Statistical significance was calculated using ANOVA.

Figure 2-9: Reduced glucose metabolism in autophagy deficient cells.

(A) 2-NBDG uptake (mean fluorescence intensity) in empty vector (BABE) and H-Ras^{V12} *atg5+/+* (WT) MEFs following 2.5h incubation.

(B) 2-NBDG uptake (mean fluorescence intensity) in H-Ras^{V12} atg5+/+ (WT) and H-Ras^{V12} *atg5-/-* MEFs following 7h suspension.

(C) Levels of ^{13}C labeled intracellular alanine detected by NMR following 24h of labeling with 1-^{13}C-glucose.

(D) Left: Lactate dehydrogenase (LDH) activity levels in MDA-MB-231 cells expressing shCNT or shATG7-2. Right: MDA-MB-231 cells were subject to immunoblotting with antibodies against LDH-A and tubulin.

(E) Empty vector (BABE) and H-Ras^{V12} expressing *atg5+/+* (WT) and *atg5-/-* MEFs were subject to immunoblotting with antibodies against LDH-A and tubulin. Results represent the mean+/-SEM from 3 or more independent experiments. For all panels, statistical significance was calculated using Student's t-test.

Figure 2-10. The proliferation and transformation of autophagy competent cells is more sensitive to diminished glucose availability than autophagy deficient cells.

(A) H-Ras^{V12} expressing WT MEFs were cultured in media containing 25mM or 5.5mM glucose for 48h, or in the complete absence of glucose (0mM) for 9h. E64d and pepstatin A (E/P) were added when indicated to measure autophagic flux. Cells were lysed and subject to immunoblotting with antibodies against LC3, p62, and tubulin as a loading control.

(B) Left: Media glucose levels from cultures of H-Ras^{V12} *atg5+/+* (WT) and *atg5-/-* MEFs grown in 5.5mM glucose over 2d. Right: Relative percentage of viable cells in 5.5mM glucose compared to 25mM glucose following 4d of culture.

(C) Left: Media glucose levels from cultures of MDA-MB-231 cells expressing shCNT or shATG7-2 grown in 2.8mM glucose over 2d. Right: Relative percentage of viable cells grown in 2.8mM and 1.4mM glucose media compared to 25mM glucose following 3d of growth.

(D) Soft agar colony formation of H-Ras^{V12} expressing *atg5+/+* (WT) and *atg5-/-* MEFs in 25mM and 5.5mM glucose conditions. Results represent the mean+/- SEM from 4 independent experiments. Statistical significance was calculated using ANOVA.

Figure 2-1

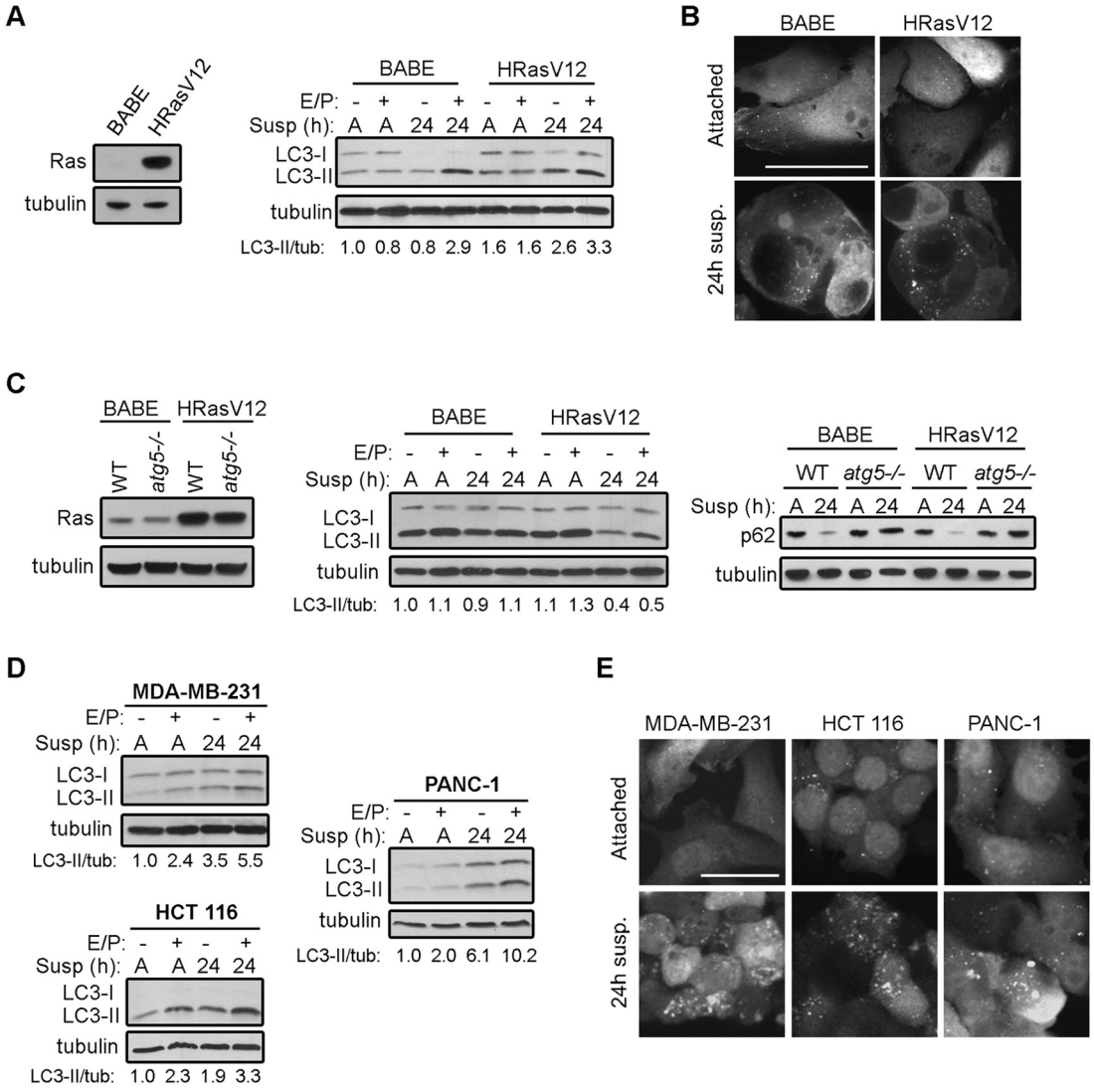
A
BABE
HRasV12
Ras
tubulin
BABE
HRasV12
E/P: - + - + - + - +
Susp (h): A A 24 24 A A 24 24
LC3-I
LC3-II
tubulin
LC3-II/tub: 1.0 0.8 0.8 2.9 1.6 1.6 2.6 3.3
B
BABE
HRasV12
Attached
24h susp.
C
BABE
HRasV12
WT
atg5-/-
WT
atg5-/-
Ras
tubulin
BABE
HRasV12
E/P: - + - + - + - +
Susp (h): A A 24 24 A A 24 24
LC3-I
LC3-II
tubulin
LC3-II/tub: 1.0 1.1 0.9 1.1 1.1 1.3 0.4 0.5
BABE
HRasV12
WT
atg5-/-
WT
atg5-/-
Susp (h): A 24 A 24 A 24 A 24
p62
tubulin
D
MDA-MB-231
E/P: - + - +
Susp (h): A A 24 24
LC3-I
LC3-II
tubulin
LC3-II/tub: 1.0 2.4 3.5 5.5
HCT 116
E/P: - + - +
Susp (h): A A 24 24
LC3-I
LC3-II
tubulin
LC3-II/tub: 1.0 2.3 1.9 3.3
PANC-1
E/P: - + - +
Susp (h): A A 24 24
LC3-I
LC3-II
tubulin
LC3-II/tub: 1.0 2.0 6.1 10.2
E
MDA-MB-231
HCT 116
PANC-1
Attached
24h susp.

Figure 2-2

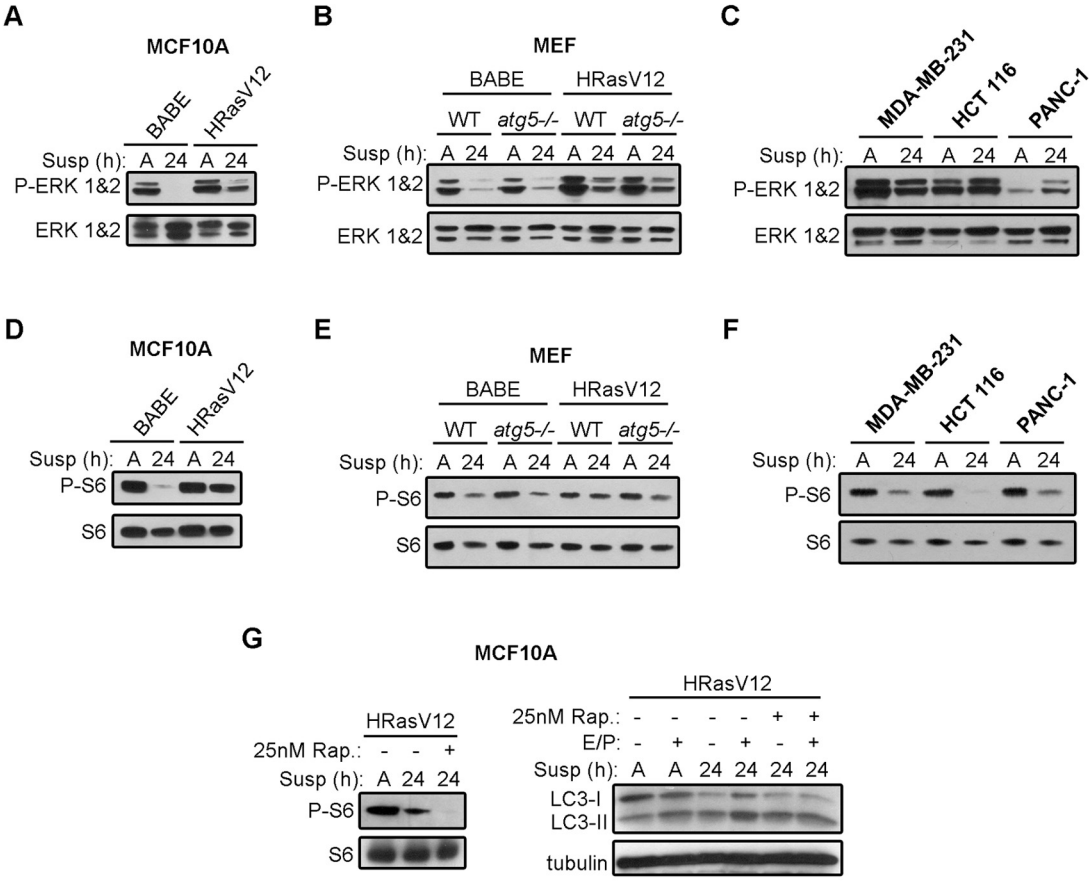
A
MCF10A
BABE
HRasV12
Susp (h): A 24 A 24
P-ERK 1&2
ERK 1&2
B
MEF
BABE
HRasV12
WT
atg5-/-
WT
atg5-/-
Susp (h): A 24 A 24 A 24 A 24
P-ERK 1&2
ERK 1&2
C
MDA-MB-231
HCT 116
PANC-1
Susp (h): A 24 A 24 A 24
P-ERK 1&2
ERK 1&2
D
MCF10A
BABE
HRasV12
Susp (h): A 24 A 24
P-S6
S6
E
MEF
BABE
HRasV12
WT
atg5-/-
WT
atg5-/-
Susp (h): A 24 A 24 A 24 A 24
P-S6
S6
F
MDA-MB-231
HCT 116
PANC-1
Susp (h): A 24 A 24 A 24
P-S6
S6
G
MCF10A
HRasV12
25nM Rap.: - - +
Susp (h): A 24 24
P-S6
S6
HRasV12
25nM Rap.: - - - - + +
E/P: - + - + - +
Susp (h): A A 24 24 24 24
LC3-I
LC3-II
tubulin

Figure 2-3

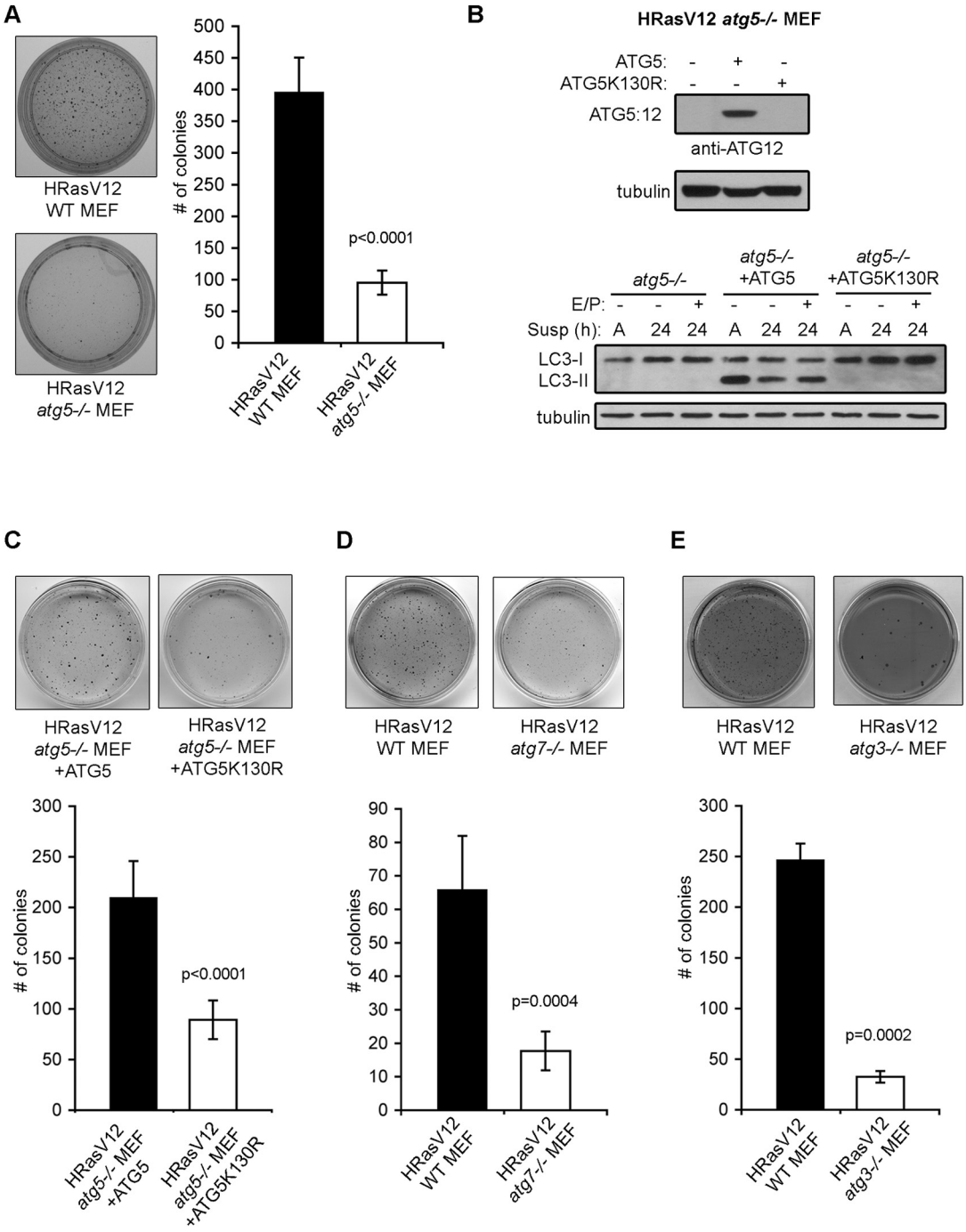
A
HRasV12
WT MEF
HRasV12
atg5-/- MEF
# of colonies
p<0.0001
HRasV12
WT MEF
HRasV12
atg5-/- MEF
B
HRasV12 atg5-/- MEF
ATG5: - + -
ATG5K130R: - - +
ATG5:12
anti-ATG12
tubulin
atg5-/-
atg5-/-
+ATG5
atg5-/-
+ATG5K130R
E/P: - - + - - + - - +
Susp (h): A 24 24 A 24 24 A 24 24
LC3-I
LC3-II
tubulin
C
HRasV12
atg5-/- MEF
+ATG5
HRasV12
atg5-/- MEF
+ATG5K130R
# of colonies
p<0.0001
HRasV12
atg5-/- MEF
+ATG5
HRasV12
atg5-/- MEF
+ATG5K130R
D
HRasV12
WT MEF
HRasV12
atg7-/- MEF
# of colonies
p=0.0004
HRasV12
WT MEF
HRasV12
atg7-/- MEF
E
HRasV12
WT MEF
HRasV12
atg3-/- MEF
# of colonies
p=0.0002
HRasV12
WT MEF
HRasV12
atg3-/- MEF

Figure 2-4

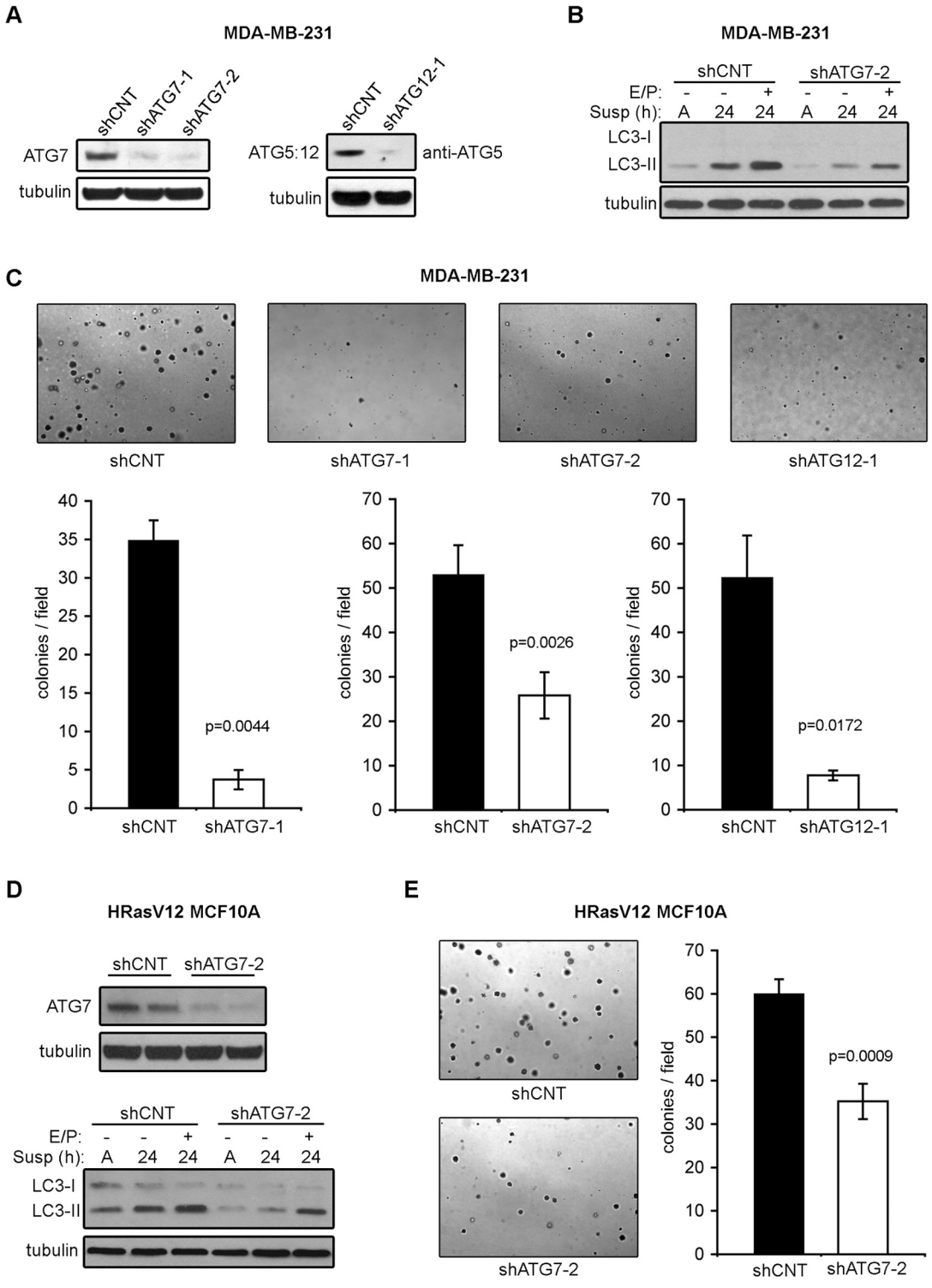
A
MDA-MB-231
shCNT
shATG7-1
shATG7-2
ATG7
tubulin
shCNT
shATG12-1
ATG5:12
anti-ATG5
tubulin
B
MDA-MB-231
shCNT
shATG7-2
E/P: - - + - - +
Susp (h): A 24 24 A 24 24
LC3-I
LC3-II
tubulin
C
MDA-MB-231
shCNT
shATG7-1
shATG7-2
shATG12-1
colonies / field
p=0.0044
shCNT
shATG7-1
p=0.0026
shCNT
shATG7-2
p=0.0172
shCNT
shATG12-1
D
HRasV12 MCF10A
shCNT
shATG7-2
ATG7
tubulin
shCNT
shATG7-2
E/P: - - + - - +
Susp (h): A 24 24 A 24 24
LC3-I
LC3-II
tubulin
E
HRasV12 MCF10A
shCNT
shATG7-2
colonies / field
p=0.0009
shCNT
shATG7-2

Figure 2-5

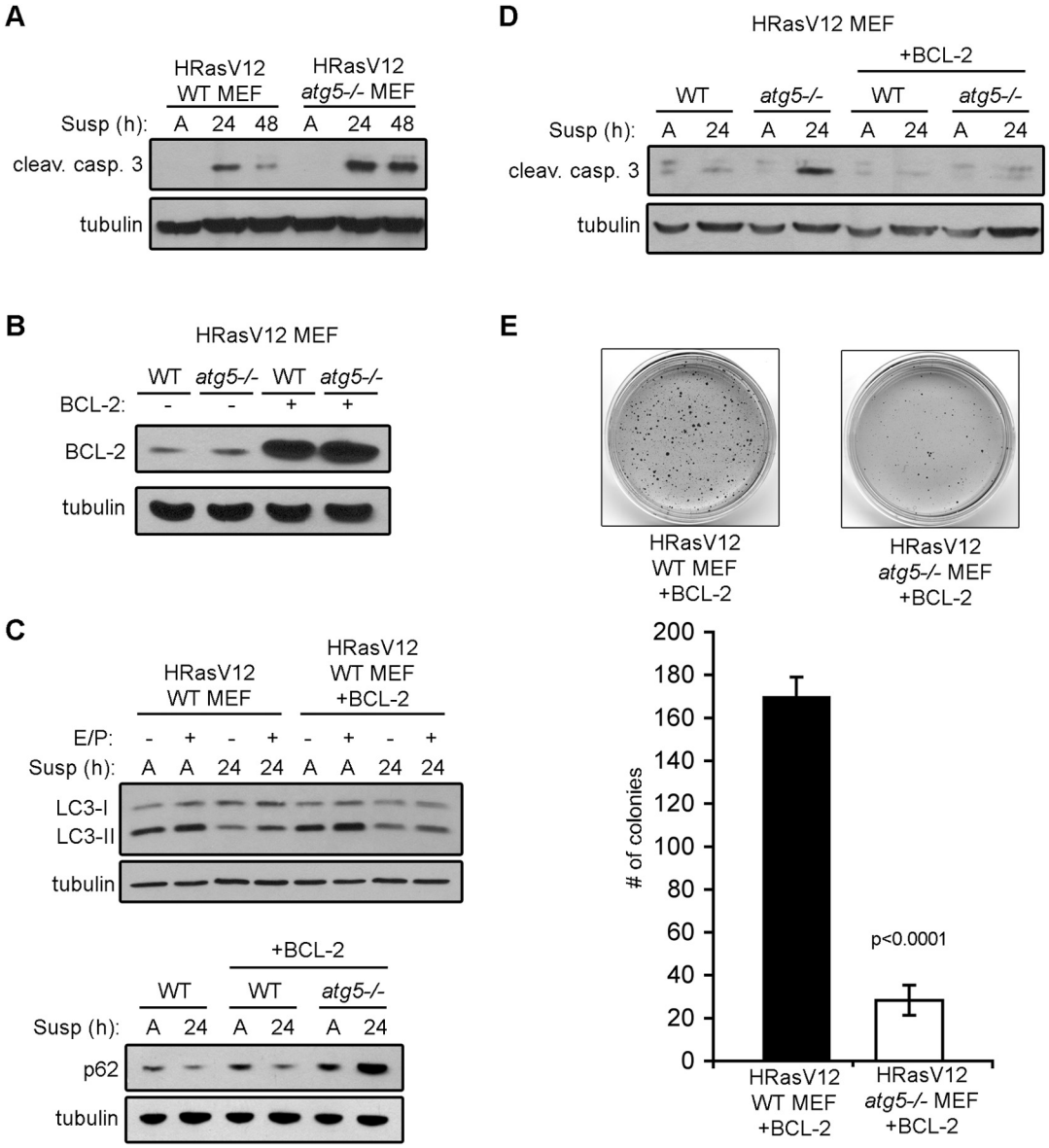
A
HRasV12 WT MEF
HRasV12 atg5-/- MEF
Susp (h): A 24 48 A 24 48
cleav. casp. 3
tubulin
B
HRasV12 MEF
WT atg5-/- WT atg5-/-
BCL-2: - - + +
BCL-2
tubulin
C
HRasV12 WT MEF
HRasV12 WT MEF +BCL-2
E/P: - + - + - + - +
Susp (h): A A 24 24 A A 24 24
LC3-I
LC3-II
tubulin
+BCL-2
WT WT atg5-/-
Susp (h): A 24 A 24 A 24
p62
tubulin
D
HRasV12 MEF
+BCL-2
WT atg5-/- WT atg5-/-
Susp (h): A 24 A 24 A 24 A 24
cleav. casp. 3
tubulin
E
HRasV12 WT MEF +BCL-2
HRasV12 atg5-/- MEF +BCL-2
# of colonies
200
180
160
140
120
100
80
60
40
20
0
p<0.0001
HRasV12 WT MEF +BCL-2
HRasV12 atg5-/- MEF +BCL-2

Figure 2-6

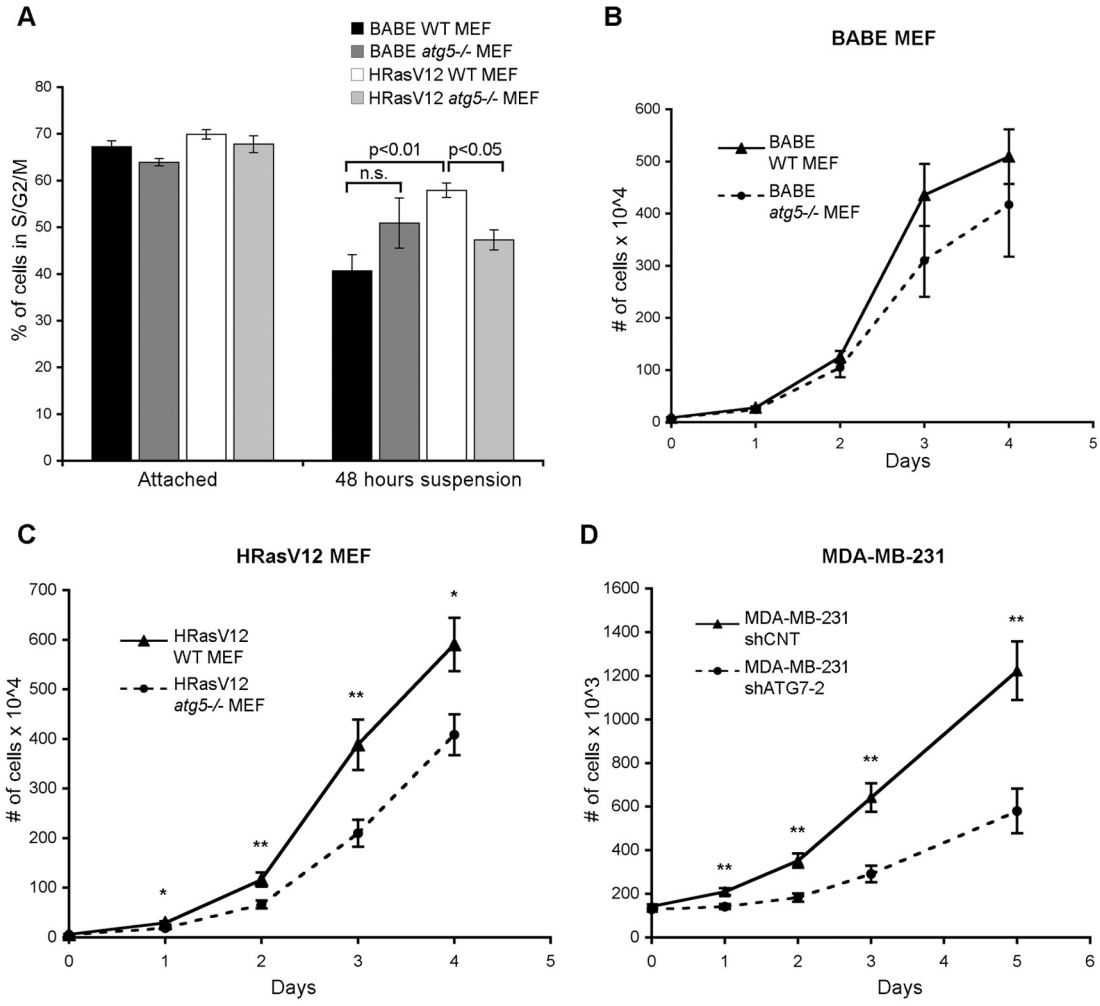
A
BABE WT MEF
BABE atg5-/- MEF
HRasV12 WT MEF
HRasV12 atg5-/- MEF
% of cells in S/G2/M
p<0.01
p<0.05
n.s.
Attached
48 hours suspension
B
BABE MEF
BABE WT MEF
BABE atg5-/- MEF
# of cells x 10^4
Days
C
HRasV12 MEF
HRasV12 WT MEF
HRasV12 atg5-/- MEF
# of cells x 10^4
Days
D
MDA-MB-231
MDA-MB-231 shCNT
MDA-MB-231 shATG7-2
# of cells x 10^3
Days

Figure 2-7

A

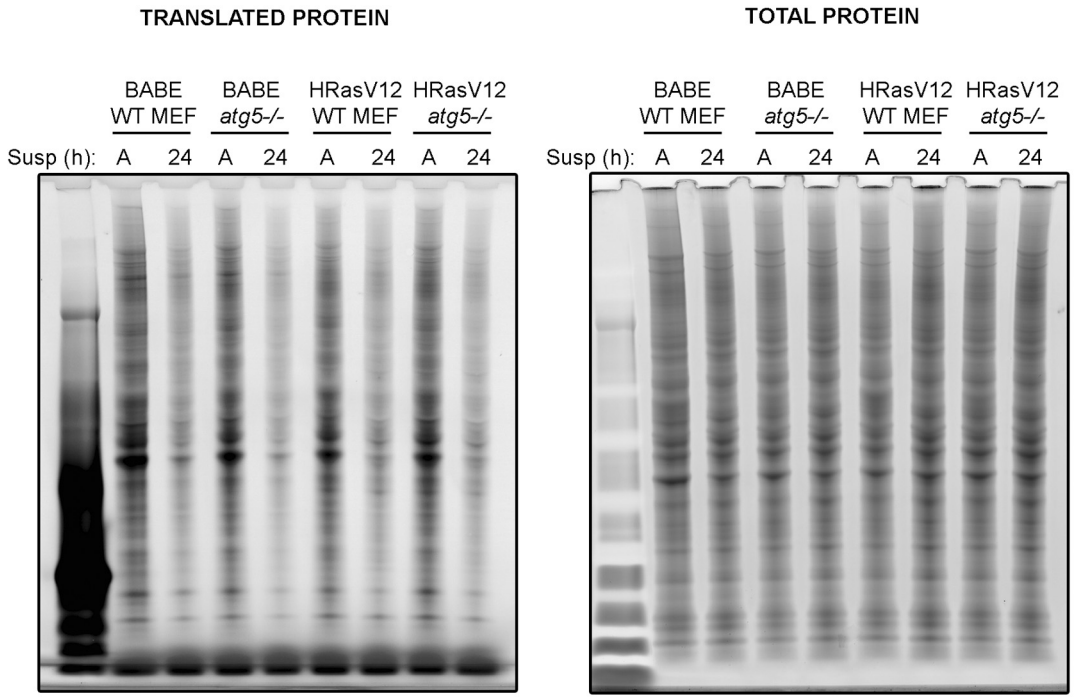

B

	TRANS. PROT. (AU)	% OF ATTACH.
BABE WT MEF Attached	903101.2	100.0
BABE WT MEF 24hr sus	251643.3	27.9
BABE atg5-/- MEF Attached	823654.5	100.0
BABE atg5-/- MEF 24hr sus	140428.3	17.0
HRasV12 WT MEF Attached	731482.6	100.0
HRasV12 WT MEF 24hr sus	199562.4	27.3
HRasV12 atg5-/- MEF Attached	747440.8	100.0
HRasV12 atg5-/- MEF 24hr sus	161101.4	21.6

Figure 2-8

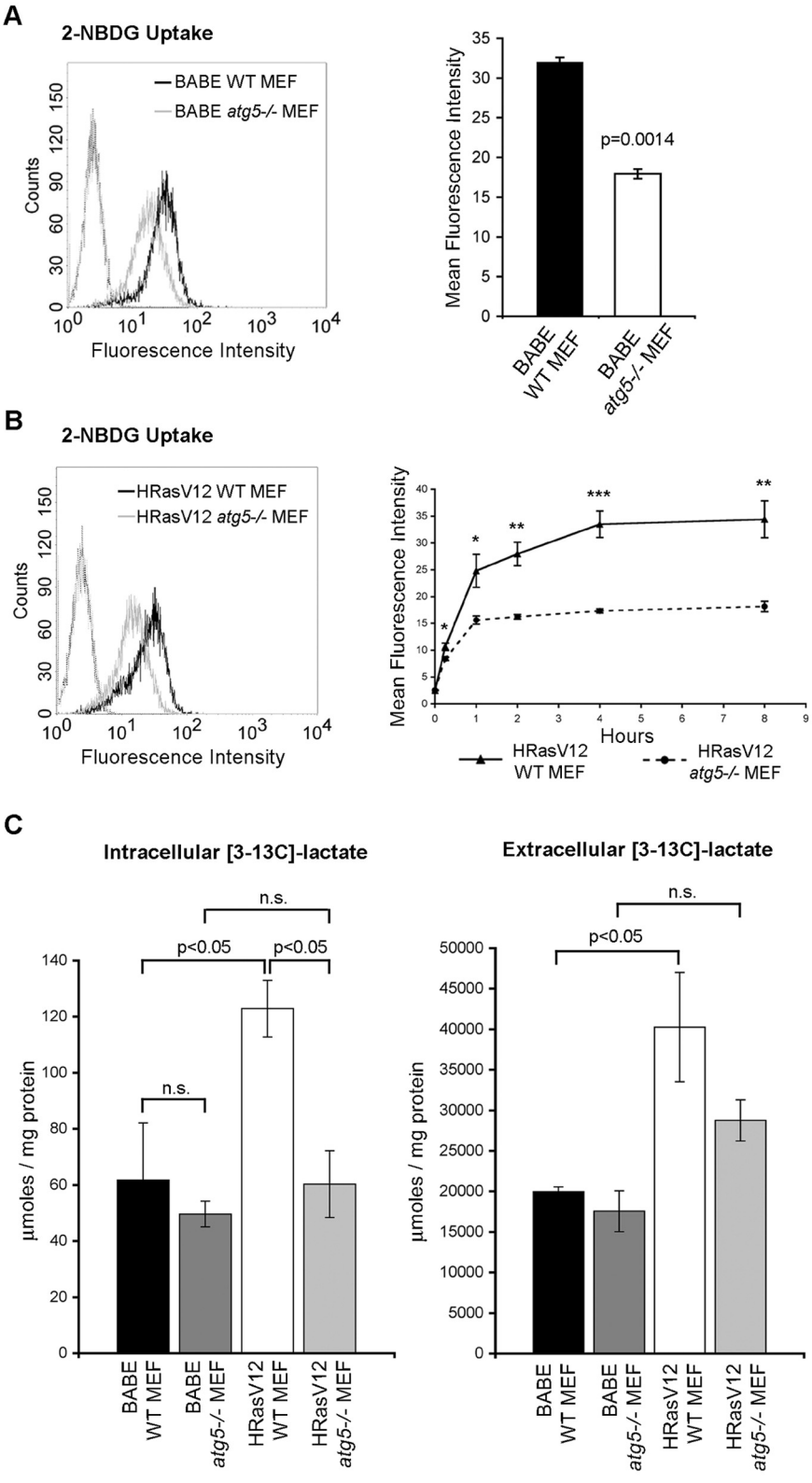
A
2-NBDG Uptake
BABE WT MEF
BABE atg5-/- MEF
Counts
Fluorescence Intensity
Mean Fluorescence Intensity
p=0.0014
BABE WT MEF
BABE atg5-/- MEF
B
2-NBDG Uptake
HRasV12 WT MEF
HRasV12 atg5-/- MEF
Counts
Fluorescence Intensity
Mean Fluorescence Intensity
Hours
HRasV12 WT MEF
HRasV12 atg5-/- MEF
C
Intracellular [3-13C]-lactate
Extracellular [3-13C]-lactate
n.s.
p<0.05
p<0.05
n.s.
µmoles / mg protein
BABE WT MEF
BABE atg5-/- MEF
HRasV12 WT MEF
HRasV12 atg5-/- MEF

Figure 2-9

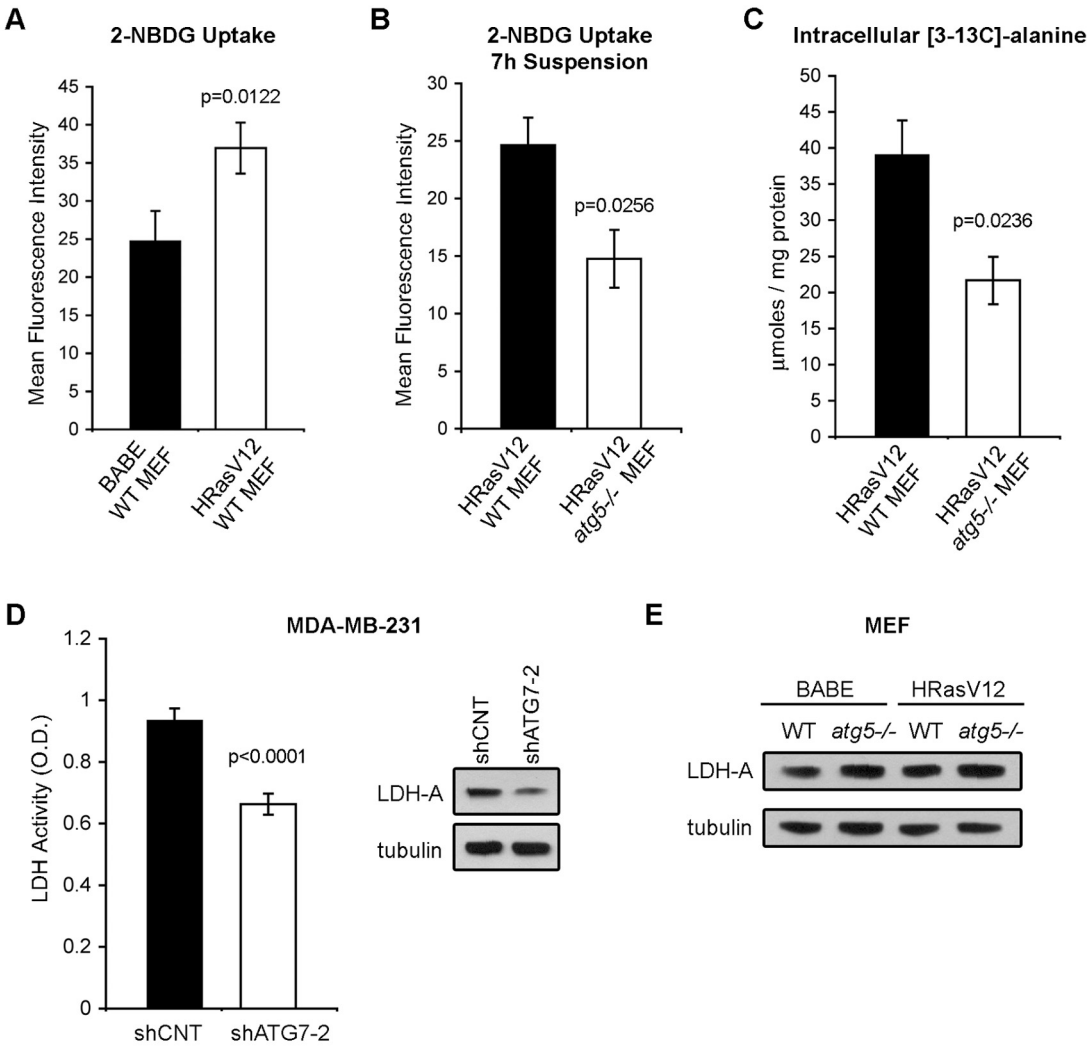
A
2-NBDG Uptake
Mean Fluorescence Intensity
p=0.0122
BABE WT MEF
HRasV12 WT MEF
B
2-NBDG Uptake 7h Suspension
Mean Fluorescence Intensity
p=0.0256
HRasV12 WT MEF
HRasV12 atg5-/- MEF
C
Intracellular [3-13C]-alanine
µmoles / mg protein
p=0.0236
HRasV12 WT MEF
HRasV12 atg5-/- MEF
D
MDA-MB-231
LDH Activity (O.D.)
p<0.0001
shCNT
shATG7-2
shCNT
shATG7-2
LDH-A
tubulin
E
MEF
BABE
HRasV12
WT
atg5-/-
WT
atg5-/-
LDH-A
tubulin

Figure 2-10

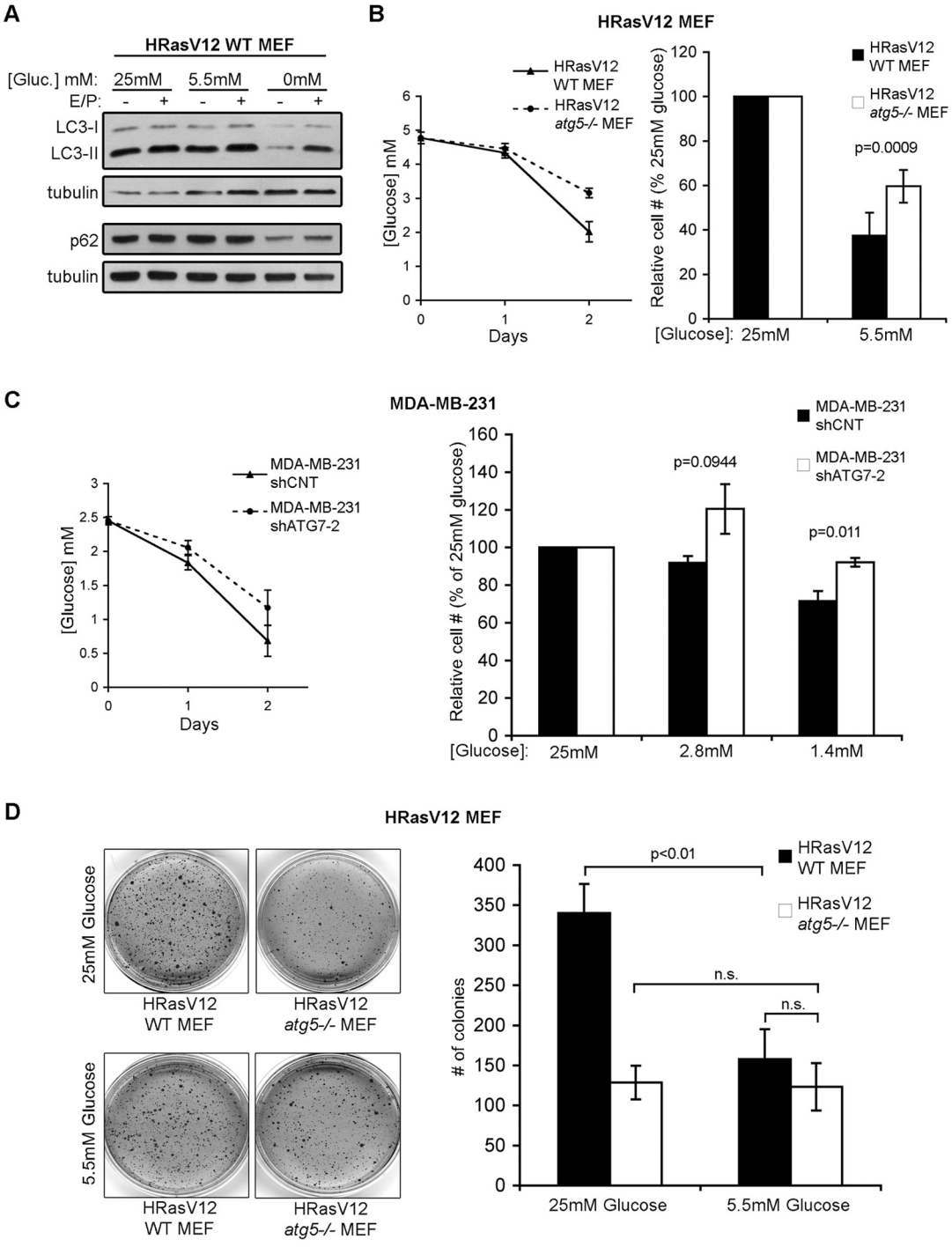
A
HRasV12 WT MEF
[Gluc.] mM: 25mM 5.5mM 0mM
E/P: - + - + - +
LC3-I
LC3-II
tubulin
p62
tubulin
B
HRasV12 MEF
HRasV12 WT MEF
HRasV12 atg5-/- MEF
[Glucose] mM
Days
Relative cell # (% 25mM glucose)
p=0.0009
[Glucose]: 25mM 5.5mM
C
MDA-MB-231
MDA-MB-231 shCNT
MDA-MB-231 shATG7-2
[Glucose] mM
Days
Relative cell # (% of 25mM glucose)
p=0.0944
p=0.011
[Glucose]: 25mM 2.8mM 1.4mM
D
HRasV12 MEF
25mM Glucose
5.5mM Glucose
HRasV12 WT MEF
HRasV12 atg5-/- MEF
p<0.01
n.s.
n.s.
# of colonies
25mM Glucose
5.5mM Glucose

Chapter 2

Autophagy supports cell invasion driven by oncogenic Ras

RNAi-mediated knockdown of critical autophagy genes (ATGs) suppresses invasion driven by oncogenic Ras in 3D culture.

To elucidate how autophagy impacts the cellular behavior of Ras-transformed epithelial cells, we utilized the established MCF10A 3D epithelial culture system to interrogate how autophagy affects the growth and morphogenesis of cells expressing oncogenic Ras (Debnath and Brugge, 2005). We generated stable pools of MCF10A human mammary epithelial cells expressing a control vector (BABE) or a mutationally active form of H-Ras (H-Ras^{V12}) that elicits high levels of anchorage independent oncogenic transformation of MCF10A cells (Lock et al., 2011). When plated as single cells on a laminin-rich ECM, control MCF10A cells clonally expand and undergo a period of luminal apoptosis resulting in the formation of hollow, spherical acini (Figure 3-2A) (Debnath et al., 2002; Petersen et al., 1992). In contrast, H-Ras^{V12} transformed cells produced grossly aberrant structures that were notable for the formation of protrusions that invaded the surrounding extracellular matrix. Individual H-Ras^{V12} structures formed these invasive protrusions as early as 3-5 days, which rapidly migrated towards each other, ultimately producing disorganized networks of cells intermingled with large cell clusters after 8 days of growth in 3D culture (Figure 3-1A and B, left columns). The 3D morphology we observed using H-Ras^{V12} MCF10A cells is similar to what has been reported using oncogenic Ras expressing mouse mammary cells grown in a 3D collagen matrix (Oft et al., 1996).

To inhibit autophagy in this experimental system we stably expressed unique short-hairpin RNAs (shRNA) against two autophagy genes (ATGs)—*atg7* (shATG7-1 and shATG7-2) or *atg12* (shATG12) in MCF10A cells stably expressing H-Ras^{V12}. Depending on the shATG utilized, these elicited a 50-90% knockdown in protein levels (Figure 3-2B), which was associated with reduced basal autophagy, as evidenced by decreased levels of PE-lipidated LC3 (LC3-II) and increased accumulation of the p62/SQSTM1, a protein selectively degraded by autophagy (Figure 3-2C). Moreover, compared to cells expressing a nontargeting control shRNA (shCNT), ATG knockdown cells exhibited decreased LC3-II turnover (autophagic flux) in response to nutrient starvation with Hank's buffered saline (Figure 3-2D).

Strikingly, when plated in 3D culture knockdown of either ATG7 or ATG12 in H-Ras^{V12} expressing cells resulted in near complete reversal of the invasive protrusions associated with oncogenic Ras activation. Rather, the majority of H-Ras^{V12} shATG expressing structures remained as tightly compact spheres that morphologically resembled non-Ras expressing structures even after 8 days of growth (Figure 3-1A-B). This decrease in invasion following autophagy inhibition was also observed upon stable knockdown of an additional autophagy gene, *atg3* (shATG3), as well as upon treatment with chloroquine or bafilomycin A, two lysosomal inhibitors that block the late steps of autophagy (Figure 3-2E). In addition, ATG knockdown cultures were notable for the presence of numerous small cell clusters, suggesting that autophagy inhibition also suppressed the proliferative outgrowth of a subset of H-Ras^{V12} cells in 3D culture. In support,

upon enumerating cells from 3D cultures derived from autophagy competent and deficient H-Ras^{V12} cells on day 8, both ATG7 and ATG12 depleted cultures exhibited reduced cell numbers compared to autophagy competent controls (shCNT) (Cell numbers, mean+/- s.d., from 5 independent experiments: H-Ras^{V12} shCNT: 196,375+/-48,900; H-Ras^{V12} shATG7-1: 89,166+/-63,500; H-Ras^{V12} shATG7-2: 122,156+/-25,900; H-Ras^{V12} shATG12: 162,263+/-44,800). Nonetheless, over 8 days, a subset of larger spherical structures did manifest in H-Ras^{V12} shATG cultures, but in stark contrast to H-Ras^{V12} shCNT structures, these larger structures failed to exhibit protrusive behavior.

Remarkably, shATG7, which produced the highest level of autophagy inhibition in H-Ras^{V12} MCF10A cells as assessed by the accumulation of p62/SQSTM1 (Figure 3-2C) elicited the largest decrease in cell number and most profound reversion in protrusive behavior, intimating that the degree of phenotypic reversion correlated with the extent of autophagy inhibition. Importantly, stable knockdown of autophagy genes in H-Ras^{V12} cells did not affect Ras expression levels or activation associated phosphorylation of a major downstream effector ERK, as observed in cells collected from 3D culture (Figure 3-2F). Thus, the morphological changes following ATG knockdown are not simply due to the loss of Ras expression or activity; rather, these results point to an important requirement for autophagy in supporting these phenotypes in the context of oncogenic Ras activation.

The disruption of basement membrane integrity is a hallmark of carcinoma invasion *in vivo* (Debnath and Brugge, 2005). To corroborate whether the

protrusions we observed in H-Ras^{V12}-transformed 3D cultures represented invasive behavior, we first evaluated basement membrane integrity by examining the expression and localization of the basement membrane protein, laminin 5 in H-Ras^{V12}-derived acini. Consistent with previous results, control non-transformed (BABE) MCF10A acini displayed polarized deposition of laminin 5 onto the basal surface (Figure 3-3A, left panel). In contrast, the expression of H-Ras^{V12} resulted in the mislocalization of laminin 5 to the cytosol, with no evidence of polarized deposition at the cell-ECM interface. Notably, this aberrant cytosolic staining pattern was especially prominent in the protrusions of H-Ras^{V12} cultures. Correlating with the decreased formation of invasive protrusions, ATG knockdown resulted in the restoration of polarized laminin 5 secretion, and based on this marker, we observed that most individual structures in ATG deficient H-Ras^{V12} cultures were encompassed by an intact basement membrane (Figure 3-3A). Hence, in addition to restricting the formation of invasive protrusions, autophagy inhibition restores polarized basement membrane secretion that is absent in H-Ras^{V12} shCNT structures.

To extend these results, we evaluated ECM proteolytic activity in control and autophagy-deficient H-Ras^{V12} cultures by assessing fluorescence emanating from the proteolytic cleavage of dye-quenched collagen IV. In control non-transformed acini (BABE), we observed a faint ring of fluorescence surrounding each structure, corresponding to collagen-IV degradation resulting from the normal outgrowth of acini during 3D morphogenesis. On the other hand, H-Ras^{V12} shCNT-expressing structures exhibited high levels of fluorescence that

extended well beyond the immediate vicinity of individual structures (Figure 3-3B). Notably, streaks of fluorescence connecting adjacent structures were frequently observed in H-Ras^{V12} shCNT cultures (Figure 3-3B), which resembled the networks of invasive protrusions (Figure 3-1B). In contrast, H-Ras^{V12} shATG-derived structures exhibited a ring-like collagen IV degradation pattern that was restricted to the cell-ECM interface, similar to that observed in non-transformed controls (Figure 3-3B). Thus, the absence of morphological protrusions in ATG deficient H-Ras^{V12} cultures was associated with the restoration of basement membrane integrity as well as with reduced ECM proteolytic activity. Together these findings indicate that intact autophagy is required for Ras-driven invasion in 3D culture.

ATG depletion in H-Ras^{V12} structures does not promote apoptosis or proliferation arrest in 3D culture.

We next evaluated the effects of autophagy inhibition on cell death and proliferation in H-Ras^{V12} 3D cultures. During normal MCF10A acinar morphogenesis, autophagy inhibition results in the enhanced apoptosis of cells occupying the luminal space (Fung et al., 2008). To test whether autophagy deficiency similarly impacted apoptosis in H-Ras^{V12} structures, we immunostained structures with an antibody against cleaved caspase-3. In contrast to the robust luminal apoptosis observed in control acini (BABE), we observed rare, isolated cleaved caspase-3 positive cells in H-Ras^{V12} shCNT structures consistent with the ability of oncogenic Ras to promote the survival of

cells in 3D culture (Figure 3-4A). Remarkably, ATG knockdown did not enhance apoptosis in H-Ras^{V12} structures. In fact, similar to their autophagy competent counterparts, only rare cleaved caspase-3 positive cells were observed in autophagy deficient H-Ras^{V12} structures (Figure 3-4A). To assess whether autophagy inhibition potentially impacted non-apoptotic death processes, we also stained day 8 3D cultures with ethidium bromide (EtBr), an intravital dye that is incorporated into all dying cells. Whereas acini derived from non-transformed (BABE) cells displayed a high levels of EtBr staining corresponding to luminal cell death (Figure 3-5), H-Ras^{V12} structures displayed only occasional EtBr cells scattered throughout the structures. Although ATG knockdown in H-Ras^{V12} cultures resulted in spherical structures that lacked invasive protrusions, we did not observe an increase in EtBr staining in these cultures (Figure 3-5). Thus, in the context of oncogenic Ras activation in 3D culture, autophagy inhibition does not enhance cell death.

We next evaluated the effects of autophagy inhibition on the proliferative capacity of H-Ras^{V12} 3D structures by immunostaining acini with the proliferation marker Ki67. On day 5, BABE, H-Ras^{V12} shCNT and H-Ras^{V12} shATG expressing structures were all highly Ki67 positive (Figure 3-4B, top panels). By day 8, few BABE structures remained Ki67 positive, indicating these acini had undergone proliferative arrest as previously described (Muthuswamy et al., 2001). On the other hand, H-Ras^{V12} cultures continued to exhibit high levels of Ki67 positive cells. Interestingly, the spherical structures derived from ATG-deficient H-Ras^{V12} cells also remained highly proliferative on day 8 (Figure 3-4B). At higher

magnification, low levels of Ki67 positive cells were observed in BABE structures, which were mostly present in the outer layer of cells that are in direct contact with the ECM. In contrast, both autophagy competent (shCNT) and autophagy depleted H-Ras^{V12} structures displayed numerous Ki67 positive cells that were located throughout the structures (Figure 3-4C). Overall these results indicate that although autophagy deficiency potently restricts H-Ras^{V12} driven invasion, it does not universally suppress the diverse oncogenic effects of H-Ras^{V12} in 3D culture, including the ability of activated Ras to inhibit apoptosis and sustain proliferation.

Autophagy supports the migration of epithelial cells expressing oncogenic Ras.

As defects in invasive capacity are often associated with diminished cell motility, we compared the rates of monolayer wound closure between autophagy competent and deficient epithelial cells. Compared to shCNT cells, ATG knockdown in H-Ras^{V12} MCF10A cells resulted in an approximately 30% decrease in wound closure at 6h following the initial wounding (Figure 3-6A). Similar results were obtained using a transwell migration assay, which demonstrated a 40-85% decrease in migration of ATG knockdown cells (Figure 3-6B). We further corroborated these results using MDA-MB-231 cells, a highly migratory, K-Ras mutant breast cancer cell line. siRNA-mediated knockdown of either ATG7 or ATG12 in MDA-MB-231 cells resulted in reduced LC3-II formation (Figure 3-6C) as well as a decrease in wound closure (Figure 3-6D). A similar

decrease in MDA-MB-231 migration was also observed in the presence of the lysosomal inhibitor bafilomycin A (Figure 3-6E). Therefore, in addition to supporting invasion of H-Ras^{V12} MCF10A cells in 3D culture, autophagy facilitates the migration of cells expressing oncogenic Ras in monolayer culture.

Altered differentiation of H-Ras^{V12} MCF10A cells upon autophagy inhibition.

In addition to promoting invasion and migration, oncogenic Ras activation has been shown to alter differentiation in epithelial cells by driving an epithelial-mesenchymal transition (EMT; (Shin et al., 2010; Thiery, 2003), a process associated with increased invasive and migratory capacity *in vitro* and with metastatic capacity *in vivo* (Polyak and Weinberg, 2009). Therefore, we evaluated how autophagy inhibition affects both gene and protein expression changes associated with Ras-induced EMT. We isolated BABE, H-Ras^{V12} shCNT and H-Ras^{V12} shATG7-1 expressing cells from day 8 3D cultures and determined the expression of a panel of EMT associated genes by qPCR array. Relative to BABE controls, H-Ras^{V12} structures displayed a significant decrease in the expression of the epithelial markers *KRT14* (keratin 14) and *CDH1* (E-cadherin) as well an increase in the expression of the mesenchymal markers, *VIM* (vimentin), *FN1* (fibronectin), and *CDH2* (N-cadherin). Strikingly, ATG7 knockdown in H-Ras^{V12} structures resulted in a partial restoration in the expression levels of the epithelial transcripts, *KRT14* and *CDH1*, and a partial decrease in the mesenchymal transcripts, *VIM* and *FN1* compared to H-Ras^{V12} shCNT (Figure 3-7A and Figure 3-8A). In contrast, no change in the

mesenchymal marker *CDH2* was observed following shATG7-1 expression (Figure 3-8A). To confirm these results, we examined the protein levels of these markers in H-Ras^{V12} shCNT and shATG expressing cells following 8 days in 3D culture. Expression of shATG7-1, as well as shATG7-2 and shATG12 in H-Ras^{V12} cells, resulted in an increase in keratin 14 protein levels and a corresponding decrease in vimentin levels compared to H-Ras^{V12} shCNT cells isolated from 3D culture (Figure 3-7B). We also observed increased E-cadherin protein levels and decreased fibronectin upon shATG7-1 expression; however, these changes were not observed in shATG7-2 or shATG12 cells (Figure 3-8B). In accordance with the qPCR array data, N-cadherin protein levels in H-Ras^{V12} structures were unchanged following ATG knockdown (Figure 3-8C).

During EMT, cells commonly lose the ability to form cell-cell junctions (Xu et al., 2009). Therefore, we analyzed the effects of autophagy inhibition on adherins junctions in H-Ras^{V12} MCF10A 3D structures by immunostaining for b-catenin. Normal MCF10A acini (BABE) displayed strong b-catenin staining at cell-cell contacts, indicating intact adherens junctions, whereas the expression of H-Ras^{V12} resulted in a near-complete loss of b-catenin junctional staining and only isolated focal areas of junctional b-catenin staining were observed (Figure 3-7C, left panels). Upon ATG knockdown in H-Ras^{V12} structures, both the expression and junctional localization of b-catenin were significantly restored (Figure 3-7C). Hence, ATG knockdown has multiple effects on H-Ras^{V12} differentiation in 3D culture, most notably the suppression of vimentin, as well as the restoration of keratin 14 expression and epithelial cell-cell contacts. Based on

these results, we construe that autophagy contributes to the maintenance of mesenchymal differentiation in H-Ras^{V12}-transformed epithelial cells in addition to supporting Ras-driven invasion and migration.

Decreased production of IL-6 contributes to reduced invasion in autophagy deficient H-Ras^{V12} cells.

Both cell migration and invasion require the secretion of multiple factors that cooperate to promote motility and to degrade the surrounding ECM (Friedl and Wolf, 2003; Scheel et al., 2011). To ascertain if the invasion defect following autophagy inhibition was due to the impaired production of pro-migratory secreted factors, we performed a co-culture assay of H-Ras^{V12} shATG7-1 cells (stably co-expressing GFP for tracking purposes) with H-Ras^{V12} shCNT cells. Whereas H-Ras^{V12} shATG7-1-GFP cells cultured alone grew as spherical structures with no evidence of invasive branches (Figure 3-9A, left panels), upon co-culture with H-Ras^{V12} shCNT cells, H-Ras^{V12} shATG7-1-GFP structures became dispersed and formed invasive protrusions (Figure 3-9A, right panels). This result indicated that factors from neighboring H-Ras^{V12} shCNT cells are sufficient to rescue in trans the invasion defect in H-Ras^{V12} shATG7-1 cells, suggesting autophagy knockdown alters the production of secreted factors that promote invasion.

During Ras-induced senescence, ATG depletion inhibits IL-6 production following acute oncogenic Ras activation in IMR90 fibroblasts indicating autophagy supports the production of IL-6 in response to oncogenic Ras

activation (Young et al., 2009). Because IL-6 has been demonstrated to support Ras-driven tumorigenesis, promote migration and invasion, as well drive epithelial-mesnchymal transition (Ancrile et al., 2007; Leslie et al., 2010; Sullivan et al., 2009), we tested whether IL-6 levels were altered in H-Ras^{V12} shATG 3D cultures. We first examined IL-6 localization in 3D cultures on day 6, a timepoint at which H-Ras^{V12} structures have formed invasive protrusions. Staining of normal MCF10A structures (BABE) revealed a low level of IL-6 expression that was concentrated at the basal surface of each structure. In contrast, H-Ras^{V12} shCNT structures displayed enhanced IL-6 staining that was most prominent in the cells comprising invasive protrusions (Figure 3-9B). In H-Ras^{V12} shATG expressing acini, IL-6 staining was primarily restricted to cells to the basal surface similar to non-transformed (BABE) acini (Figure 3-9B). Because of this restricted IL-6 expression pattern observed in autophagy-deficient H-Ras^{V12} structures, we hypothesized that the levels of secreted IL-6 may be reduced in shATG expressing 3D cultures. In support, analysis of IL-6 levels in conditioned media collected from 3D cultures by ELISA indicated IL-6 levels in H-Ras^{V12} shATG expressing 3D cultures were significantly reduced in comparison to H-Ras^{V12} shCNT cultures (Figure 3-9C). qPCR analysis of cells collected from 3D culture revealed an increase (rather than decrease) in *IL-6* transcript levels in H-Ras^{V12} shATG cells compared to autophagy competent (shCNT) cells indicating the decrease in IL-6 secretion was not due to reduced gene expression (Figure 3-9D). These results are consistent with previous findings in models of Ras-induced senescence, which also demonstrated a decrease in IL-6 protein levels,

but not transcripts, in autophagy deficient cells (Narita et al., 2011; Young et al., 2009). Thus, in H-Ras^{V12} transformed cells grown in 3D culture, autophagy facilitates the production of IL-6 by a post-transcriptional mechanism.

To ascertain the functional significance of these results, we tested whether treatment with exogenous IL-6 was sufficient to restore invasion in H-Ras^{V12} shATG expressing cells during 3D morphogenesis. Addition of recombinant IL-6 to 3D cultures of H-Ras^{V12} shATG7 and shATG12 cells disrupted structure integrity, resulting in large globular structures, and enhanced the formation of invasive branches compared to their untreated counterparts (Figure 3-9E). These results indicate that autophagy supports the production of IL-6 in H-Ras^{V12} cells grown in 3D culture. Furthermore, the partial restoration in invasive capacity of H-Ras^{V12} shATG structures following the addition of recombinant IL-6 suggests that the decreased IL-6 production resulting from autophagy inhibition contributes to the decrease in invasion.

Autophagy facilitates *MMP-2* and *WNT5A* expression by H-Ras^{V12} cells in 3D culture.

In addition, we further analyzed the qPCR array data of EMT-associated factors from the studies above and identified *WNT5A* and *MMP2* as two secreted factors that were upregulated in H-Ras^{V12} cells, but potently suppressed upon ATG7 knockdown. Further qPCR analysis of cells collected from 3D cultures confirmed a 2-fold decrease in *MMP2* and *WNT5A* expression following ATG knockdown (Figure 3-10A and B). Because these secreted factors have been

implicated in facilitating cell migration, invasion and mesenchymal differentiation, we further evaluated whether the decrease in their expression following ATG knockdown also contributed to the reduced invasive potential of H-Ras^{V12} shATG cells. First, we utilized gelatin zymography to assess MMP2 activity in conditioned media from 3D cultures. As expected, MMP2 activity was enhanced in H-Ras^{V12} cells compared to non-transformed (BABE) controls, and upon ATG knockdown in H-Ras^{V12} cells, this activity was reduced (Figure 3-10C). In addition, we found the increase in MMP-2 expression and secretion that occurs following constitutive Ras activation is necessary for Ras-driven invasion as addition of an MMP-2 inhibitor, Arp-100, was sufficient to inhibit the formation of invasive protrusions in H-Ras^{V12} 3D cultures (Figure 3-10D). Furthermore, using cells isolated from 3D culture, we found that the decrease in *WNT5A* expression correlated with a slight decrease in Wnt5a protein levels in H-Ras^{V12} shATG cells by immunoblot analysis on cells collected from 3D culture (Figure 3-10E). Moreover, the addition of recombinant Wnt5a to H-Ras^{V12} shATG7-1 3D cultures promoted the dissociation of cells within the structures and enhanced the formation of invasive protrusions (Figure 3-10F). Overall, these data indicate that autophagy supports the production of multiple secreted pro-migratory and invasive factors in cells expressing oncogenic Ras, which contribute to Ras-driven invasion in 3D culture.

References

Ancrile, B., K.H. Lim, and C.M. Counter. 2007. Oncogenic Ras-induced secretion of IL6 is required for tumorigenesis. *Genes Dev*. 21:1714-9.

Debnath, J., and J.S. Brugge. 2005. Modelling glandular epithelial cancers in three-dimensional cultures. *Nat Rev Cancer*. 5:675-88.

Debnath, J., K.R. Mills, N.L. Collins, M.J. Reginato, S.K. Muthuswamy, and J.S. Brugge. 2002. The role of apoptosis in creating and maintaining luminal space within normal and oncogene-expressing mammary acini. *Cell*. 111:29-40.

Friedl, P., and K. Wolf. 2003. Tumour-cell invasion and migration: diversity and escape mechanisms. *Nat Rev Cancer*. 3:362-74.

Fung, C., R. Lock, S. Gao, E. Salas, and J. Debnath. 2008. Induction of Autophagy during Extracellular Matrix Detachment Promotes Cell Survival. *Mol Biol Cell*. 19:797-806.

Leslie, K., S.P. Gao, M. Berishaj, K. Podsypanina, H. Ho, L. Ivashkiv, and J. Bromberg. 2010. Differential interleukin-6/Stat3 signaling as a function of cellular context mediates Ras-induced transformation. *Breast Cancer Res*. 12:R80.

Lock, R., S. Roy, C.M. Kenific, J.S. Su, E. Salas, S.M. Ronen, and J. Debnath. 2011. Autophagy facilitates glycolysis during Ras-mediated oncogenic transformation. *Mol Biol Cell*. 22:165-78.

Muthuswamy, S.K., D. Li, S. Lelievre, M.J. Bissell, and J.S. Brugge. 2001. ErbB2, but not ErbB1, reinitiates proliferation and induces luminal repopulation in epithelial acini. *Nat Cell Biol*. 3:785-92.

Narita, M., A.R. Young, S. Arakawa, S.A. Samarajiwa, T. Nakashima, S. Yoshida, S. Hong, L.S. Berry, S. Reichelt, M. Ferreira, S. Tavare, K. Inoki, S. Shimizu, and M. Narita. 2011. Spatial coupling of mTOR and autophagy augments secretory phenotypes. *Science*. 332:966-70.

Oft, M., J. Peli, C. Rudaz, H. Schwarz, H. Beug, and E. Reichmann. 1996. TGF-beta1 and Ha-Ras collaborate in modulating the phenotypic plasticity and invasiveness of epithelial tumor cells. *Genes Dev*. 10:2462-77.

Petersen, O.W., L. Ronnov-Jessen, A.R. Howlett, and M.J. Bissell. 1992. Interaction with basement membrane serves to rapidly distinguish growth and differentiation pattern of normal and malignant human breast epithelial cells. *Proc Natl Acad Sci U S A*. 89:9064-8.

Polyak, K., and R.A. Weinberg. 2009. Transitions between epithelial and mesenchymal states: acquisition of malignant and stem cell traits. *Nat Rev Cancer*. 9:265-73.

Scheel, C., E.N. Eaton, S.H. Li, C.L. Chaffer, F. Reinhardt, K.J. Kah, G. Bell, W. Guo, J. Rubin, A.L. Richardson, and R.A. Weinberg. 2011. Paracrine and autocrine signals induce and maintain mesenchymal and stem cell States in the breast. *Cell*. 145:926-40.

Shin, S., C.A. Dimitri, S.O. Yoon, W. Dowdle, and J. Blenis. 2010. ERK2 but not ERK1 induces epithelial-to-mesenchymal transformation via DEF motif-dependent signaling events. *Mol Cell*. 38:114-27.

Sullivan, N.J., A.K. Sasser, A.E. Axel, F. Vesuna, V. Raman, N. Ramirez, T.M. Oberyszyn, and B.M. Hall. 2009. Interleukin-6 induces an epithelial-mesenchymal transition phenotype in human breast cancer cells. *Oncogene*. 28:2940-7.

Thiery, J.P. 2003. Epithelial-mesenchymal transitions in development and pathologies. *Curr Opin Cell Biol*. 15:740-6.

Xu, J., S. Lamouille, and R. Derynck. 2009. TGF-beta-induced epithelial to mesenchymal transition. *Cell Res*. 19:156-72.

Young, A.R., M. Narita, M. Ferreira, K. Kirschner, M. Sadaie, J.F. Darot, S. Tavare, S. Arakawa, S. Shimizu, F.M. Watt, and M. Narita. 2009. Autophagy mediates the mitotic senescence transition. *Genes Dev*. 23:798-803.

FIGURE LEGENDS

Figure 3-1. Autophagy is required for the elaboration of invasive protrusions mediated by H-Ras^{V12} in 3D culture.

(A-B) H-Ras^{V12} MCF10A cells stably expressing non-targeting control shRNA (shCNT) or shRNAs against autophagy genes (shATGs) were cultured on Matrigel for the indicated number of days. Representative phase contrast images at the indicated magnifications are shown. Bar, 100mm.

Figure 3-2. ATG knockdown inhibits Ras-driven invasion in 3D culture.

(A) MCF10A cells expressing an empty vector control (BABE) were grown in 3D culture and imaged at the indicated times by phase contrast microscopy. Bar, 100mm.

(B) MCF10A H-Ras^{V12} cells expressing shCNT or shATGs were lysed and subject to immunoblot analysis with the indicated antibodies.

(C) MCF10A H-Ras^{V12} cells expressing shCNT or shATGs were grown in monolayer (top) or 3D culture for 8 days (bottom), lysed, and subject to immunoblotting with the indicated antibodies.

(D) H-Ras^{V12} shCNT or shATG expressing cells were grown in full media or starved in HBSS in the presence or absence of E64d and pepstatin A (E/P). Cells were lysed and subject to immunoblotting with antibodies against LC3 and a-tubulin.

(E) Top: MCF10A H-Ras^{V12} shCNT and shATG3 cells were grown in 3D culture for 8 days. Bottom: MCF10A H-Ras^{V12} cells were grown untreated in 3D culture or in the presence of 5mM chloroquine or 5nM bafilomycin A (Baf-A). Acini were imaged by phase contrast microscopy. Bar, 100mm.

(F) BABE, H-Ras^{V12} shCNT, and H-Ras^{V12} shATG cells were grown in 3D culture for 8 days. Cells were collected and lysed and the levels of Ras and phospho-ERK1&2 were determined by immunoblot analysis.

Figure 3-3. Autophagy inhibition in H-Ras^{V12} cells restores basement membrane integrity and restricts ECM proteolysis in 3D culture.

(A) H-Ras^{V12} MCF10A cells expressing shCNT or shATGs were cultured in 3D for 8 days. Structures were fixed and immunostained with antibodies against the basement membrane protein laminin 5 (human specific), counterstained with DAPI to detect nuclei, and imaged by confocal microscopy. Bar, 50mm.

(B) H-Ras^{V12} MCF10A cells were cultured on Matrigel containing 25mg/mL fluorescein DQ-collagen IV for 5 days. Structures were fixed, counterstained with phalloidin (to visualize F-actin) and DAPI (to detect cell nuclei) and imaged by confocal microscopy. Green fluorescence represents areas of proteolytic cleavage of the DQ-collagen present in the extracellular matrix. Bar, 50mm.

Figure 3-4. Autophagy inhibition in MCF10A H-Ras^{V12} structures does not promote apoptosis or proliferative arrest.

(A) H-Ras^{V12} MCF10A cells expressing shCNT or shATGs were cultured in 3D for 8 days, fixed, and immunostained with anti-cleaved caspase-3 to detect apoptotic cells, counterstained with DAPI to detect nuclei, and imaged by confocal microscopy. Bar, 50mm.

(B) H-Ras^{V12} MCF10A cells expressing shCNT or shATGs were grown in 3D for either 5 or 8 days. Structures were fixed, and immunostained with anti-Ki67 and imaged using wide-field fluorescence microscopy. Representative Ki-67 positive structures and the corresponding phase contrast images are shown. Bar, 100mm.

(C) H-Ras^{V12} MCF10A cells expressing shCNT or shATGs were cultured in 3D for 8 days. Structures were fixed, stained with anti-Ki67 and DAPI and imaged by confocal microscopy. Bar, 50mm.

Figure 3-5. Autophagy knockdown in H-Ras^{V12} MCF10A cells does not enhance cell death in 3D culture.

BABE, H-Ras^{V12} shCNT, and H-Ras^{V12} shATG cells were grown in 3D culture for 8 days. Cultures were stained with the intravital dye ethidium bromide (EtBr); representative phase contrast and wide-field fluorescence images are shown. Bar, 100mm.

Figure 3-6. ATG knockdown diminishes the motility of cells expressing oncogenic Ras.

(A) Representative phase contrast images and quantification of wounding assay on H-Ras^{V12} MCF10A cells expressing shCNT or shATGs. Confluent monolayers were scratched and wound width was measured at 0 and 6 hours after initial wounding to quantify the decrease in scratch width. Results are expressed as the mean +/- s.d. (shCNT n=16, shATG7-2 n=8, shATG12 n=14; p-values determined by Student's t-test). Bar, 100mm.

(B) Transwell migration of H-Ras^{V12} MCF10A cells expressing shCNT or shATGs. Twenty-four hours after plating, cells that migrated to the bottom of the filter were stained with crystal violet. Results are expressed as the mean crystal violet extracted from stained cells +/- s.d. (n=9; p-values determined by Student's t-test).

(C) Levels of ATG7, ATG5:12 complex, and LC3-I and LC3-II were determined by immunoblot analysis in MDA-MB-231 cells transfected with siCNT, siATG7 or siATG12.

(D-E) Wounding assay of MDA-MB-231 cells expressing siATGs or in presence of 10nM bafilomycin A. Graphs represent the mean decrease in scratch width at 10 hours or 9 hours after initial wounding, respectively +/- s.d. (siCNT n=16, siATG7 n=16, siATG12 n=10, Untreated and BafA n=6; p-values determined by Student's t-test)

Figure 3-7. ATG depletion in H-Ras^{V12} MCF10A cells alters differentiation and restores cell-cell junctions in 3D culture.

(A) MCF10A cells expressing an empty vector (BABE, non-Ras expressing control), H-Ras^{V12} shCNT or H-Ras^{V12} shATG7-1 cells were grown in 3D for 8 days, upon which cells were collected for RNA isolation. Levels of *KRT14* (keratin 14) and *VIM* (vimentin) were determined using a qPCR array for EMT genes. Graphs represent the expression levels relative to non-Ras (BABE) cells.

(B) Immunoblot analysis of protein levels of keratin 14 and vimentin in lysates collected from day 8 3D cultures derived from BABE, H-Ras^{V12} shCNT and H-Ras^{V12} shATG MCF10A cells.

(C) H-Ras^{V12} MCF10A cells expressing shCNT or shATGs were cultured in 3D for 8 days. Structures were fixed, immunostained with anti-b-catenin to detect cell-cell junctions, counterstained with DAPI, and imaged by confocal microscopy. Note that only isolated focal areas of junctional b-catenin staining are detected in H-Ras^{V12} shCNT cultures, whereas robust b-catenin staining is evident at cell-cell junctions throughout BABE and H-Ras^{V12} shATG cultures. Bar, 50mm.

Figure 3-8. ATG depletion in H-Ras^{V12} MCF10A alters differentiation.

(A) RNA was isolated from MCF10A non-Ras expressing (BABE), H-Ras^{V12} shCNT or H-Ras^{V12} shATG7-1 cells grown in 3D culture for 8 days. Expression levels of *CDH1* (E-cadherin), *FN1* (Fibronectin), and *CDH2* (N-cadherin) were

determined using a qPCR array for EMT genes and graphs represent the expression levels relative to BABE cells.

(B) Protein levels of E-cadherin were determined by immunoblot analysis in BABE, H-Ras^{V12} shCNT and shATG7-1 cells collected from 3D culture on day 8.

(C) Protein levels of N-cadherin were determined by immunoblot analysis in BABE and H-Ras^{V12} MCF10A cells expressing shCNT or shATGs collected from 3D culture on day 8.

Figure 3-9. ATG knockdown in H-Ras^{V12} cells inhibits the production of pro-invasive secreted factors, including interleukin 6 (IL6).

(A) MCF10A H-Ras^{V12} shATG7-1 cells co-expressing GFP were cultured for 8 days in 3D either alone (left) or together with H-Ras^{V12} shCNT cells co-expressing an empty vector (BABE). Structures were imaged by phase contrast and wide-field fluorescence microscopy or fixed, counterstained with anti-phalloidin (to visualize F-actin) and DAPI and imaged by confocal microscopy. Phase: Bar, 100mm. Confocal: Bar, 50 mm.

(B) H-Ras^{V12} MCF10A cells expressing shCNT or shATGs were cultured in 3D for 6 days. Structures were fixed and immunostained with anti-IL-6 antibody, counterstained with DAPI and imaged by confocal microscopy. Bar, 50mm.

(C) Levels of IL-6 were determined by ELISA from conditioned media collected over 18h on days 5-6 from 3D cultures of the indicated cell types. Results are expressed as the mean +/- s.d. (n=3; p-values determined by ANOVA).

(D) *IL-6* expression levels from the indicated cell types grown in 3D culture for 8 days were determined by qPCR and normalized to an internal control *GAPDH.* Results represent mean expression relative to BABE, +/- s.d. (n=3; p-value determined by Student's t-test). (E) H-Ras^{V12} MCF10A shATG cells were grown in 3D in the presence or absence of 200ng/mL recombinant human IL-6 for 7 days and imaged by phase contrast microscopy. Bar, 100mm.

Figure 3-10. Wnt5a and MMP2 are reduced following autophagy inhibition in 3D culture.

(A-B) RNA was isolated from MCF10A BABE, H-Ras^{V12} shCNT, and H-Ras^{V12} shATG cells cultured in 3D for 8 days. Expression levels of *MMP2* and *WNT5A* were determined by qPCR and normalized to an internal control *GAPDH*. Results represent the mean expression levels relative to BABE +/- s.d. (*MMP2,* n=4; *WNT5A*, n=3; p-values determined by Student's t-test).

(C) Conditioned media was collected from MCF10A BABE, H-Ras^{V12} shCNT and H-Ras^{V12} shATG MCF10A cells grown in 3D culture. Activity levels of MMP9 and MMP2 in the conditioned media were determined by zymography.

(D) H-Ras^{V12} shCNT MCF10A cells were grown in the absence (top) or presence (bottom) of 25mm Arp-100. Left: Structures were imaged on day 8 by phase contrast microscopy. Right: Representative confocal images of structures immunostained with anti-phospho-ERM to detect cell borders and counterstained with DAPI. Bars, 100mm.

(E) MCF10A Babe, H-Ras^{V12} shCNT, and H-RasV12 shATG cells were collected from 3D culture on day 8, lysed, and protein levels of Wnt5a were determined by immunoblot analysis. (F) MCF10A H-Ras^{V12} shATG7-1 cells were grown in 3D for 8 days in the absence (top) or presence (bottom) of 500ng/mL Wnt5a. Left: Structures were imaged on day 8 by phase contrast microscopy. Right: Representative confocal images of structures immunostained with anti-phospho-ERM to detect cell borders and counterstained with DAPI. Bars, 100mm.

Figure 3-1

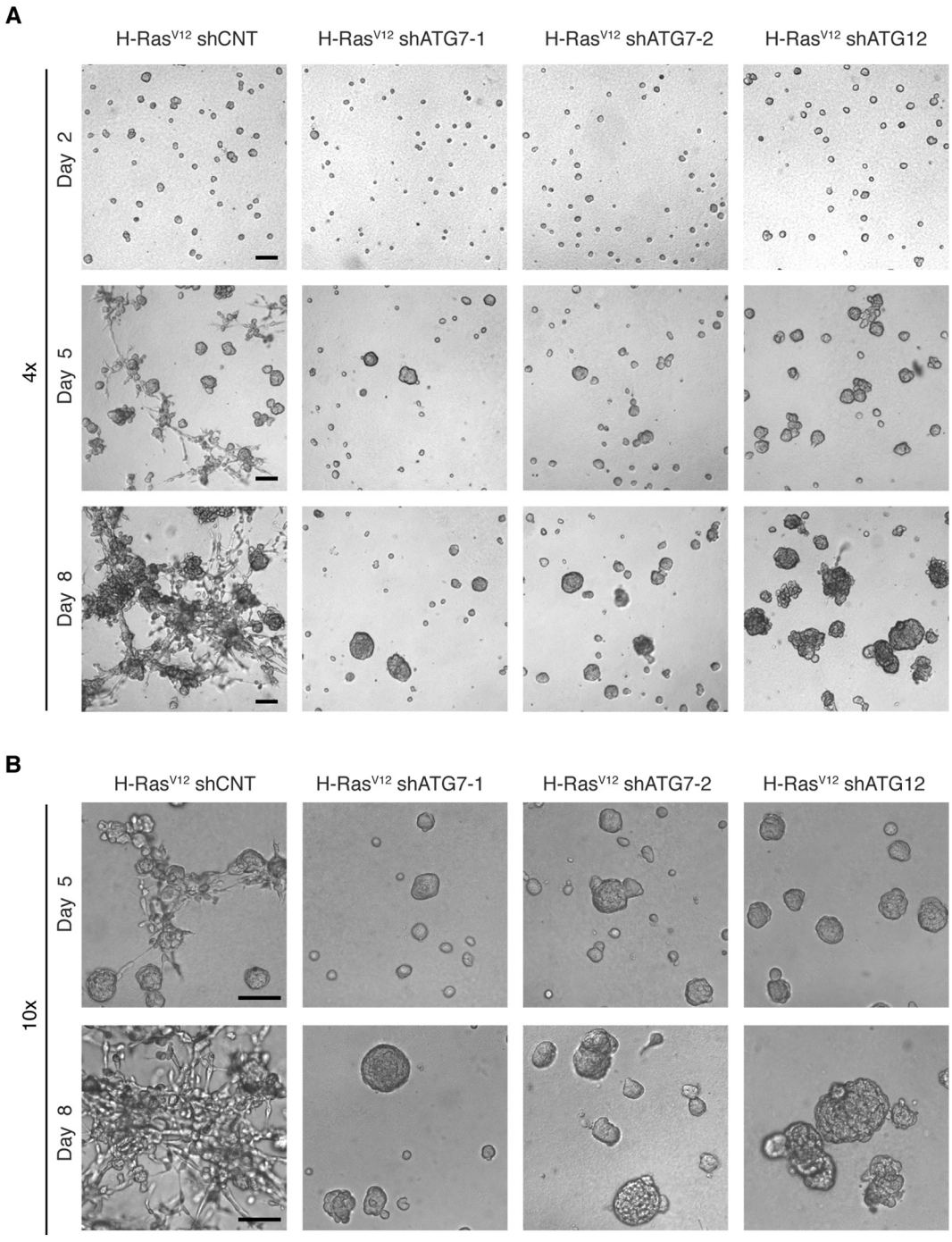
A
H-Ras^{V12} shCNT
H-Ras^{V12} shATG7-1
H-Ras^{V12} shATG7-2
H-Ras^{V12} shATG12
4x
Day 2
Day 5
Day 8
B
H-Ras^{V12} shCNT
H-Ras^{V12} shATG7-1
H-Ras^{V12} shATG7-2
H-Ras^{V12} shATG12
10x
Day 5
Day 8

Figure 3-2

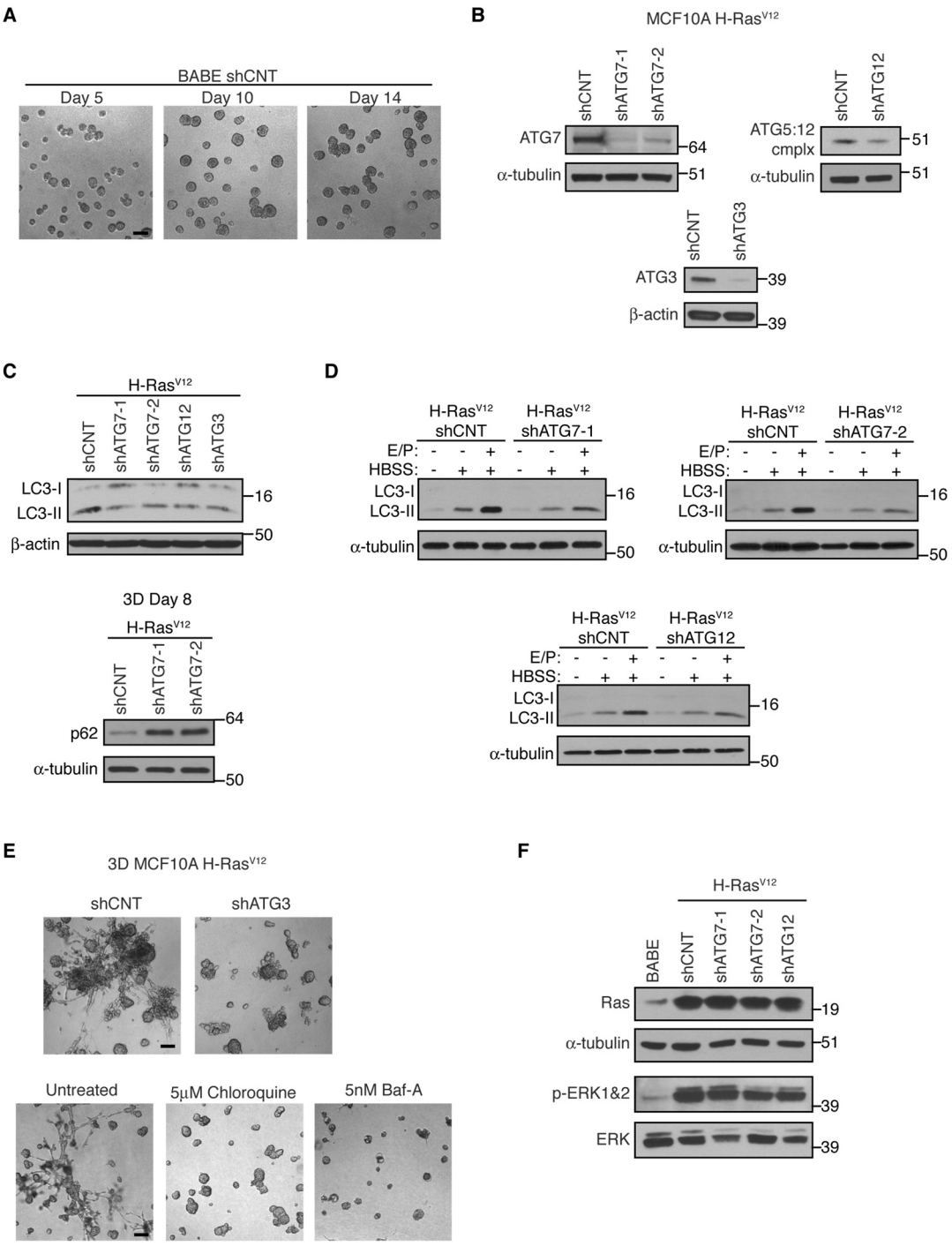
A
BABE shCNT
Day 5
Day 10
Day 14
B
MCF10A H-Ras^{V12}
shCNT
shATG7-1
shATG7-2
ATG7
64
α-tubulin
51
shCNT
shATG12
ATG5:12 cmplx
51
α-tubulin
51
shCNT
shATG3
ATG3
39
β-actin
39
C
H-Ras^{V12}
shCNT
shATG7-1
shATG7-2
shATG12
shATG3
LC3-I
LC3-II
16
β-actin
50
3D Day 8
H-Ras^{V12}
shCNT
shATG7-1
shATG7-2
p62
64
α-tubulin
50
D
H-Ras^{V12} shCNT
H-Ras^{V12} shATG7-1
E/P: - - + - - +
HBSS: - + + - + +
LC3-I
LC3-II
16
α-tubulin
50
H-Ras^{V12} shCNT
H-Ras^{V12} shATG7-2
E/P: - - + - - +
HBSS: - + + - + +
LC3-I
LC3-II
16
α-tubulin
50
H-Ras^{V12} shCNT
H-Ras^{V12} shATG12
E/P: - - + - - +
HBSS: - + + - + +
LC3-I
LC3-II
16
α-tubulin
50
E
3D MCF10A H-Ras^{V12}
shCNT
shATG3
Untreated
5μM Chloroquine
5nM Baf-A
F
H-Ras^{V12}
BABE
shCNT
shATG7-1
shATG7-2
shATG12
Ras
19
α-tubulin
51
p-ERK1&2
39
ERK
39

Figure 3-3

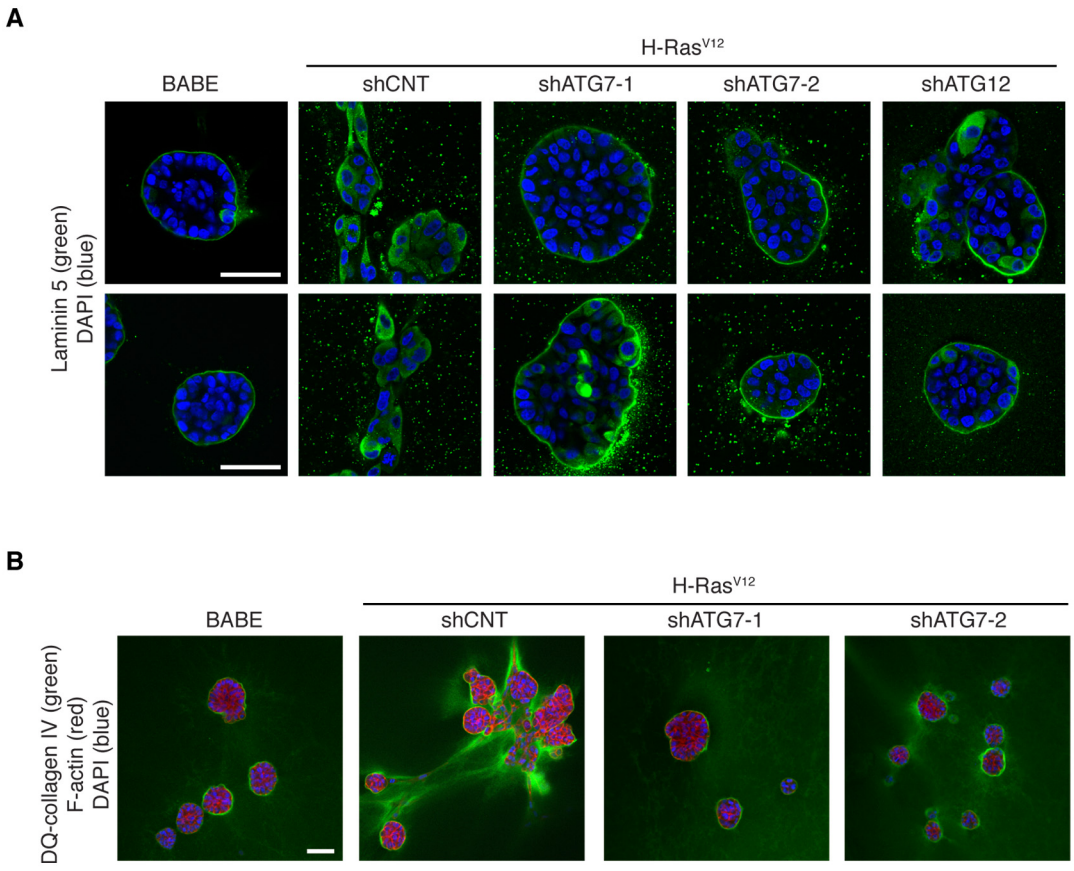
A
H-Ras^{V12}
BABE
shCNT
shATG7-1
shATG7-2
shATG12
Laminin 5 (green)
DAPI (blue)
B
H-Ras^{V12}
BABE
shCNT
shATG7-1
shATG7-2
DQ-collagen IV (green)
F-actin (red)
DAPI (blue)

Figure 3-4

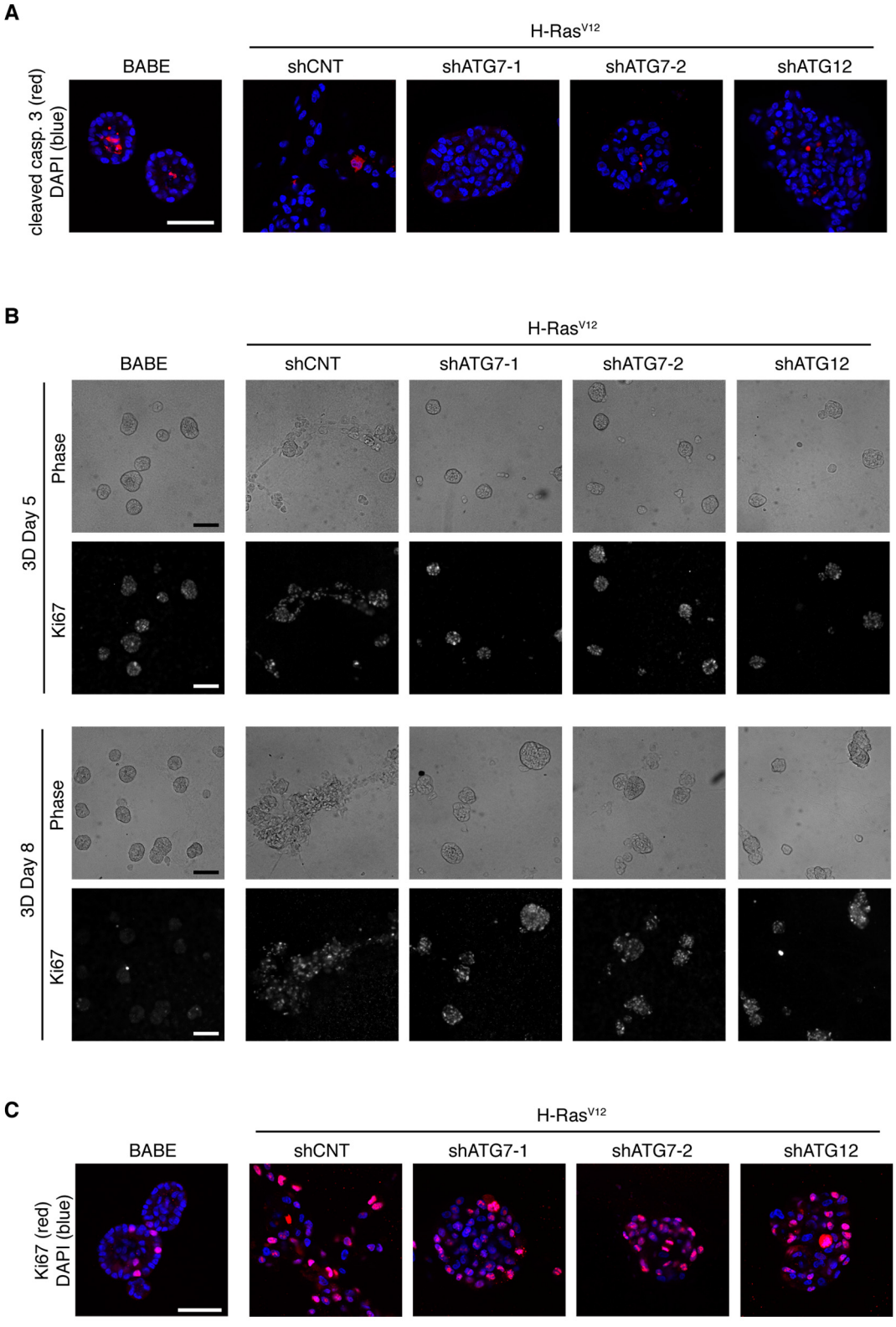
A
H-Ras^{V12}
BABE
shCNT
shATG7-1
shATG7-2
shATG12
cleaved casp. 3 (red)
DAPI (blue)
B
H-Ras^{V12}
BABE
shCNT
shATG7-1
shATG7-2
shATG12
3D Day 5
Phase
Ki67
3D Day 8
Phase
Ki67
C
H-Ras^{V12}
BABE
shCNT
shATG7-1
shATG7-2
shATG12
Ki67 (red)
DAPI (blue)

Figure 3-5

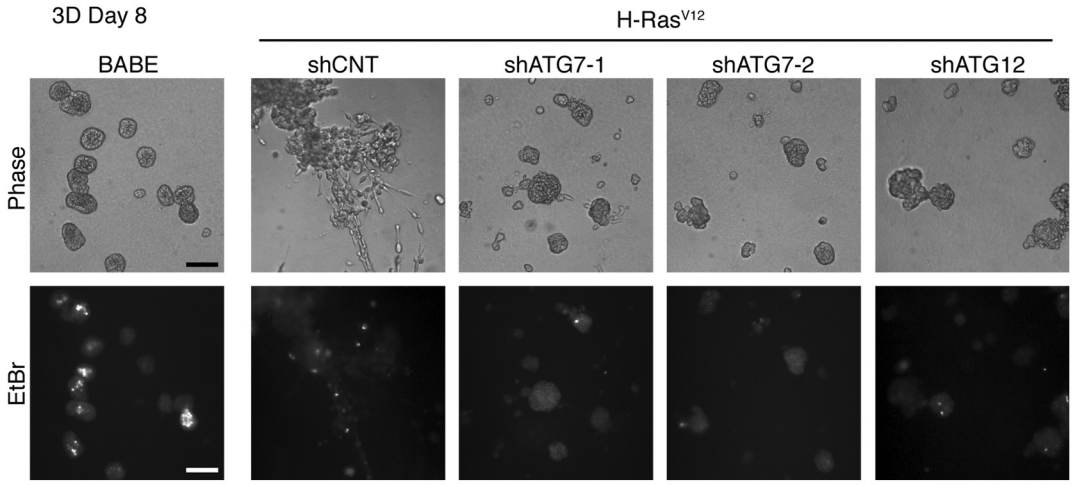
3D Day 8
H-Ras^{V12}
BABE
shCNT
shATG7-1
shATG7-2
shATG12
Phase
EtBr

Figure 3-6

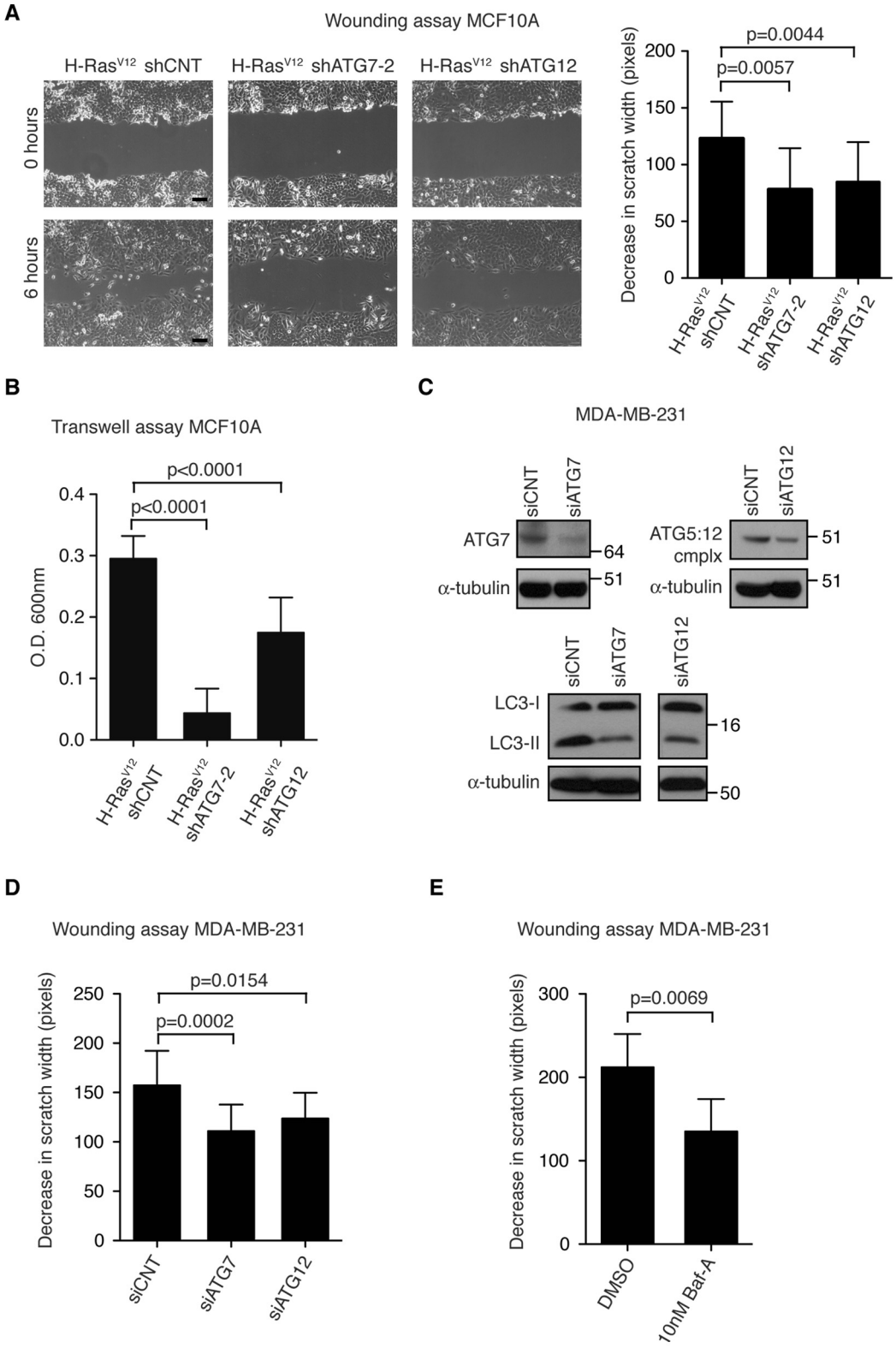
A
Wounding assay MCF10A
H-Ras^{V12} shCNT
H-Ras^{V12} shATG7-2
H-Ras^{V12} shATG12
0 hours
6 hours
Decrease in scratch width (pixels)
p=0.0044
p=0.0057
B
Transwell assay MCF10A
O.D. 600nm
p<0.0001
p<0.0001
C
MDA-MB-231
siCNT
siATG7
siATG12
ATG7
ATG5:12 cmplx
α-tubulin
LC3-I
LC3-II
64
51
16
50
D
Wounding assay MDA-MB-231
p=0.0154
p=0.0002
E
Wounding assay MDA-MB-231
p=0.0069
DMSO
10nM Baf-A

Figure 3-7

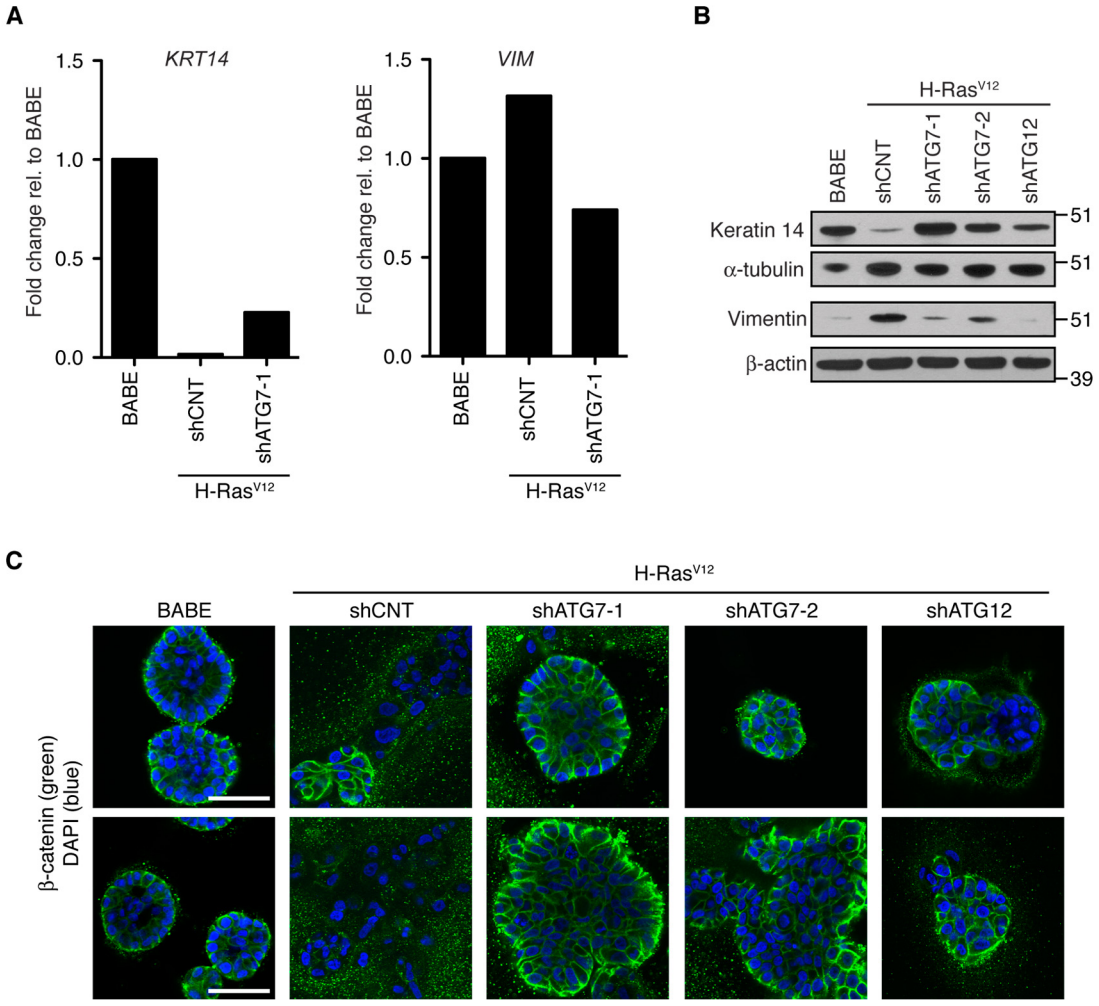
A
KRT14
VIM
Fold change rel. to BABE
1.5
1.0
0.5
0.0
BABE
shCNT
shATG7-1
H-RasV12
B
H-RasV12
BABE
shCNT
shATG7-1
shATG7-2
shATG12
Keratin 14
α-tubulin
Vimentin
β-actin
51
51
51
39
C
H-RasV12
BABE
shCNT
shATG7-1
shATG7-2
shATG12
β-catenin (green)
DAPI (blue)

Figure 3-8

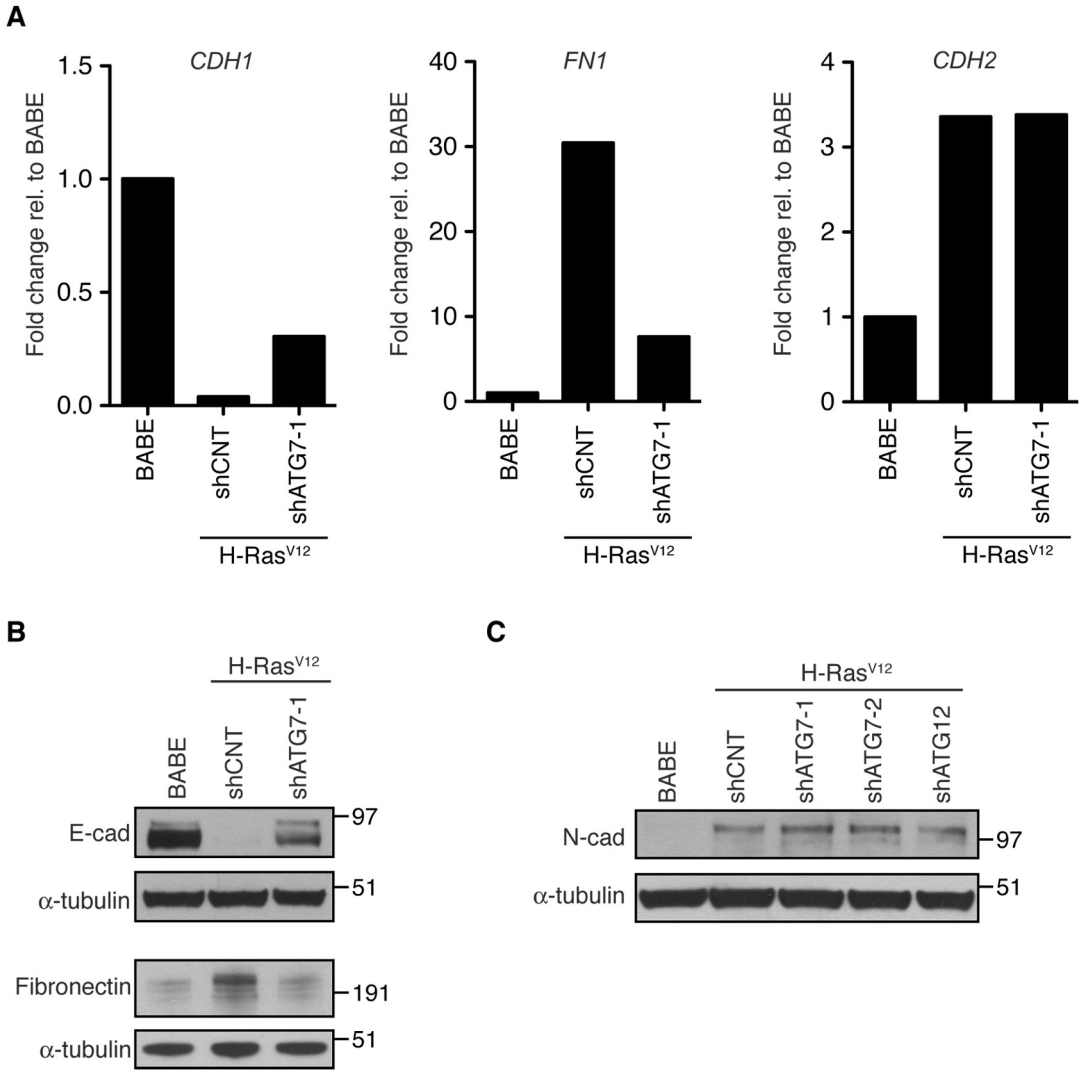
A
CDH1
FN1
CDH2
Fold change rel. to BABE
1.5
1.0
0.5
0.0
40
30
20
10
0
4
3
2
1
0
BABE
shCNT
shATG7-1
H-RasV12
B
C
E-cad
α-tubulin
Fibronectin
N-cad
97
51
191
shATG7-2
shATG12

Figure 3-9

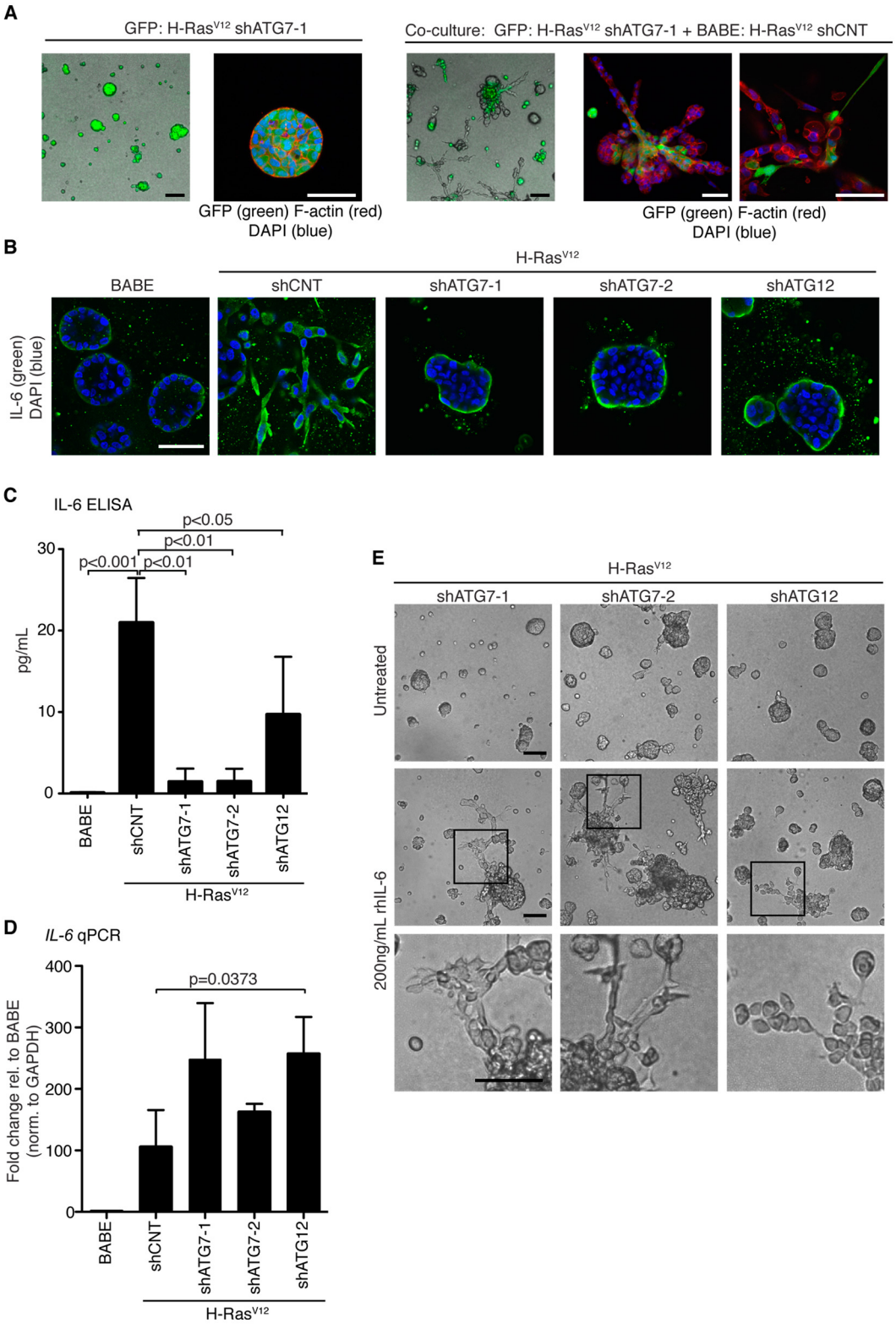
A
GFP: H-Ras^{V12} shATG7-1
Co-culture: GFP: H-Ras^{V12} shATG7-1 + BABE: H-Ras^{V12} shCNT
GFP (green) F-actin (red)
DAPI (blue)
GFP (green) F-actin (red)
DAPI (blue)
B
H-Ras^{V12}
BABE
shCNT
shATG7-1
shATG7-2
shATG12
IL-6 (green)
DAPI (blue)
C
IL-6 ELISA
p<0.05
p<0.01
p<0.001
p<0.01
pg/mL
30
20
10
0
BABE
shCNT
shATG7-1
shATG7-2
shATG12
H-Ras^{V12}
D
IL-6 qPCR
p=0.0373
Fold change rel. to BABE
(norm. to GAPDH)
400
300
200
100
0
BABE
shCNT
shATG7-1
shATG7-2
shATG12
H-Ras^{V12}
E
H-Ras^{V12}
shATG7-1
shATG7-2
shATG12
Untreated
200ng/mL rhIL-6

Figure 3-10

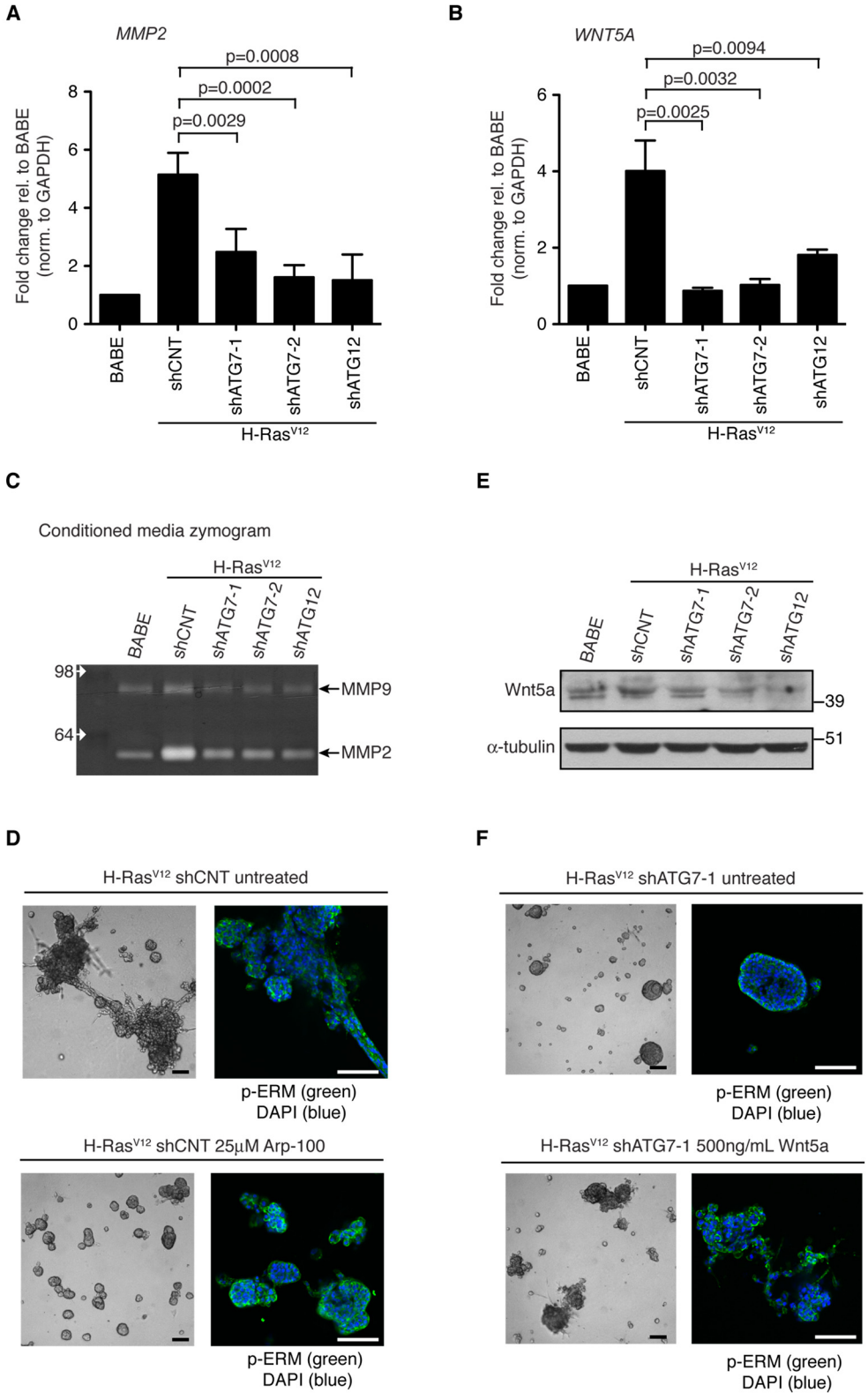
A
MMP2
p=0.0008
p=0.0002
p=0.0029
Fold change rel. to BABE (norm. to GAPDH)
BABE
shCNT
shATG7-1
shATG7-2
shATG12
H-Ras^{V12}
B
WNT5A
p=0.0094
p=0.0032
p=0.0025
C
Conditioned media zymogram
98
64
MMP9
MMP2
E
Wnt5a
α-tubulin
39
51
D
H-Ras^{V12} shCNT untreated
p-ERM (green)
DAPI (blue)
H-Ras^{V12} shCNT 25μM Arp-100
F
H-Ras^{V12} shATG7-1 untreated
H-Ras^{V12} shATG7-1 500ng/mL Wnt5a

Discussion

Autophagy facilitates glycolysis during Ras mediated oncogenic transformation

Autophagy, a highly conserved and tightly regulated catabolic process, is thought to have both pro-tumor and anti-tumor functions (Chen and Debnath, 2010). Several studies have elucidated mechanisms explaining tumor suppressive roles for autophagy. However, less is known about the mechanisms mediating autophagy's pro-tumor functions beyond its role in promoting survival in response to stress. In particular, it was previously unknown how autophagy, a key pathway proposed to sustain core metabolic functions during starvation or stress, contributes to oncogenic transformation. Our studies demonstrate that in the context of a potent oncogene, mutationally active Ras, autophagy promotes adhesion-independent transformation and facilitates glycolysis. The genetic deletion or RNAi-mediated knockdown of autophagy genes (ATGs) causes a potent decrease in anchorage-independent growth in soft agar, indicating that an intact autophagy pathway is required for robust adhesion-independent transformation by oncogenic Ras. Furthermore, autophagy inhibition during Ras transformation results in reduced proliferation and decreased glucose metabolism. The decreased rate of glycolysis observed in Ras-transformed autophagy deficient cells correlates with decreased sensitivity to declining glucose concentrations in comparison to autophagy competent counterparts, both in terms of proliferation and adhesion-independent transformation.

In addition, our results indicate that constitutive Ras activation does not suppress autophagy during ECM detachment. These data differ from previous

reports in both Ras expressing cells *in vitro* as well as Drosophila development *in vivo* (Berry and Baehrecke, 2007; Furuta et al., 2004), both of which demonstrate that Ras activation suppresses autophagy. Ras-mediated suppression of autophagy is proposed to arise secondary to the constitutive activation of the PI3K/mTOR pathway, a negative regulator of autophagy induction. However, upon ECM detachment of several KRas mutant cancer lines, ribosomal protein S6 phosphorylation, an established readout of mTORC1 activity, is rapidly decreased, indicating that Ras is unable to sustain mTORC1 activation in cells deprived of matrix contact. Furthermore, detached MEFs expressing H-Ras^{V12} exhibit decreased S6 phosphorylation comparable to non-transformed controls. On the other hand, in H-Ras^{V12} transformed MCF10A cells, S6 phosphorylation is only slightly reduced following matrix detachment compared to nontransformed counterparts. Interestingly, although we were able to completely inhibit mTORC1 activity by treating H-Ras^{V12} MCF10A cells with rapamycin during suspension, this did not further augment autophagy. This result indicates the enhanced level of mTORC1 activity that persists in H-Ras^{V12} MCF10A cells following detachment is not sufficient to suppress autophagy induction. From these results, we speculate that a partial reduction in mTORC1 activity in H-Ras^{V12} expressing MCF10A cells may be sufficient to promote detachment-induced autophagy. Alternatively, other mTORC1-independent pathways may promote autophagy in detached cells expressing oncogenic Ras. Importantly, our results indicate that oncogenic Ras activation does not inhibit detachment-induced autophagy in mammalian cells.

In addition to confirming that autophagy can be enhanced in the presence of constitutively active Ras, two other groups report enhanced levels of basal autophagy in MCF10A cells or immortalized mouse kidney cells following expression of oncogenic Ras compared to non-Ras expressing controls (Guo et al., 2011; Kim et al., 2011). In MCF10A cells the expression of mutant K-Ras enhances reactive oxygen species and JNK signaling culminating in increased transcription of autophagy genes indicating a potential mechanism through which Ras upregulates basal autophagy (Kim et al., 2011). Although we did not carefully compare basal autophagy levels between non-Ras and Ras-expressing cells in our studies, our observations support these findings. We have observed increased levels of GFP-LC3 puncta in normal growth condition in H-Ras^{V12} cells compared to controls (unpublished observations) and expression of H-Ras^{V12} in mouse embryonic fibroblasts results in a slight decrease in basal p62 levels (Figure 2-1C).

We demonstrate that autophagy is required for robust Ras-driven transformation; cells deleted or depleted of multiple independent ATGs all exhibit decreased anchorage-independent transformation in soft agar. Our results have been corroborated by recent studies from three separate groups demonstrating that autophagy inhibition in MCF10A cells and immortalized kidney epithelial cells expressing activated Ras, or in pancreatic ductal adenocarcinoma cells lines (which have endogenous KRas mutations) results in decreased colony formation and decreased xenograft growth in immunodeficient mice (Guo et al., 2011; Kim

et al., 2011; Yang et al., 2011). Taken together, these results reveal a critical function for autophagy in supporting Ras-driven transformation.

Based on our previous findings that autophagy inhibition promotes extracellular matrix detachment mediated apoptosis (termed anoikis), we initially predicted that decreased Ras-mediated transformation in autophagy deficient cells was due to increased levels of anoikis (Fung et al., 2008). Although apoptosis was increased in H-Ras^{V12} autophagy deficient cells following matrix detachment and could be inhibited by BCL-2 overexpression, inhibiting apoptosis by overexpressing BCL-2 was not sufficient to rescue defects in adhesion-independent transformation. Thus, the ability of autophagy to facilitate Ras transformation cannot be completely explained by its capacity to protect cells from apoptosis during ECM detachment.

These studies point to a previously unrecognized tumor-promoting function for autophagy that manifests during oncogenic Ras transformation. For example, upon matrix detachment, increased numbers of *Atg5-/-* cells continue to proliferate compared to *Atg5+/+* controls. In fact, the enhanced proliferation of autophagy deficient cells has been proposed as a potential mechanism by which autophagy might exert tumor suppressive effects (Fimia et al., 2007; Qu et al., 2003). However, unlike non-transformed autophagy-deficient cells, *Atg5* genetic deletion impedes, rather than enhances, the ability of H-Ras^{V12} transformed MEFs to proliferate during ECM detachment. Similarly, when cultured in attached nutrient-rich conditions, Ras-transformed *Atg5-/-* cells exhibit a marked decrease in proliferation compared to their autophagy-competent counterparts. In addition,

we have also found that MCF10A cells expressing H-Ras^{V12} occasionally undergo growth arrest or cell death following lentiviral-driven introduction of shRNAs against ATGs. In contrast, nontransformed cells consistently remain viable and continue to proliferate upon ATG knockdown (data not shown). Based on these results we conclude that autophagy competence is required for cells to proliferate and expand specifically in the context of constitutive Ras activation.

Increasing evidence indicates that stress response pathways play diverse, multifaceted roles that contribute to oncogenic transformation. For example, heat shock protein 1 (HSP1), an important mediator of the heat shock response, has been implicated as an important facilitator of Ras transformation, which correlates with its ability to modulate both proliferative capacity and glucose metabolism (Dai et al., 2007). Here, we demonstrate that autophagy similarly supports increased glucose metabolism, suggesting a previously unrecognized mechanism by which autophagy may contribute to tumorigenesis. H-Ras^{V12} transformed, autophagy competent MEFs display enhanced glucose uptake compared to their autophagy deficient counterparts. In addition, using ^{13}C-NMR analysis of glucose metabolism, we observe augmented glycolytic flux in H-Ras^{V12} expressing autophagy competent cells as evidenced by increased production of lactate and alanine from glucose. Notably, we have also observed reduced glucose uptake in nontransformed, autophagy deficient cells, but unlike H-Ras^{V12}-transformed cells, these reductions do not correlate with significant changes in lactate production or in monolayer proliferation. Increased glycolysis in tumors, first observed by Otto Warburg, is crucial to support both the increased

energy and synthetic demands required for high rates of proliferation. This metabolic shift in tumor cells is coordinated by upregulating critical components of glycolysis resulting in enhanced glucose uptake and lactate production even in the presence of ample oxygen (Vander Heiden et al., 2009). It is currently unclear whether reduced autophagy specifically elicits changes in glucose metabolism or causes more global metabolic shifts during Ras transformation. We are presently evaluating whether and how other metabolic pathways are affected by the loss or reduction of autophagy.

Although glucose withdrawal and energy depletion have been found to be potent activators of autophagy as a survival response, we have unexpectedly found that the reduction or elimination of autophagy competence can actually reduce glycolytic capacity in a Ras-transformed cell. Hence, we speculate that autophagy may promote oncogenic Ras-driven tumor growth in specific metabolic microenvironments. In support of this hypothesis, decreasing glucose concentrations inhibit soft agar colony formation in H-Ras^{V12} expressing wild-type cells to levels approaching that of H-Ras^{V12} autophagy deficient cells. In contrast, both the proliferation and adhesion independent transformation of autophagy deficient cells is relatively insensitive to reductions in glucose availability.

These data indicate autophagy possess additional pro-tumorigenic functions beyond its established role in supporting the survival of tumor cells exposed to harsh environments. While increased autophagy levels are likely to sustain the viability of tumor cells lacking access to nutrients and oxygen, we propose that basal autophagy supports the rapid proliferation of all cells within

the tumor, in part by enhancing glycolytic capacity (Figure 4). In addition to glycolysis, autophagy may impact other metabolic pathways. For example, in Ras-transformed kidney epithelial cells and pancreatic ductal adenocarcinoma cells the loss of autophagy is associated with reduced oxygen consumption and decreased levels of tricarboxylic acid (TCA) cycle intermediates (Guo et al., 2011; Yang et al., 2011). Nonetheless, how autophagy deficiency alters glycolysis, either directly or indirectly, remains an important question for future investigation. Another important area is delineating how autophagy generally impacts metabolism in cells expressing other oncogenes, such as Myc and activated PI3K, which also elicit metabolic changes that support the transformed phenotype.

Autophagy supports oncogenic Ras-driven invasion, migration and mesenchymal differentiation

Previous studies demonstrate a critical role for autophagy in suppressing tumor initiation and in promoting the growth and survival of tumor cells. However, little is known about how autophagy influences cell biological processes that support tumor cell invasion and metastasis. Using a 3D culture system, we demonstrate that inhibition of autophagy in H-Ras^{V12} MCF10A cells restricts the formation of invasive protrusions, restores the polarized secretion of basement membrane proteins, and attenuates ECM proteolysis. Furthermore, upon ATG depletion in H-Ras^{V12} MCF10A cells and MDA-MB-231 cells, a K-Ras mutant breast cancer cell line, we observe significantly decreased cell motility. In

addition, we find that autophagy inhibition in H-Ras^{V12} cells elicits the coordinate reduction of multiple molecules that favor invasion. These include a decrease in the production of the pro-migratory cytokine IL-6 via a post-transcriptional mechanism, as well as the diminished transcription of additional pro-invasive factors, including MMP2 and Wnt5a.

Although we find that autophagy inhibition is sufficient to suppress invasion in 3D culture, it does not completely restore the formation of normal acini. Rather, the oncogenic activation of Ras continues to disrupt fundamental aspects of 3D morphogenesis even in autophagy deficient cells. Autophagy inhibition does not alter the ability of H-Ras^{V12} to suppress apoptosis in 3D culture. Whereas the cells occupying the lumen of normal MCF10A acini readily undergo apoptosis due to the lack of ECM contact, we demonstrate here that H-Ras^{V12} expression potently suppresses cell death, resulting in only occasional apoptotic cells in these structures. Similarly, ATG deficient H-Ras^{V12} structures do not exhibit luminal apoptosis or evidence of hollow lumen formation, despite the restoration of a grossly spheroidal morphology and the deposition of a polarized basement membrane. Thus, in contrast to normal MCF10A acini, where autophagy protects ECM-detached cells from luminal apoptosis, Ras-transformed cells lacking direct ECM contact are able to survive even upon inhibiting autophagy in 3D culture (Fung et al., 2008). Moreover, autophagy inhibition does not elicit a global proliferative arrest in H-Ras^{V12} 3D cultures. Interestingly, ATG depletion induces two distinct phenotypes of 3D structures: smaller cell clusters that exhibit low levels of proliferation and larger spherical

outgrowths that remain highly proliferative over extended periods in 3D culture. Similar dichotomous effects on proliferation have previously been described in studies of Notch pathway activation in MCF10A 3D culture (Mazzone et al., 2010). Despite increased Ki-67 activity and the absence of apoptosis, these large, proliferative structures display no evidence of invasive protrusions. Hence, we conclude that decreased invasion due to autophagy inhibition represents a distinct phenotype in 3D culture.

Cell invasion requires the production and directed secretion of factors that stimulate migration and degrade the surrounding ECM (Friedl and Wolf, 2003). Upon co-culture of autophagy depleted H-Ras^{V12} cells with their autophagy competent counterparts, the ability of autophagy deficient cells to form invasive protrusions in 3D culture is restored, suggesting that autophagy is required for the efficient production of secreted factors that promote invasion and migration of H-Ras^{V12} cells. In support, we observed a decrease in multiple pro-migratory factors, including IL-6, an inflammatory cytokine known to promote cell migration and invasion in a variety of cell types (Leslie et al., 2010; Sullivan et al., 2009; Tang et al., 2011). Importantly, upon addition of recombinant IL-6, we were able to significantly restore the formation of invasive protrusions in H-Ras^{V12} shATG 3D cultures, indicating that depletion of this cytokine following ATG knockdown is an important mediator of the reduction in invasive capacity. However, as this rescue is still partial, we speculate that autophagy facilitates the production of additional unidentified secreted factors that promote invasion.

Whereas *IL-6* transcript levels are slightly increased following autophagy knockdown in H-Ras^{V12} cells, the secreted levels of IL-6 in 3D culture are significantly reduced, indicating that autophagy is required for robust IL-6 production through a post-transcriptional mechanism. These results are strikingly reminiscent of recent work demonstrating that autophagy is required for the production of cytokines during Ras-induced senescence in fibroblasts. Remarkably, in this model, autophagy inhibition has no effect on *IL-6* transcript levels, but elicits a reduction in IL-6 intracellular protein levels (Young et al., 2009). Although it remains unclear how autophagy precisely contributes to the post-transcriptional production of IL-6, our immunofluorescence analysis indicates a marked absence of cells expressing high levels of IL-6 protein upon ATG knockdown, suggesting that autophagy may contribute to the translation or stability of IL-6 protein in H-Ras^{V12} cells.

In addition to IL-6 production, we demonstrate that autophagy also promotes the expression of Wnt5a, a growth factor that positively influences cell migration and invasion, as well as MMP2, a matrix metalloprotease that promotes ECM degradation. Interestingly, in contrast to *IL-6*, ATG knockdown in H-Ras^{V12} cells is associated with reduced transcription of *WNT5A* and *MMP2*. Although these findings do not rule out an additional contribution for autophagy in regulating translation and secretion of these molecules, we speculate that these transcriptional effects on *WNT5A* and *MMP2* expression are likely an indirect consequence of autophagy inhibition. Nevertheless, several lines of evidence indicate that the autophagy-dependent production of both Wnt5a and MMP2 are

important contributors to invasion driven by H-Ras^{V12} in 3D culture. First, the addition of recombinant Wnt5a to autophagy deficient H-Ras^{V12} cells in 3D culture promotes the dissociation of cells within structures and enhances the formation of invasive branches. Second, treatment with a pharmacological MMP-2 inhibitor is sufficient to inhibit Ras-driven invasion in 3D culture. Lastly, the decrease in MMP2 activity found in H-Ras^{V12} shATG conditioned media correlates with a more restricted ECM degradation pattern in 3D culture, as delineated by attenuated fluorescence emanating from the proteolytic cleavage of dye-quenched collagen IV.

In addition to facilitating Ras-induced invasion, we find that intact autophagy is required for certain molecular features of Ras-driven mesenchymal differentiation. Previous studies indicate that oncogenic Ras activation is a potent inducer of epithelial-mesenchymal transition (EMT), which we corroborate here in H-Ras^{V12} MCF10A 3D cultures. Interestingly, ATG knockdown in H-Ras^{V12} cells restores keratin 14 levels, while concomitantly reducing vimentin levels, suggesting that autophagy inhibition suppresses mesenchymal differentiation in Ras-transformed cells. Nonetheless, broad-based changes across all EMT genes are not observed. For example, no changes in the mesenchymal marker *CDH2* (N-cadherin) were found in ATG knockdown cells. Based on these results, we conclude that autophagy deficiency is not sufficient to completely reverse a Ras-induced EMT. However, it is important to recognize that the partial effects we have observed may arise from the fact that we only partly reduce, rather than completely inhibit autophagy in ATG knockdown cells. How autophagy inhibition

alters the differentiation status of H-Ras^{V12}-transformed cells remains an important topic for future study. Intriguingly, in a recent study focusing on the mechanisms that govern EMT, multiple secreted factors were found to collaborate to induce a mesenchymal state in immortalized human mammary epithelial cells. Specifically, Wnt5a was identified as a key secreted factor critical for mesenchymal differentiation (Scheel et al., 2011). Accordingly, one can speculate that the reversion to a more epithelial state following autophagy inhibition may partly arise from decreased Wnt5a production and subsequent downstream signaling necessary to maintain the mesenchymal state. An additional implication of these finding is that autophagy may support the maintenance or function of cancer stem cells as the EMT program has been associated with the generation and maintenance of cancer stem cells (Mani et al., 2008; Polyak and Weinberg, 2009).

To date, research examining how autophagy contributes to cancer development has been focused on tumor initiation and expansion of the primary tumor. However, less is understood about how autophagy impacts the later stages of tumorigenesis. Recently, the deletion of *FIP200*, a gene involved in the early steps of autophagosome induction, was demonstrated to dramatically reduce the development of lung metastases in the MMTV-PyMT genetic mouse model of breast cancer (Wei et al., 2011). Our findings here demonstrate a unique requirement for autophagy during Ras transformation in facilitating cell migration, invasion and mesenchymal differentiation. Because these properties have long been associated with tumor dissemination and metastasis, an

important outstanding question is whether and how autophagy supports these novel tumor-promoting functions during carcinoma progression *in vivo*.

References

Berry, D.L., and E.H. Baehrecke. 2007. Growth arrest and autophagy are required for salivary gland cell degradation in Drosophila. *Cell*. 131:1137-48.

Chen, N., and J. Debnath. 2010. Autophagy and tumorigenesis. *FEBS Lett*. 584:1427-35.

Dai, C., L. Whitesell, A.B. Rogers, and S. Lindquist. 2007. Heat shock factor 1 is a powerful multifaceted modifier of carcinogenesis. *Cell*. 130:1005-18.

Fimia, G.M., A. Stoykova, A. Romagnoli, L. Giunta, S. Di Bartolomeo, R. Nardacci, M. Corazzari, C. Fuoco, A. Ucar, P. Schwartz, P. Gruss, M. Piacentini, K. Chowdhury, and F. Cecconi. 2007. Ambra1 regulates autophagy and development of the nervous system. *Nature*. 447:1121-5.

Friedl, P., and K. Wolf. 2003. Tumour-cell invasion and migration: diversity and escape mechanisms. *Nat Rev Cancer*. 3:362-74.

Fung, C., R. Lock, S. Gao, E. Salas, and J. Debnath. 2008. Induction of Autophagy during Extracellular Matrix Detachment Promotes Cell Survival. *Mol Biol Cell*. 19:797-806.

Furuta, S., E. Hidaka, A. Ogata, S. Yokota, and T. Kamata. 2004. Ras is involved in the negative control of autophagy through the class I PI3-kinase. *Oncogene*. 23:3898-904.

Guo, J.Y., H.Y. Chen, R. Mathew, J. Fan, A.M. Strohecker, G. Karsli-Uzunbas, J.J. Kamphorst, G. Chen, J.M. Lemons, V. Karantza, H.A. Coller, R.S. Dipaola, C. Gelinas, J.D. Rabinowitz, and E. White. 2011. Activated Ras requires autophagy to maintain oxidative metabolism and tumorigenesis. *Genes Dev*. 25:460-70.

Kim, M.J., S.J. Woo, C.H. Yoon, J.S. Lee, S. An, Y.H. Choi, S.G. Hwang, G. Yoon, and S.J. Lee. 2011. Involvement of autophagy in oncogenic K-Ras-induced malignant cell transformation. *J Biol Chem*. 286:12924-32.

Leslie, K., S.P. Gao, M. Berishaj, K. Podsypanina, H. Ho, L. Ivashkiv, and J. Bromberg. 2010. Differential interleukin-6/Stat3 signaling as a function of cellular context mediates Ras-induced transformation. *Breast Cancer Res*. 12:R80.

Mani, S.A., W. Guo, M.J. Liao, E.N. Eaton, A. Ayyanan, A.Y. Zhou, M. Brooks, F. Reinhard, C.C. Zhang, M. Shipitsin, L.L. Campbell, K. Polyak, C. Brisken,

J. Yang, and R.A. Weinberg. 2008. The epithelial-mesenchymal transition generates cells with properties of stem cells. *Cell*. 133:704-15.

Mazzone, M., L.M. Selfors, J. Albeck, M. Overholtzer, S. Sale, D.L. Carroll, D. Pandya, Y. Lu, G.B. Mills, J.C. Aster, S. Artavanis-Tsakonas, and J.S. Brugge. 2010. Dose-dependent induction of distinct phenotypic responses to Notch pathway activation in mammary epithelial cells. *Proc Natl Acad Sci U S A*. 107:5012-7.

Polyak, K., and R.A. Weinberg. 2009. Transitions between epithelial and mesenchymal states: acquisition of malignant and stem cell traits. *Nat Rev Cancer*. 9:265-73.

Qu, X., J. Yu, G. Bhagat, N. Furuya, H. Hibshoosh, A. Troxel, J. Rosen, E.L. Eskelinen, N. Mizushima, Y. Ohsumi, G. Cattoretti, and B. Levine. 2003. Promotion of tumorigenesis by heterozygous disruption of the beclin 1 autophagy gene. *J Clin Invest*. 112:1809-20.

Scheel, C., E.N. Eaton, S.H. Li, C.L. Chaffer, F. Reinhardt, K.J. Kah, G. Bell, W. Guo, J. Rubin, A.L. Richardson, and R.A. Weinberg. 2011. Paracrine and autocrine signals induce and maintain mesenchymal and stem cell States in the breast. *Cell*. 145:926-40.

Sullivan, N.J., A.K. Sasser, A.E. Axel, F. Vesuna, V. Raman, N. Ramirez, T.M. Oberyszyn, and B.M. Hall. 2009. Interleukin-6 induces an epithelial-mesenchymal transition phenotype in human breast cancer cells. *Oncogene*. 28:2940-7.

Tang, C.H., C.F. Chen, W.M. Chen, and Y.C. Fong. 2011. IL-6 increases MMP-13 expression and motility in human chondrosarcoma cells. *J Biol Chem*. 286:11056-66.

Vander Heiden, M.G., L.C. Cantley, and C.B. Thompson. 2009. Understanding the Warburg effect: the metabolic requirements of cell proliferation. *Science*. 324:1029-33.

Wei, H., S. Wei, B. Gan, X. Peng, W. Zou, and J.L. Guan. 2011. Suppression of autophagy by FIP200 deletion inhibits mammary tumorigenesis. *Genes Dev*. 25:1510-27.

Yang, S., X. Wang, G. Contino, M. Liesa, E. Sahin, H. Ying, A. Bause, Y. Li, J.M. Stommel, G. Dell'antonio, J. Mautner, G. Tonon, M. Haigis, O.S. Shirihai, C. Doglioni, N. Bardeesy, and A.C. Kimmelman. 2011. Pancreatic cancers require autophagy for tumor growth. *Genes Dev*. 25:717-29.

Young, A.R., M. Narita, M. Ferreira, K. Kirschner, M. Sadaie, J.F. Darot, S. Tavare, S. Arakawa, S. Shimizu, F.M. Watt, and M. Narita. 2009. Autophagy mediates the mitotic senescence transition. *Genes Dev*. 23:798-803.

FIGURE LEGEND

Figure 4. Potential pro-tumor functions for autophagy in mutant Ras tumors.

Tumor cells attached to the basement membrane and with ample supply of nutrients and oxygen rely on basal autophagy to support metabolism and promote rapid proliferation (left). When tumor cells lack access to nutrients, oxygen, or basement membrane contact autophagy levels are increased to promote survival (right).

Figure 4

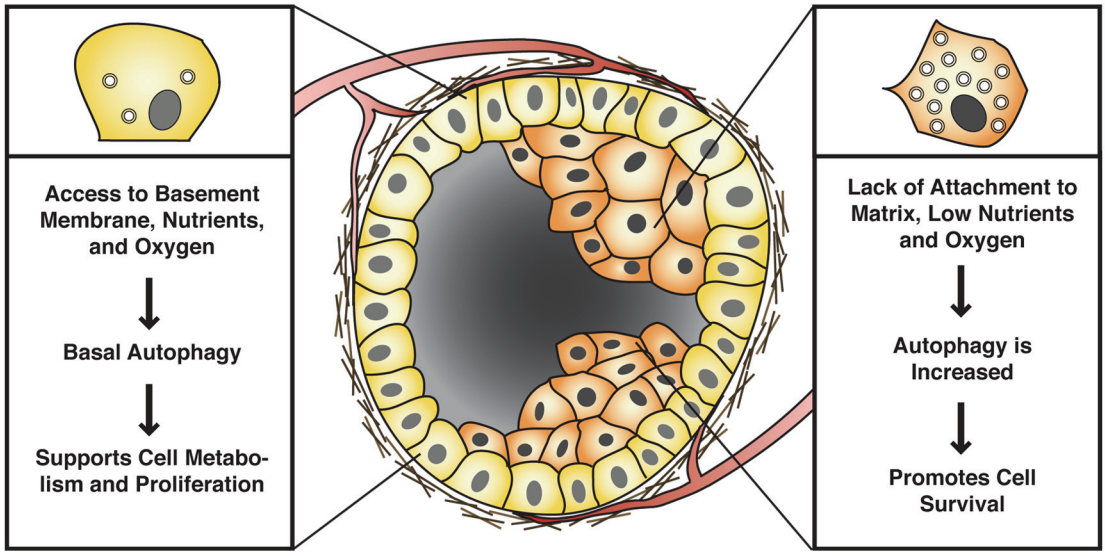
Access to Basement Membrane, Nutrients, and Oxygen
Basal Autophagy
Supports Cell Metabo-lism and Proliferation
Lack of Attachment to Matrix, Low Nutrients and Oxygen
Autophagy is Increased
Promotes Cell Survival

Publishing Agreement

It is the policy of the University to encourage the distribution of all theses, dissertations, and manuscripts. Copies of all UCSF theses, dissertations, and manuscripts will be routed to the library via the Graduate Division. The library will make all theses, dissertations, and manuscripts accessible to the public and will preserve these to the best of their abilities, in perpetuity.

Please sign the following statement:

I hereby grant permission to the Graduate Division of the University of California, San Francisco to release copies of my thesis, dissertation, or manuscript to the Campus Library to provide access and preservation, in whole or in part, in perpetuity.

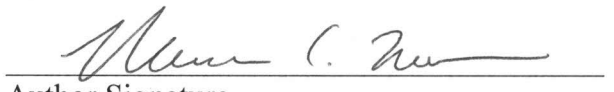

Author Signature

12/28/2011

Date